10-1-2021 2:00 PM

Evaluating Cranial Nonmetric Traits in Mummies from Pachacamac, Peru: The Utility of Semi-Automated Image Segmentation in Paleoradiology

Cameron J. Beason, *The University of Western Ontario*

Supervisor: Nelson, Andrew J., *The University of Western Ontario*

A thesis submitted in partial fulfillment of the requirements for the Master of Arts degree in Anthropology

Abstract

Anthropologists employ biodistance analysis to understand past population interactions and relatedness. The objectives of this thesis are twofold: to determine whether a sample of five mummies from the pilgrimage centre, Pachacamac, on the Central Coast of Peru comprised local or non-local individuals through an analysis of cranial nonmetric traits using comparative samples from the North and Central Coasts of Peru and Chile; and to test the utility of machine-learning-based image segmentation in the image analysis software, Dragonfly, to automatically segment CT scans of the mummies such that the cranial nonmetric traits are visible. Results show that while fully automated segmentation was not achieved, a semi-automated procedure was adequate for visualizing and scoring the skulls and saved time over manual segmentation methods. The sample from Pachacamac was too small to make significant inter-site comparisons, but a broader regional analysis suggests there are significant biological differences between geographical regions along the coast.

Keywords

Mummies, Pachacamac, Peru, Biodistance, Cranial Nonmetric Traits, Pilgrimage, Population Dynamics, Computed Tomography, Paleoradiology, Image Segmentation, Deep Learning

Summary for Lay Audience

This thesis focuses on a sample of five mummies from the Pachacamac sanctuary on the Central Coast of Peru. Pachacamac served as a ceremonial centre to which many groups of people travelled to engage in various forms of ritual behavior, indicating that it was a significant cosmopolitan centre throughout multiple Andean cultural phases from the Early Intermediate Period (200 BCE-AD 600) to the Spanish Conquest (AD 1532). The two central objectives of this study are anthropological and methodological. The anthropological objective is to conduct a biodistance analysis of cranial nonmetric traits to assess the dissimilarity between samples from the North and Central Coasts of Peru and the coast of Chile to determine whether the sample from Pachacamac represents the local population or pilgrims drawn from a wide area. Biodistance studies can reveal both genetic and environmental differences between populations by measuring divergence based on polygenic traits.

Because the skulls are inside mummy bundles, or *fardos*, Computed Tomographic (CT) scans of the mummies were studied using the image analysis software, Dragonfly. The methodological objective of this study is to test the utility of the machine-learning-based image segmentation tools in Dragonfly to automatically segment CT scans of the mummies such that the skulls can be scored for these traits. Image segmentation is the process of separating the components of images into meaningful segments for analysis. Currently, researchers rely on manual segmentation of CT images, a process that is tedious and difficult to replicate.

The findings show that while fully automated segmentation was not achieved, a semi-automated procedure proved adequate for visualization and scoring of the skulls and saved time over manual segmentation methods. The sample from Pachacamac was too small to make significant inter-site comparisons, but a broader regional analysis suggests there are significant biological differences between geographical regions along the coast. Previous studies of cranial nonmetric traits have focused on dry bone. This project is the first to examine these traits on mummified individuals using CT and demonstrates the benefits of investigating more complex methodologies in paleoimaging.

Acknowledgements

This project was made possible with the help of many people for whom I am immensely grateful. First and foremost, I must thank my supervisor, Dr. Andrew Nelson. Andrew has been the best supervisor I could ask for and even during my brief time at Western, it quickly became clear that Andrew works tirelessly for his students. Whether he is providing unique and engaging course content, offering valuable advice, being a receptive and patient point of contact, or organizing museum trips, Andrew has consistently shown his passion for anthropology and his aptitude for teaching. I must also thank him for providing numerous resources in this interest of a successful project, including sharing his data from San Jose de Moro, sharing connections with his Peruvian colleagues, organizing scanning sessions, and being available for any inquiries and assistance that was needed.

Thank you to my advisor, Dr. Jay Stock, who provided guidance on the theoretical components of the project in its early phases. I am also thankful for your advice during my first semester as a teaching assistant and for being approachable and always willing to help. I thoroughly enjoyed being in your theory course and learned a lot about the impact of one's paradigm on their interpretive lens. I also thank Dr. Andrea Waters-Rist for offering valuable feedback on my thesis. I also appreciate the unique projects in your methods course and the opportunities to explore creative avenues while honing my methodological knowledge as I began to develop this project.

I must also thank the entire faculty in the anthropology department at Western for being friendly and approachable throughout my time in the program. I am honored to have been a part of this department and I look forward to seeing the fascinating research that comes. Additional thanks to Christine Wall who answered my countless questions while I was sorting out all the study permit paperwork and administrative details of making the move to Western.

My access to the datasets analyzed in this thesis would not have been possible without the work of many people. Firstly, I must thank the contributors to the Mummies as Microcosms project for the Pachacamac datasets, including Andrew Nelson, Lucía Watson, Jocelyn Williams, Suellen Gauld, Joanna Motley, Lauren Poeta, Elizabeth

Gómez, Jhon Baldeos, Sarita Fuentes, and Denise Pozzi-Escot. Although I was not able to travel to Pachacamac myself, I am honored that I was able to analyze the data that you collected several years before I was involved with the project.

The comparative samples make up the backbone of the anthropological research question addressed in this thesis. I must thank Dr. Lucía Watson and the HORUS Group for the Ancón datasets. Thank you to Maria Ordoñez, Drs. Ronald Beckett, Andrew Nelson, and Gerald Conlogue for the Maranga datasets. Thank you to Dr. Nancy Ossenberg for publishing her analysis of the Chilean samples. Lastly, thank you to Andrew Nelson for the San Jose de Moro data.

Several individuals contributed significantly to the early phases of the project, especially learning how to master the analytical tools used in paleoradiology. Thank you to Dr. Natalie Reznikov for her tutorial and advice on the deep learning segmentation in Dragonfly. I must also thank CT technologist Alisha Goosens and Drs. David Hocking and Greg Garvin at St. Joseph's Medical Centre for opening their facility to obtain test scans for visualization of the nonmetric traits.

Thank you to my cohort for being so welcoming and for their assistance and friendship during our transition to a new city in a new country. Thank you, also, to my friends back home who connected with me virtually and provided me with occasional respite from the challenges of grad school.

I must also thank my family for their love and support throughout this whole process. I appreciate you check-in calls and care packages and especially appreciate you being understanding while we had to miss holidays and other milestones during this time. Thank you for taking interest in my work and for encouraging me to explore.

Finally, to Alexandria, few words capture how deeply grateful I am that you moved to London with me for this chapter. Your laughs, your lightness, and your support made this process so special, and I absolutely could not have done it without you. I will always treasure our time in our very fine house with Kiki, Wabi, and Basil. Thank you, for being there when our friends and families could not and for helping us both find growth in such an isolating and challenging time. You are truly one of a kind.

Table of Contents

List of Tables

List of Figures

List of Appendices

Chapter 1 Introduction

1.1 Background and research questions

Bioarchaeologists are interested in understanding past population interactions and mobility through the examination of skeletal markers. One method for studying group affinity, or biodistance, is to study the biological divergence between groups using nonmetric traits of the skull. The purpose of this thesis is to conduct a biodistance analysis focused on a sample of mummies from the pilgrimage centre, Pachacamac, Peru, in order to test the research question whether the sample represents the local population, or a pilgrimage sample drawn from a wide area, as expected. Pachacamac is a large ritual centre located on the Central Coast of Peru that contains large temples, pyramids, oracular seats for the deities, and sacrificial offering burials (Eeckhout, 2013). The site attracted many pilgrims from various locations throughout the Andes (Takigami et al., 2014). The assessment of this sample's status as pilgrims will be done through a comparative analysis of cranial nonmetric traits from skulls from other Middle Horizon, Late Intermediate Period, and Late Horizon sites on the Central and North Coasts of Peru as well as the North and South-central Coasts of Chile.

This thesis seeks to address both anthropological and methodological questions, the aims of which can be divided into two major components: (1) an anthropological model comparing the degree of divergence between the sample from Pachacamac and various sites from the Central and North Coasts of Peru and Chile and (2) an evaluation of the cranial nonmetric traits in the mummies using CT scans, comparing both manual and automated (machine-learning-based) methods of image segmentation for the visualization of the skulls. The goal of the first component is to elucidate the extent of regional interaction and the evidence of pilgrimage to centres like Pachacamac throughout the Andes around the Late Intermediate Period (AD 1100-1470). The goal of the second component is to assess the applicability of a new methodology for future paleoradiological studies of mummified remains.

1.1.1 Anthropological research question

Pachacamac is situated on the northern bank of the Lurín River, roughly half a kilometer from the Pacific Ocean and 30 km south of modern-day Lima on the Central Coast of Peru (Eeckhout, 2003). It was first excavated by Max Uhle in the late 19th century (Uhle, 1903). Many groups of people travelled to Pachacamac to engage in various forms of ritual behavior, indicating that it was a significant gathering centre across multiple Andean cultural phases from the Early Intermediate Period (200 BCE-AD 600) to the Spanish Conquest (AD 1532) (Eeckhout, 2013).

There is an abundance of archaeological and architectural evidence demonstrating the ceremonial and sacred nature of this site, including temples, pyramids, oracular seats of various deities, and burials of sacrificial offerings (e.g., Eeckhout, 2013; Shimada, 2006, Uhle, 1903). Furthermore, a substantial body of ethnohistoric accounts of the Ychsma and Inca highlight Pachacamac as a sacred location that was used as an administrative centre by dominant cultural and political groups (e.g., Cieza de Leon, 1941 [1553]; Cobo, 1979 [1653]; De Molina, 2011 [1575]). The long-standing ceremonial significance of Pachacamac's occupation is also illustrated by the series of modifications, additions, and expansions made by successive groups of occupants throughout the site's roughly 1,300-year use before the arrival of the Spanish (Eeckhout, 2013). This includes the construction of additional sectors that contained temples and pyramids (both on top of and adjacent to previous structures), residential buildings, walls, and cemeteries.

The sample from Pachacamac examined in this thesis was excavated in 2015 by Jhon Baldeos and studied and scanned in 2019 by the SSHRC-funded "Mummies as Microcosms" project, directed by Andrew Nelson, Lucía Watson, and Jocelyn Williams (Baldeos, 2015; Nelson et al., 2021). Eighteen CT scans are available from Pachacamac. This is the first attempt to assess this sample's status as pilgrims. The sample observed in this study most likely corresponds with the Late Intermediate Period with possible overlap with the Middle and Late Horizons (between 700 and 1400 A.D.) (Baldeos, 2015). Preliminary assessment of the sample from Pachacamac indicates a high degree of variability in fardo shape and size and the presence of textiles from the North Coast supports the hypothesis that this is a sample of pilgrims (Baldeos, 2015).

Biodistance analysis is a means of assessing relatedness in bioarchaeological samples by examining the variability in bone and tooth form and shape that is thought to reflect genetic relatedness (Buikstra et al., 1990). Biodistance analysis using nonmetric traits most frequently employs the Mean Measure of Divergence (MMD) to assess the dissimilarity between samples. The MMD converts a battery of trait frequencies into a numerical value such that the more dissimilar two groups are, the greater the value (Harris & Sjøvold, 2004).

The first step to address the anthropological research question of this thesis is to develop a model of the typical variation of local, non-pilgrim populations. This requires a comparison with other coastal sites in the Andes. This project examines a sample from Ancón, another cosmopolitan centre on the Central Coast (Slovak, 2020; Watson, 2016). Twenty-seven scans were made available from Ancón, courtesy of the "Mummies as Microcosms" co-director, Dr. Lucía Watson Jiménez and the Horus Project. Previous isotopic analysis suggests that the Ancón mortuary population is largely local (Slovak, 2020; Slovak et al., 2009), and so it will be used to represent the local baseline for determining whether the sample from Pachacamac is local or non-local.

In additional to Ancón, comparative samples were drawn from other regions along the Andean coast. These comparative samples include: (1) CT scans of two mummies from the Maranga Complex, a collection of monumental remains located in modern Lima; (2) a sample of 23 individuals from San Jose de Moro, an important Moche and Lambayeque ceremonial center on the North Coast of Peru; and (3) several sites (cultural affiliation unknown) along the coast of Chile that were examined by Dr. Nancy Ossenberg (2013). Regional patterning may be inferred according to the geographic distribution of the sites. Groups that lived closer together are expected to have reproduced with each other more frequently than with groups from greater distances. Therefore, sites from the Central Coast (Maranga and Ancón) should cluster together with one another and then with the sample from the North Coast (San Jose de Moro). The sites from Chile are expected to be a separate group from both the North and Central Coast sites. Possible disruptions in this expected patterning may come from the distribution of past trade routes or the relative ceremonial importance of Pachacamac to various groups of people throughout the Andes.

If the sample from Pachacamac is local, they should be more closely related to the sample from Ancón (low MMD values) than the other samples outside of the Central Coast (high MMD values). If the individuals from Pachacamac are pilgrims (and, therefore, non-local), they should not cluster closely with Ancón (high MMD values), and perhaps cluster more closely with the either San Jose de Moro or the Chilean sites (low MMD values). However, the Pachacamac sample may not cluster consistently with any static sample if they were derived from a sample not included in this study.

1.1.2 Methodological research questions

Previous studies of nonmetric variants of the skull have focused on dry bone (Berry & Berry, 1967; Corruccini, 1974; Molto, 1980; Ossenberg, 1976; Sutter & Mertz, 2004; Velasco, 2018; Verano, 1987). This project will be the first to investigate nonmetric traits as an indicator of biodistance on the skulls of mummified individuals using computed tomography (CT) imaging methods. Whether nonmetric traits can be visualized using CT scans is a central question of this project. The skulls from Pachacamac are not observable via traditional visual methods because they are inside mummy bundles, or *fardos*, that still have desiccated soft tissue. The visibility of the skull within the fardos is further limited by the relatively poor state of preservation and the presence of other grave goods inside the bundles, including ceramics, *spondylus* shells, and thousands of cotton seeds. The presence of these additional artifacts introduces further difficulties in the visualization process due to their similar densities as bone.

CT scans of the mummies were studied using the image analysis software, ORS Dragonfly (2020.0 and 2021.1). This software is used to create 3-dimensional reconstructions of the fardos and for segmentation of the crania for the biodistance analysis. Image segmentation is the process of separating the components of images into meaningful segments for analysis. By segmenting CT volumes, we can differentiate materials according to their densities within the object being scanned; in other words, bones, tissues, and other internal contents of mummies can be identified and examined separately. We currently rely on manual segmentation of CT images, a process that is tedious and difficult to replicate. This creates several methodological questions that I aim

to address: (1) Can nonmetric cranial data be collected from the CT scans? (2) Can this be done using manual image segmentation techniques? (3) Can the traditional (manual) process be automated using the recently implemented deep learning architecture in ORS Dragonfly? (4) If the fardos can be segmented automatically, is this quicker than the traditional method and can it produce a model of the skull suitable for scoring the nonmetric variants in both the two- and three-dimensional views?

1.2 Theoretical framework

My analysis of the sample from Pachacamac will draw from the biocultural approach, which blends elements of the two major paradigms in archaeological theory (processual and post-processual archaeology). This approach relies on empirical interpretations of archaeological data and materials and considers the broader, phenomenological analyses of these materials (Martin et al., 2015).

Analysis of the sample from Pachacamac will draw from Skousen's (2018) overview of the archaeology of pilgrimage and its importance in the archaeological literature on population mobility. A common thread throughout archaeological research on pilgrimage is a consideration of what types of archaeological materials are left behind by pilgrimage activities and how these materials fit into the broader religious or spiritual context under study (Skousen, 2018). Furthermore, biodistance studies and isotopic analyses can reveal bioarchaeological signatures of pilgrimage activity by determining the degree to which nonlocal skeletal samples differ from local populations (Sutter, 2000; Torres-Rouff et a1., 2013; Turner et al., 2013; White & Nelson, 2009). The biodistance analysis in this study may reveal the degree of divergence of the sample from Pachacamac from other local samples as well as samples from other regions along the Andean coast. The extensive history of archaeological work done at Pachacamac establishes the prevalence of pilgrimage to the site. The analysis of this specific sample may inform whether Pachacamac served, for these individuals, as a local ritual centre or the destination for pilgrims drawn from more distant regions.

1.3 Organization of this thesis

This thesis is organized into five chapters. Chapter two is a literature review covering both the anthropological background and the methodological background of this thesis. The anthropological background will introduce the samples under analysis, the culture history of the Central Coast with respect to perspectives of landscape and mobility, and an overview of biodistance analysis using nonmetric variants of the skull. The methodological background will cover the history of paleoradiology and CT in mummy studies as well as an overview of artificial intelligence and deep learning with respect to image segmentation and recent advances in automated image segmentation.

Chapter three will discuss the materials and methods employed in this study. It will introduce the samples from each site, including the hardware specifications of the CT scans of fardos from Pachacamac, Maranga, and Ancón. This chapter will also summarize the development and training of deep learning models and the steps taken to obtain finalized segmentations that are usable for scoring the nonmetric traits on the scans. This section will conclude with a summary of the statistical analyses used in biodistance studies using cranial nonmetric traits as well as common data screening techniques used for trait list reduction.

Chapter four will present the results of the automated image segmentation using deep learning in Dragonfly, the scoring of nonmetric traits and the process of selecting traits for statistical analysis; and the resultant biodistance analyses of inter-site and inter-regional divergence.

Chapter five will discuss the results of the CT image analysis with a consideration of deep learning's applicability in paleoradiological analyses. It will also discuss the results of the biodistance analysis and the assessment of biological affiliation along the Andean Coast.

Finally, chapter six will conclude with a summary of the overall aims of this study and a brief discussion of recommended future directions regarding both the study of the sample from Pachacamac and paleoradiological approaches to mummy studies in general.

Chapter 2 Literature Review

This chapter will provide an overview of the literature relevant to the aims of this thesis. It will begin with a brief overview of the culture history of the Central Coast of Peru from the Early Horizon to the Late Horizon (Table 2.1) followed by a summary of the history of archaeological investigations at Pachacamac, including the work of Max Uhle. This chapter will also cover the sites from which comparative samples were drawn, including Maranga and Ancón on the Central Coast, San Jose de Moro on the North Coast, and the six Chilean samples examined by Ossenberg (2013). A discussion of archaeological perspectives on pilgrimage will be followed by a discussion of Andean ecological and sacred landscapes. This chapter will then introduce biodistance analysis using cranial nonmetric traits and a brief history of paleoradiology and the application of CT in mummy studies and will conclude with an introduction to artificial intelligence and image segmentation and an overview of how these concepts have been applied recently in anthropology.

2.1 Culture history of the Central Coast

Table 2.1 Temporal sequence of the Andean cultural phases and the predominant cultures on the Central Coast, following Rowe (1962) and Moseley (2001).

Phase	Culture	Dates
Late Horizon (LH)	Inca	AD 1470-1532
Late Intermediate Period (LIP)	Ychsma	AD 1100-1470
Middle Horizon (MH)	Wari	AD 600-1100
Early Intermediate Period (EIP)	Lima	200 BCE-600 AD
Early Horizon (EH)		800-200 BCE

2.1.1 Early Horizon (800-200 BCE)

In the Early Horizon along the Central Coast (Figure 2.1), and especially surrounding Lima, there was a mass abandonment of the use of the earlier population's U-shaped ceremonial centres (previously common in the Rimac Valley) that was followed by the coexistence of two primary ceramic traditions- the Chavín de Huantár tradition influencing the northern part of Lima and Casma-Norte Chico tradition in the

Figure 2.1 Map of Peru with North Coast and Central Coast sites labelled. Modern Lima is labelled with the blue marker. Image by Google Earth, labelled by Cameron Beason.

Lurín valley (Flores, 2019; Tello, 1943). In Ancón, a local style of ceramics also known as ‘Miramar’ emerged (Lanning, 1963).

The end of the Early Horizon is marked by the emergence of the “White on Red” ceramic tradition that was subsequently replaced with a tri-color tradition that would become emblematic of the Lima culture in the Early Intermediate Period. Recent evidence also suggests that camelid domestication on the Central Coast first occurred as early as the Early Horizon (Szpak et al., 2014). It was previously believed that camelids were primarily bred in the highlands and brought down to the coastal valleys along commercial routes (cf. Shimada & Shimada, 1985; Szpak et al., 2015).

2.1.2 Early Intermediate Period (200 BCE- AD 600)

The Early Intermediate Period on the Central Coast is characterized by increased agricultural intensification and modifications made to the landscape (such as irrigation systems), resulting in an expansion of agriculture into the valleys (Earle, 1972). The Lima culture is associated with a specific tri-color ceramic type with geometric patterning, the use of hand-made adobe bricks in construction, which were positioned vertically and known as *adobitos*, and extended burials wrapped in cane (Flores, 2019). The Lima culture maintained a cultural hegemony in the region throughout this period, until the beginning of the Middle Horizon. Toward the end of the period, there is a population decline and the abandonment of public sites, which is associated with periods of intense drought and flooding due to El Niño Seasonal Oscillation (ENSO) (Flores, 2019).

The construction of the large urban settlement of Cajamarquilla (near Pachacamac) in the Rimac valley, dates to the Early Intermediate Period. While Pachacamac is considered the main ceremonial centre of the Lima culture, Cajamarquilla was the main urban centre (Conklin & Moseley, 1988). However, Cajamarquilla’s significance is debated because the population density of Cajamarquilla did not grow significantly until the end of the Early Intermediate Period. Shimada and colleagues (1991) argue that the site of Maranga (Figure 2.1) may have been a more likely urban centre of the Lima culture. The construction of some of the first temples at Pachacamac took place during this period.

2.1.3 Middle Horizon (AD 600-1100)

The reconstruction of culture history of the Central Coast during the Middle Horizon is characterized by a long-standing debate regarding the imperial presence of the Wari, an imperial power from the highlands. This debate arose in the 1980s and 90s on the basis of evidence of Wari presence on the coast centered around Wari ceramic styles associated with the highland site of Ayacucho and the role of the Wari in coastal urban and ceremonial centres. However, there has not yet been any clear evidence of a foreign settler population in the region (Flores, 2019). The second half of the Middle Horizon is characterized by shifts in Wari presence along the coast and the rise of regional elites that eventually formed the Yschma culture into the Late Intermediate Period.

2.1.4 Late Intermediate Period (AD 1100-1470)

The Late Intermediate Period on the Central Coast is associated with a reduction in Wari influence and the emergence of the Ychsma culture. This region also experienced considerable population growth and climatic fluctuations during the emergence of the Chimú (on the North Coast) and eventually the Inca (Covey, 2008).

One notable element of our understanding of this period is that it is not solely based on ceramic typology, but also on readings of ethnohistoric accounts (16^{th}-17^{th}-century chronicles). Maria Rostworowski de Díez Canseco is the most heavily cited interpreter of Ychsma lifeways through ethnohistoric accounts. According to Rostworowski's analysis of colonial sources, the Ychsma were composed of a handful of separate polities/groups that were united by their common worship of the *Pacha Kamaq* deity and whose administrative centre was situated at Pachacamac (Rostworowski, 1972, 1977).

The collapse of the Wari in the Cusco region is associated with the emergence of the early Inca state. The Inca soon began to annex neighboring territories, eventually reaching the territories along the Central Coast by the early 13^{th} century (Covey, 2008). The arrival of the Inca to the Central Coast resulted in the unification of the loosely affiliated polities that previously made up the Ychsma.

2.1.5 Late Horizon (AD 1470-1532)

The Late Horizon on the Central Coast is characterized by the incorporation of the region into the Inca empire. The Inca state expanded through warfare, marriage alliances, and the establishment of administrative and religious architecture (Covey, 2006; 2008). Flores (2019) suggests that the Inca occupation of the coast differed slightly than in the highlands. Initially, the coastal settlements were maintained in a relatively peripheral state. The Inca built roads and other structures throughout the coast but maintained control through local elites rather than state administrators from Cusco, as they did in the highlands (Burger & Salazar, 2014; Flores, 2019). Eventually, the Inca co-opted Pachacamac as the regional administrative and ceremonial centre and spread its influence throughout the neighboring valleys. The creation of the state province of Pachacamac unified the inhabitants of the coastal valleys, resulting in a reorganization of social relations between groups. The Late Horizon ends with arrival of the Spanish in 1532 which marks the beginning of the Spanish Conquest in Peru.

Moore (2005) describes a common practice in this body of research to overextend the wealth of information from analyses/syntheses of ethnohistoric accounts of the Inca to all other Andean cultures through space and time. He cautions against this use of the Inca as *lo andino*, suggesting that such perspectives can obscure the underlying complexity and variability of these cultures. This will have to be taken into account when considering the samples in my thesis as they are either directly associated with the Inca or are associated with a period before the arrival of the Inca but are situated at sites that later came under Inca rule.

2.2 Archaeological background

2.2.1 Pachacamac and Max Uhle

The Pachacamac sanctuary is a large ceremonial centre located on the northern bank of the Lurín River, the southernmost river in the Central Coast. It is one of the most important ritual sites in the Andes. The site covers 600 hectares of coastal desert and is situated roughly 500 metres from the Pacific Ocean. Unlike many sites along the

Central Coast with ritual architecture that were abandoned following the disappearance of their founding culture, Pachacamac was used continuously as a ceremonial centre over a span of about 1,300 years across multiple cultural phases (Lima (AD 200-600) - Wari (AD 600-1100) - Ychsma (AD 1100-1470) - Inca (AD 1470-1532)) from the Early Horizon to the Spanish Conquest in 1532 (Eeckhout, 2013).

The spatial organization of the site consists of four sectors divided by concentric walls (Uhle, 1903) (Figure 2.2). Sector I is the innermost sector of the site and is also known as the "Sacred Precinct". It is located at the southernmost and topographically highest point on the site. The earliest inhabitants lived and worshipped in the southwestern portion of the site, within Sector I. In this sector are the Temple of the Sun, the Painted Temple (Pachacamac Temple), and the Old Pachacamac Temple (Franco Jordan, 1998). The Old Pachacamac Temple (Lima Temple) was constructed during the Early Intermediate Period, the Painted Temple was constructed in the earlier phase of the Middle Horizon, and the Temple of the Sun was constructed by the Inca during the Late Horizon (Takigami et al., 2014; Uhle, 1903). The distinct *adobito* architectural style of the Lima culture is also found in the Old Pachacamac Temple, now situated below the Temple of the Sun (Eeckhout, 2004a).

During the later phases of the Middle Horizon, Pachamac underwent a period of apparent increase in power. Menzel et al. (1964) argue that the site served as a central administrative center subject to Wari rule or incursion. The site's influence and power is illustrated by the presence of textiles and ceramics found at Pacatnamú bearing iconography of the Pachacamac deity (Keatinge, 1978). By the end of the Middle Horizon, there was also a resurgence in local religious practices, indicated by an increase in offerings made at the temples in Sector I which had previously lost status and use under Wari control (Shimada et al., 1991). The collapse of the Wari is associated with an increase in construction at Pachacamac; this is consistent with Rostworowski's assertion that it was the Ychsma centre of worship and ideology in the Late Intermediate Period (Rostworowski, 1972).

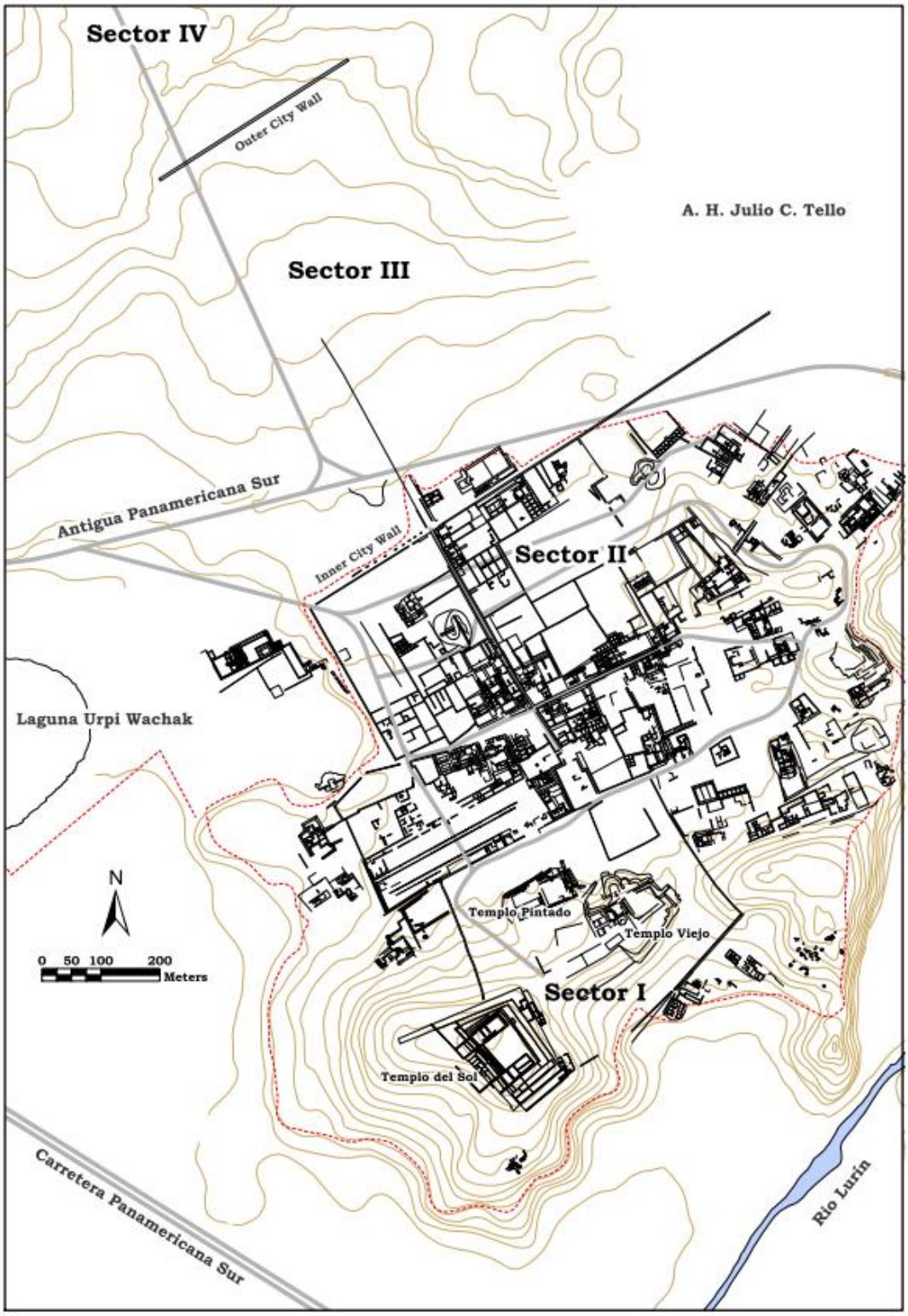

Figure 2.2 Map of the Pachacamac sanctuary with sectors labelled. Image by Go Matsumoto (2005, p. 55).

Sector II encompasses Sector I and is bordered by a prominent wall. These first two sectors make up the "Inner City" and Uhle described Sector II as the "Old City". Sector II contains fourteen Pyramids with Ramps; these are the dominant architectural features constructed during the Late Intermediate Period. There are two opposing models explaining the purpose of the Pyramids with Ramps. The traditional "Embassy Model" argues that the structures served as embassies or outposts for the various ethnic groups that were united due to their worship of the Pachacamac deity at the site (Bueno Mendoza, 1982; Burger, 1988; Hyslop, 1990; Rostworowski, 1972, 1977). Alternatively, Eeckhout's (1999) "Dynastic Model" suggests that the palaces were inhabited by local leaders or chiefs who succeeded one another. When one chief died, they were buried in their temple, the temple was abandoned, and the next chief constructed a new temple. This model is supported by Michczyński and colleagues' (2003) carbon dating of Pyramid with Ramp III, indicating successive stages of occupation, construction, and abandonment of the temples.

Sector III is known as the "Outer city" and contains numerous habitations and cemeteries dating to the Late Intermediate Period and the Late Horizon (Uhle, 1903). This sector also contains important Inca structures, including the Pilgrim's Plaza, the Convent of the Mamacona, the Quipu House, and the Tauri Chumpi palace (Shimada et al., 2004; Uhle, 1903). Finally, Sector IV is situated outside of the northern extent of Sector III and contains sections of floodplains and the Urpi Wachak Lagoon.

Pachacamac was first excavated by the German archaeologist, Max Uhle (1856-1944) in 1896, marking a significant turning point in Andean archeology by ushering the beginning of professional South American archaeology (Ramos, 2013). This illustrates the important role of Pachacamac not only in regional culture history, but also in the history of Andean studies and archaeology. Uhle's early excavations took place between 1892 and 1895 in Northwestern Argentina and Bolivia. In January of 1896, Uhle left the region in frustration after being prohibited from digging at Tiwanaku and travelled westward where he arrived in Lima a week later, and after a brief excavation at Ancon, Uhle began his year-long excavation at Pachacamac in February of 1896 (Uhle, 1903). He conducted a general survey, extensive photography, and stratigraphic sections and

diagrams of the temples and architecture. Uhle also excavated gravesites throughout Pachacamac, estimating that the site contained anywhere from 60,000 to 80,000 burials, and he collected and described extensive collections of ceramics and textiles (Uhle, 1903). Here, Uhle also uncovered the first physical evidence of Inca human sacrifice (Fleming, 1986; Uhle, 1903; Verano, 2001). Max Uhle's work in Argentina, Bolivia, and Peru also led him to create a general chronology independent of the colonial accounts that were written by 19th-century travelers. These travelers primarily wrote memoirs of their expeditions, racialized descriptions of Indigenous intelligence, and collected artifacts from Tiwanaku and Cuzco (Covey, 2018).

2.2.2 Ancón

The archaeological site of Ancón is located between the Chancay and Chillón river valleys roughly 40 km north of Lima (Slovack, 2020) (Figure 2.1). It has been thoroughly investigated for roughly a century and a half, most notably by George Dorsey in 1891, Max Uhle in 1904, and Tello and Carrion Cachot in the 1940's (Slovack, 2020 citing Dorsey, 1894, Uhle, 1968 [1912], and Carrion Cachot, 1951). The site is adjacent to the Bay of Ancón which provided rich marine resources throughout its occupation. It is divided into two primary sectors: the early Ancón sector which includes several small sites that functioned as a small-scale intensive fishing community and the Necropolis of Ancón (Slovack, 2020). The settlement of the site shifted from the early Ancón sector to the Necropolis in the beginning of the Middle Horizon (Patterson, 1966). The occupation of the Necropolis continued through the Late Horizon.

Twenty-nine individuals from this sample were CT scanned in 2013 in collaboration with the HORUS group. The fardos are housed at the Museo del Sitio-Ancón in Peru. The individuals studied in this thesis are associated with the Chancay culture (ca. AD 1100-1532) and correspond with the end of the Middle Horizon, into the Late Intermediate Period, and Late Horizon (Watson, 2016, 2019).

2.2.3 Maranga

The archaeological complex of Maranga, or Maranga Complex, encompasses a series of monumental remains, including the Pyramids with ramps, in the southern margin of the Rímac River valley and is associated with the Lima and Ychsma cultures (Eeckhout, 2004b) (Figure 2.1). The complex was occupied since the Early Intermediate Period (AD 1-750) through the Colonial Period (AD 1532). The site consists of large *huacas* (artificial mounds) built in a 'bookshelf' style, so named for the walls made of vertically positioned bricks (*aboditos*) that appear as books on a shelf and are characteristic of the Early Intermediate Period. The *huacas* served as domestic and administrative buildings, storage areas, workshops, and cemeteries (Mackay & Santa Cruz, 2000). During the Late Intermediate Period, the Maranga Complex contained Pyramids with Ramps, associated with the Ychsma (Villacorta, 2004). The individuals from Maranga studied in this thesis are associated with the Late Intermediate Period and/or the Late Horizon but their exact location from the Maranga Complex is unknown (Ordoñez et al., 2015). They are likely associated with Huaca San Marcos, Huaca Middendorf, or the Concha Complex (Ordoñez et al., 2015).

2.2.4 San Jose de Moro

San Jose de Moro was an important Moche ceremonial center located in the Jequetepeque Valley on the North Coast of Peru (Figure 2.1). It is located between the modern cities of Trujillo and Chiclayo and the most notable features of the site are large adobe huacas. The site was occupied by fragmented and competing Moche polities and initial occupation began in the Middle Moche Period (AD 450) during the Early Intermediate Period (Castillo & Quilter, 2010; Conlogue & Nelson, 1999; Sutter & Chhatiawala, 2016). Following the demise of the Moche, the site underwent a Transitional period (AD 850-950) and a Lambayeque occupation throughout the Middle Horizon (Castillo, 2012; Nelson et al., 2000). Finally, the Chimu, and eventually the Inca, occupied the site, using the large adobe huacas as administrative buildings.

The sample examined in this thesis was studied and x-rayed by Drs. Andrew Nelson and Gerald Conlogue from 1995 to 1999. It is mostly comprised of local

individuals associated with the latter half of the Moche period (AD 450-750) during the Early Intermediate Period and Middle Horizon. The sample serves as an outgroup Peruvian population that was not located on the Central Coast.

2.2.5 Chilean datasets from Ossenberg (2013) online database

The material from northern Chile was derived from Nancy Ossenberg's (2013) cranial nonmetric trait database. The database contains scores for 8,016 crania from a variety of geographic regions and time periods. Individuals are separated by geographic region and by site; the only South American material was from Chile and Argentina. While Ossenberg's (2013) database did not provide any Peruvian samples, the sites in the Chilean sample are coastal and were thus useful for comparison as a southern outgroup.

Most of the individuals from the Chilean sample were excavated by Junius Bird, who, at the time of his death in 1982, was the curator emeritus of South American archaeology at the American Museum of Natural History. Six localities are included in the Chilean sample scored by Ossenberg: Arica, Araucanian, Coquimbo, Iquique, and Punta Pichalo (Figure 2.3). Information on the

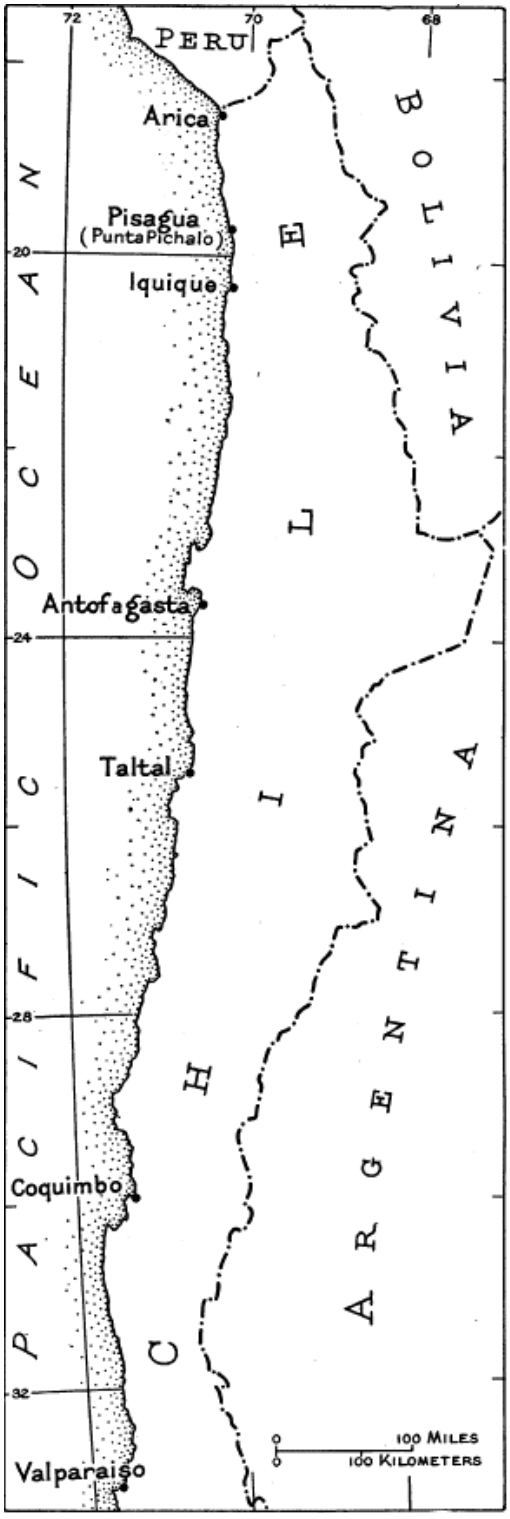

Figure 2.3 Map of localities along the Chilean Coast excavated during Bird's 1941 expedition. Image by Junius Bird (1943, p. 180).

specific sites studied in each of these localities is limited; only the sites in Arica and Iquique are specified in the collections information as well as the report published by Bird in 1943. The crania were collected during Bird's 1941 expedition to various coastal sites in the northern half of Chile (Bird, 1943). Bird's expedition began in Arica, where he spent 65 days excavating sites in the region, including the Salinas Mound and Playa Miller. From there, he travelled roughly 150 kilometers south to Punta Pichalo (also referred to as Pisagua in Figure 2.3) where he spent a month and a half. The 'Junin Grave' individuals were excavated about 5 km south of Punta Pichalo. Bird then excavated in Iquique for ten days, Antofagasta for ten days, Taltal for a month, and finally Coquimbo for another month (Bird, 1943, pp. 179-181).

2.3 Mobility, pilgrimage, and the Andean landscape

2.3.1 Bioarchaeology of mobility and pilgrimage in the Andes

Prehispanic Andean populations moved throughout the landscape for a multitude of reasons, including migration, economic activity, conflict, subsistence and agriculture, responses to environmental conditions and catastrophes, and pilgrimage to sacred sites (Barbarena et al., 2017; Eeckhout, 2013; Knudson et al., 2004; Sutter & Mertz, 2004; White et al., 2009). Bioarchaeological investigations of population mobility throughout the Andes are often tied to an analysis of the associated landscapes. For instance, several recent isotopic studies have examined the mobility of past populations in the Andes, most often assessing place of origin and estimating spatial scales of mobility to understand the interaction between groups of people (Barbarena et al., 2017; Knudson & Tung, 2011; Slovak et al., 2009; Toyne et al., 2017; White et al., 2009). The scale of these investigations varies according to specific regions of interest and associated research questions. These analyses elucidate the extent of small-scale interactions between remote groups or larger scale interactions, such as the dynamics between imperial heartlands and peripheral settlements or assessing interactions within or among remote settlements (e.g., Knudson & Tung, 2011; Shady & Ruiz, 1979; Slovack et al., 2009).

Pilgrimage has been thoroughly described in the archaeological literature of various regions throughout the world, including Mesoamerica (Harrison-Buck et al.,

2018; Lucero & Kinkella, 2014); North America (Huffman & Earley, 2019; Van Pool & Van Pool, 2018); Europe (Lash, 2018; Locker, 2015); The Levant (Coleman & Elsner, 1994; Lymer, 2004; Ullinger, 2002); and Asia (Davis & Coningham, 2018). Skousen (2018) discusses the importance of pilgrimage as a concept in archaeological analysis, highlighting the phenomenological value of materials, features, and landscapes associated with pilgrimage. He defines pilgrimage simply as "religiously motivated journeys to special places" (Skousen, 2018, p. 262). He also proposes a relational approach that emphasizes the interaction that pilgrimages promote between people, places, and artifacts (Skousen, 2018).

2.3.2 Evidence that suggests the presence of pilgrimage

As previously mentioned, a consideration of the types of archaeological materials left behind by pilgrimage activities and how these materials fit into the site's broader ideological and sacred context is a central component of archaeological interpretations of pilgrimage. These assessments often rely on a combination of artifactual, architectural, and ethnohistoric evidence of pilgrimage (when available) to determine if the cause or purpose of a group's movement is associated with pilgrimage activities rather than the other motivations listed in the previous section. Assessments of pilgrimage can expand on the ideological contexts associated with these previous mobility studies. For instance, if a site did attract pilgrims, they would have been outsiders compared to the local group, their stays may have been of variable length and may have been recurring at various points in their life (White et al., 2009).

2.3.3 The Andean landscape(s)

Andean archaeologists have long been interested in the topography and paleoecology of the Andean region. With respect to Andean cultural history, much of this research emphasizes the connection between the natural environmental processes and the complexity and diversity of past human interactions. The descriptions of these landscapes and how they have changed as a result of climatic processes throughout time are used to the trace developments in subsistence and agriculture as well as broader political and social contexts (e.g., Aldenderfer, 1999; Contreras, 2010; Flores, 2019; Sandweiss &

Richardson, 2008). Similarly, catastrophic events, such as earthquakes, floods, and drought, have been of interest to archaeologists in Peru to study periods of dramatic cultural change and expansion as well as societal collapse (Binford et al., 1997; Eeckhout, 2013; Jennings, 2008; Kolata, 2000; Paulsen, 1976). Archaeologists working in the coastal regions of the Andes during the 1970s began to study the El Niño/Southern Oscillation as culturally influential events (Osborn, 1977; Parsons, 1970; Paulsen, 1976; Sandweiss & Richardson, 2008).

The earliest scholarship of the Andean landscape dates to the 17th-century geographer, Guaman Poma de Ayala (Contreras, 2010). Archaeological notions of the 'environment' and 'landscape' have long been central to investigations of past population dynamics of the central Andes. Julio Tello described the relationship between environmental diversity and Prehispanic cultural development as early as 1930 (Contreras, 2010; Tello, 1930). The formation and shaping of this sacred landscape are often attributed to the unique natural features of the region, such as the sliding of the oceanic Nazca plate under the continental South American plate creating a prevalence of seismic and volcanic activity as well as coast uplift, affecting the region's irrigation. Additionally, frequent climatic fluctuations result from both El Nino Seasonal Oscillation (ENSO) events and the stark shifts in altitude throughout the landscape (Sandweiss & Richardson, 2008). Complementing these stark shifts in altitude and climate is a vast sacred landscape that encompasses ritual sites throughout the region (Contreras, 2010).

In his modern classification, Peruvian geographer Javier Pulgar Vidal (2014 [1987]) divides Peru into eight distinct 'natural regions' (Figure 2.4), forming a west-east gradient based on climate, altitude, and indigenous land use. This model can be used to describe the ecological zones of the Central Andes and has been used to help situate the human-environment interactions of this region (Sandweiss & Richardson, 2008; Stone et al., 2015). Three of the four sites discussed in this thesis (Pachacamac, Ancón, and Maranga) are located on the Central Coast of Peru and one (San Jose de Moro) is located on the North Coast.

All of the sites are situated in Pulgar Vidal's first zone, known as the *chala*. This zone is a coastal desert that runs from the Pacific coast to the quebradas of the western

slopes of the Andes up to 500 metres above sea level (Pulgar Vidal, 2014 [1987]; Sandweiss & Richardson, 2008). The Peruvian Coast is segmented by rivers that run perpendicular to the coast and have provided vital sources of water, plant and animal resources, and transport throughout the history of human occupation in this region. The lower boundary of the Lurin valley is located in both this first zone and Pulgar Vidal's second zone, the *yunga*. The *yunga* is present on the western slopes between 500 masl and 2,300 masl. It is characterized by arid hillsides and mountain slopes cut by the deep river valleys and quebradas. The first intensive farming and irrigation of the coastal valley floors began around 4,400 years ago and as early as 6,100 years ago in the western slopes (Burger, 1992; Dillehay et al., 2005).

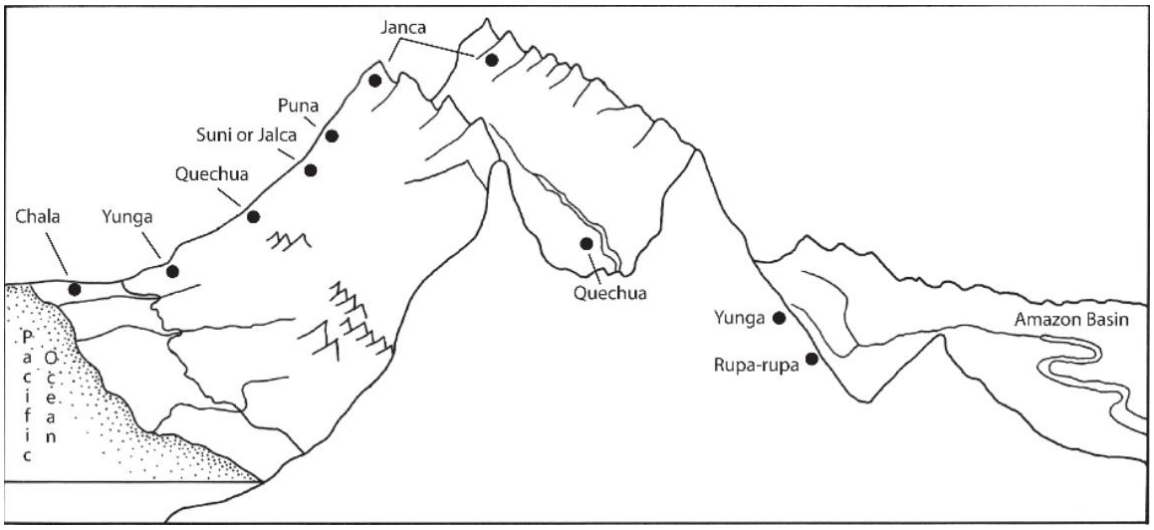

Figure 2.4 Cross-section of the Central Andes showing Pulgar Vidal's (2014 [1987]) natural regions, image adapted from Richardson (1994) by Sandweiss & Richardson (2008, p. 95).

Between 200 and 1,000 masl, the Pacific winds bring in a dense fog, known as *garúa*, along the coast during the austral winter. This moisture sustains *lomas*, communities of vegetation that are unique to the coastal deserts of the Andes and provided food and resources to the earliest inhabitants of the region (Matos Mar & Mendoza, 1964; Sandweiss & Richardson, 2008). Other flora found in the region of Pachacamac are also typical of the Central Coast, including varieties of domesticated legumes and a variety of fruits and vegetables. Camelids were a common source of wool and meat in the region. Some authors associate camelid herding and wool production with the highland regions (e.g., Murra, 1980 [1955]) while others have suggested that

camelids were raised in some coastal regions (cf. Shimada & Shimada, 1985; Szpak et al., 2014). Other forms of terrestrial fauna include small rodents and guinea pigs, domesticated dogs, insects, and the rich marine resources of the coast also offered numerous species of fish and mollusks. *Spondylus*, a shell occasionally placed in the fardos observed in this thesis, was also imported from the coast of Ecuador and northern Peru (Bauer, 2007; Paulsen, 1974).

2.3.4 Sacred landscapes

As noted in the previous section, the environmental settings of the Andes have been traditionally studied and interpreted with respect to the productive capacities and constraints of the landscape. These capacities and constraints are understood as pressures that have guided changes in subsistence strategies throughout the ancient Andean past.

The term, *sacred* landscapes, refers to the ideological or ritual significance that is associated with both the landscape as a whole and with distinct features of that landscape (Contreras, 2010). Scholars of Andean archaeology have long sought to reconstruct and interpret the sacred or ritual elements of the Andean landscape. This is often done with a grounding in ethnohistoric documentation (in the case of the Inca and less frequently among the Yschma, see Rostworowski 1972, 1977) (Bauer & Stanish, 2001; Reinhard & Ceruti, 2005). A considerable amount of ethnohistoric evidence points to conceptions of certain landscape features (e.g., springs, rivers, rocks features, caves, mountain peaks, etc.) as sacred elements. Many of these recent studies employ the Inca concept of the *waka* or *huaca*, a term that refers to these sacred elements, at which sacrifices, ceremonies, and offerings were often made, and apply this significance to describe the entire sacred landscape (Contreras, 2010, 2017; Silverman, 2004).

2.4 Biodistance analysis

Biodistance is “the measurement of the population divergence based on polygenic traits” and can reveal both genetic and environmental differences between groups (Buikstra et al., 1990, p. 1). This assessment of relatedness is conducted through the use of multivariate statistical methods. Although modern applications have incorporated

increasingly complex methods of analysis, the underlying assumption of biodistance studies has generally remained the same since the early studies of the late 19th century: people who share similar morphological features are more closely related or share a common ancestry when compared to people with fewer similarities (Hefner et al., 2016, p. 4). Biodistance analysis has been used for many purposes, including: tracing temporal and spatial biological relationships; assessing geographical influence on microevolutionary forces (gene flow, genetic drift, and selection); identifying postmarital residence patterns, inter- and intracemetery variation and structure, familial/kinship ties, and genetic admixture; reconstructing mobility, migration, and pilgrimage; and sorting commingled remains and the assignment of unknown individuals to a reference group (relevant to both repatriation claims and forensic cases) (Pietrusewsky, 2014).

Biodistance analysis is concerned with the effects of gene flow (usually within the context of migration) and genetic drift. These processes have greater impacts on variability over relatively short time spans than over longer periods of time (Stojanowski & Schillaci, 2006). When gene flow occurs between two populations, the mean variances for metric traits become increasingly similar while the variability in nonmetric traits gradually decreases.

Biodistance has been a prominent realm of human skeletal analysis since the 18th century, but modern bioanthropologists have since moved away from the racial typological perspective. The so-called natural philosophers of this time used characteristics of soft tissue (such as skin, color, hair color, and eye shape) along with skeletal form (such as limb proportions) to group people into “biological packages” (Hefner et al., 2016, p. 4). At the turn of the 19th century, researchers began to notice the remarkable diversity of human populations but continued to focus on a small suite of traits with little regard for an analysis of within-group variation (Armelagos et al., 1982; Hefner et al., 2016).

There are several types of variables that are traditionally used in biodistance analysis, including craniofacial measurements, cranial nonmetric traits, dental morphology, dental measurements, and ancient DNA. Cranial metrics have a similarly typological history as nonmetric studies. Martin’s (1926) textbook marks one of the first

systematic attempts to standardize not only craniometric data collection, but also physical anthropological methods in general, such as in osteology and 'craniology' (Hefner et al., 2016 citing Martin, 1926). Howells (1973) applies multivariate analysis to the classification of skulls using craniometrics and offers a more recent treatment of craniometric data, refining variables such as the definitions of bony landmarks and the coding of measurements to be incorporated into workable statistical analysis. Studies of dental morphology and measurements follow a similar development as the late 19th-century descriptions of cranial 'anomalies'. Anthropological approaches to dental morphology were not standardized until Turner et al.'s (1991) description of the Arizona State University Dental Anthropology System (ASUDAS). Ancient DNA is the most recent realm of modern biodistance analysis (e.g., Torres et al., 2013); the first extraction and sequencing of ancient DNA was conducted by Higuchi et al. (1984) on a "150-year-old" museum specimen.

2.4.1 Cranial nonmetric traits

Cranial non-metric traits were first described by the natural philosophers as skeletal anomalies. Chambellan's (1883) dissertation on wormian bones was the first scholarly attempt to connect these anomalies in a racial context with anthropological research (Hefner et al., 2016 citing Chambellan, 1883). During this time and around the turn of the 20th century, a consideration of statistical approaches was incorporated in these analyses. However, much of biological anthropology remained typological through the 1930 and 40s; many biodistance studies of this period were still describing nonmetric traits as anomalies rather than indicators of human variation. A significant shift in this perspective occurred following Washburn's "The New Physical Anthropology" (Washburn, 1951) that emphasized hypothesis-driven analysis, biochemical mechanisms of human evolution, and anticipated the processual approach to data collection and interpretation that arose in the 1960s (Hefner et al., 2016). This shift also coincided with Grüneberg's and Berry and Berry's genetic and morphological studies of mice during the 1950s and 1960s (Berry & Berry, 1967; Lane & Sublett, 1972; Hauser & DeStefano, 1989).

2.4.2 Biodistance studies in Peru

The Andes, and particularly Peru, is an interesting region to study population variability because the rugged landscape features multiple ecozones of varying high and low altitudes and climatic fluctuations from coastal processes have created numerous isolated populations, as discussed above (Pulgar Vidal, 2014 [1987]; Stone et al., 2015). This has, coupled with a rich assemblage of archaeological and ethnohistoric data, made the Andes a frequent region of interest for biodistance researchers. Biodistance studies in the Andes have analyzed a suite of craniofacial characteristics to assess population structure and dynamics, including dental morphology (Corruccini & Shimada, 2002; Sutter, 2000; Sutter & Castillo, 2015; Sutter & Verano, 2007), craniometrics (Ross et al., 2008; Rothhammer et al., 1982; Rothhammer & Silva, 1989; Stone et al., 2015), and nonmetric cranial traits (Rothhammer et al., 1984; Sutter & Mertz, 2004; Torres-Rouff et al., 2013; Verano, 1987). These studies can serve as useful references for determining the variability within sites with local, relatively homogenous makeup.

In the previous chapter, I summarized the expected results of the biodistance analysis regarding the geographic distribution of sites. Richard Sutter's (2000, 2005, 2009) work with Andean populations has found significant geographic trends in dental nonmetric trait frequencies across numerous samples that span all chronological periods in both highland and coastal sites of the Andes. His (2009) study of dental nonmetric trait frequencies among 44 Andean samples suggests a closer relationship between the northern and central Peruvian samples. This work supports the possibility of geographic trends in the sample observed in this thesis. If group clusters form according to the geographic distributions of the sites, I expect the Central and North Coast groups to cluster more closely than with the Chilean group. This expectation is also supported by the greater cultural similarities between the North and Central coasts compared to the Chilean sites.

2.4.3 Cranial modification

One of the most common issues in studies of ancient Andean population dynamics is the prevalence of cranial vault modification (Blom, 2005; White, 1996).

Many ancient Andean people used special apparatuses to alter the shape of the head during infancy as the crania is still soft and pliable at this stage (Torres-Rouff, 2019). The modification of skulls has been thoroughly discussed in studies of Andean population dynamics (Del Papa & Perez, 2007; Pomeroy et al., 2010; Torres-Rouff, 2019). There are several different types of modification; the two main forms described in Peru are tabular or fronto-occipital and annular (Figure 2.5) (Anton, 1989; Nelson et al., 2021; Torres-Rouff, 2019). The motivations for cranial modification are thought to be markers of either social status (see Blom et al., 1998; Las Casas, 1967 [1552-1561]: p. 338) or ethnic identity (see Cieza de Leon, 1984 [1553]: pp. 594-595; Sutter, 2005) according to the interpretations of ethnohistoric accounts of Inca practices. Recently, scholars have cautioned against a broad territorial perspective and emphasize the importance of a more contextualized approach to understanding patterns of modification (Blom & Knudson, 2014; Velasco, 2018).

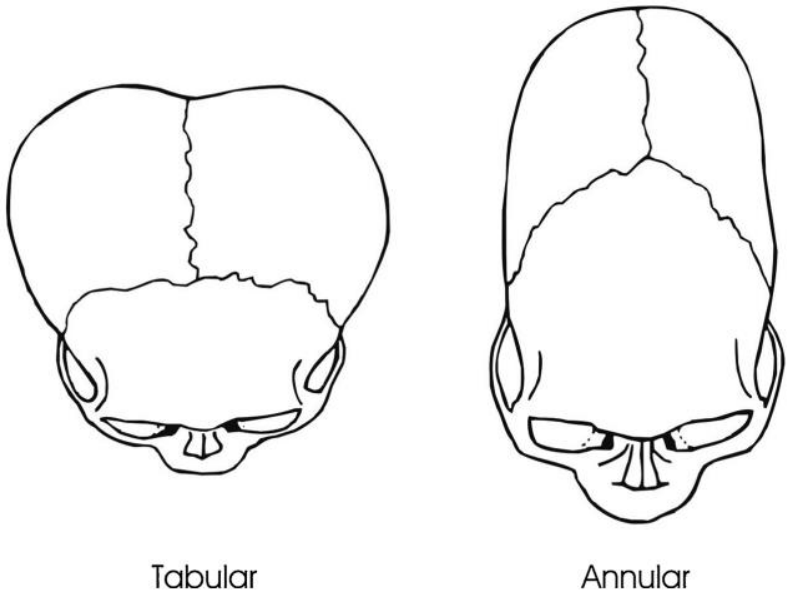

Figure 2.5 Broad categories of Andean head shaping. Image by Torres-Rouff (2019, p. 3) after Anton (1989).

Many studies examine the potential influence of cranial modification on the expression of nonmetric traits (Del Papa & Perez, 2007; Konigsberg et al., 1993, O'Loughlin, 2004). The most commonly mentioned trait affected by modification is the presence of wormian bones (Del Papa & Perez, 2007; White, 1996). Additionally, some

studies compare the effects of various forms of modification on the expression of other nonmetric traits. Konigsberg et al., (1993) note that annular modification is correlated with a decrease in epipteric bones and an increase in extrasutural bones of the parietal notch and occipitomastoid suture. However, these studies suggest that the implications of cranial modification on the ability to assess population dynamics with nonmetric cranial traits are negligible overall. The effects of cranial modification are more pronounced for metric analyses (Boston et al., 2015).

2.4.4 Critiques of biodistance and paradigmatic shifts in epigenetics

Some modern researchers have dismissed recent approaches to biodistance, arguing that recent studies are too heavily concerned with racial histories and typological, mean-based perspectives (Armelagos & Van Gerven, 2003). Armelagos and Van Gerven (2003) also argue that the underlying questions addressed in interregional comparisons have not changed in roughly 100 years. However, this is not necessarily problematic when considering the updates in methodology and central research questions since these early racialized typologies. Stojanowski and Buikstra (2004), in their response to this critique, argue that advancements in model-bound genetic analyses that consider both means and variances contradict this perspective and indicate that biodistance analyses still have much to offer anthropology (Relethford & Blangero, 1990; Stojanowski & Buikstra, 2004). They also point out the shift to ‘model-bound’ quantitative genetic approaches (Knudson & Stojanowski, 2008; Stojanowski & Schillaci, 2006) as well advances in evolutionary theory and improvements in computing and statistical procedures (Harris & Sjøvold, 2004; Irish, 2010). Stojanowksi and Schillaci (2006) also argue that modern biodistance analyses have moved away from the typological perspective by focusing on phenetic variability, rather than just means. For example, research on ethnicity, identity, and regional histories has benefited from a consideration of genetic population structure.

2.4.5 Heritability of nonmetric traits

There is also some debate surrounding the heritability of nonmetric cranial traits (Carson, 2006; Cheverud & Buikstra, 1981; Richtsmeier et al., 1981; Richtsmeier &

McGrath, 1986; Sjøvold, 1984). Numerous studies have been conducted on non-human subjects, such as Grüneberg's (1952) and Berry's (1962) studies on mice and Cheverud and Buikstra's (1981a; 1981b) study on rhesus macaques. Several more recent studies have been done to assess the heritability of nonmetric traits in human samples (Carson, 2006; Sjøvold, 1984). For instance, Sjøvold (1984) calculated the heritabilities of nonmetric traits in a skeletal sample of known pedigree from Austria, finding a range of heritability coefficient values from 0.0 to 0.954 across various traits (Pink et al., 2016; Sjøvold, 1984). Carson (2006) reexamined heritability in the same sample as Sjøvold (1984), using a more advanced statistical procedure (maximum likelihood variance components analysis) and found uniformly low heritabilities in nonmetric traits when scored as dichotomous (presence versus absence, the method used in this thesis and by Sjøvold (1984)) or multilevel (sliding scale) (Carson, 2006; Pink et al., 2016). Carson (2006) attributed this low heritability to large standard errors across estimates as well as variability in the dichotomization standards when scoring traits. Despite the low heritabilities, the dichotomous scoring method achieved relatively higher values than the multilevel scoring method. Furthermore, recent comparisons have reported a high degree of concordance between morphological and genetic data (see Herrera et al., 2014; Ricaut et al., 2010).

2.4.6 Epigenetics

The term, epigenetics, has been used in a variety of ways in the past. It was originally coined in 1942 by Conrad Waddington (Waddington, 1942). During these early years, epigenetics was defined as "the study of the processes by which the genotype brings the phenotype into being" in the context of development (Cavalli & Heard, 2019, p. 491). Waddington's conceptualization of the term had a substantial impact on many fields, especially developmental researcher interested in understanding the nature of the environment and its interaction with genes on the eventual phenotype of an organism (Tronick & Hunter, 2016, 2).

Early biodistance studies considered the variability of nonmetric craniofacial traits within this early context of epigenetic variation. Early epigenetic studies on humans

argued that epigenetic variants of morphological traits may reflect genetic differences between populations because these traits exhibit high heritability (Berry & Berry, 1967; Buikstra et al., 1990). Hauser and De Stefano's (1989) atlas, *Epigenetic Variants of the Human Skull,* has been widely used in bioarchaeological studies of cranial nonmetrics to develop trait lists for biodistance analysis. However, recent advances in our understanding of epigenetics may suggest that these traits do not necessarily follow a direct model of genetic inheritance and that the processes that guide epigenetic control of genomic function are more complex than some of the early studies suggested (e.g., Berger et al., 2009; Cavalli & Heard, 2019).

Weinhold (2016) uses the term to refer to the processes that alter gene expression without modifying the DNA sequence itself. Some of the known environmental agents of epigenetic processes include basic nutrients, viruses, bacteria, tobacco smoke, heavy metals, hormones, and air pollution. In a recent review of the current state of knowledge on epigenetics, Cavalli and Heard (2019) use the term to mean "the study of molecules and mechanisms that can perpetuate alternative gene activity states in the context of the same DNA sequence" (Cavalli & Heard, 2019: 489). Furthermore, recent biodistance analyses using these traits prefer the term *nonmetric* over *epigenetic* traits (e.g., Ricaut et al., 2010; Sutter & Mertz, 2004) while others abandon the term entirely, using only the term *nonmetric* (e.g., Velasco, 2018). Based on these recent reconsiderations, the updated use of terminology in biodistance analyses, and personal communication with Dr. Jay Stock, it was advised to disregard the use of the term, *epigenetics*, when referring to the nonmetric traits in this analysis.

2.4.7 Rationale for the use of nonmetric cranial traits

Despite the variable heritability reported for nonmetric traits, nonmetric trait analysis is the most conducive to the nature of the samples and the goals of this thesis. Nonmetric traits are also better suited for fragmentary samples and can mitigate the effects of cranial modification; both of these conditions apply to the samples studied in this thesis. While DNA analysis is the most obvious and effective way to understand the genetic makeup of a population, its costliness and its requirement to disturb the bundles

do not make it a viable method for this study. Similarly, craniometric analysis was discarded due to the prevalence of cranial modification and the fragmentary nature of the remains. It is assumed that nonmetric traits can reflect, at least partially, the genetic background of a population while being non-destructive and low-cost compared to alternative approaches (Hauser & DeStefano, 1989; Buisktra & Ubelaker, 1994).

2.5 Paleoradiology and computed tomography (CT)

2.5.1 Tomography and Computed Tomography (CT)

The term tomography is used today to refer, simply, to slice imaging, encompassing the "methods used to reconstruct the internal structure of a solid object from external measurements" (Epstein, 2007: 53). Tomography can also be defined as "the class of devices and procedures used to produce 2-dimensional cross-sections of a 3-dimensional object" which can be used to produce 3D images (Leahy & Clackdoyle, 2005: 1155). The mathematical basis of tomography, the Radon Transform, was published in 1917 by Austrian mathematician, Johann Radon. For an image represented by the function, f(x,y), the Radon Transform is a series of line integrals through f(x,y) at different angles from the source. The reconstruction of the image is obtained using the inverse Radon transform (for more detail on vector calculus and the mathematical principles of tomography, see Toft, 1996 and Epstein, 2007).

In two papers published nearly fifty years after the Radon Transform, Allan Cormack demonstrated how to represent a function (i.e., an image) by its line integral (Cormack, 1963; 1964). These mathematical principles were incorporated in the first CT scanner, that was invented by Godfrey Hounsfield in 1972. Both Cormack and Hounsfield received the Nobel Prize in Physiology and Medicine for their work in 1979 (Beckett & Conlogue, 2020).

Computed tomography (CT) is an imaging modality by which x-ray photons pass through an object from an x-ray source that rotates around the object and projects a 2-dimmensional image (known as a projection image) of that object onto a planar image receptor (Beckett & Conlogue, 2020; Leahy & Clackdoyle, 2005). The image receptor is

a photon detector that converts the energy of the photons into digital information that is then transmitted to a computer, where it is reconstructed into a 3D volumetric reconstruction of the object (Beckett & Conlogue, 2020). This conferred a major advantage over traditional plain film radiography, which represented a 3-dimensional object on a 2-dimensional plane. This makes it difficult to determine the depth of certain features in the scan and creates problems with superimposition of features in the volume.

The first generation of CT scanners used parallel beam x-rays. This required the coordinated rotation and translation of the x-ray source and a single detector and took a considerable amount of time. The early CT aperture was limited to scans of the head; full body scans were made possible with the development of more effective computing power. Initially, the data acquired from the CT detector had to be stored on magnetic tape and sent to remote computing facilities for image reconstruction. With the advent of minicomputers, scans could be processed locally, thus increasing patient throughput (Hughes, 2011). With the use of the fan beam x-ray source and an array of multiple detectors, the entire object can be exposed to x-rays simultaneously and images can be reconstructed much faster. Many modern clinical CT scanners use fan-beam x-ray sources. Some scanners, including most bench-top and industrial scanners use a non-collimated, cone-shaped beam (Beckett & Conlogue, 2020). A collimator is a mechanism of the scanner that allows the user to shape the x-ray beam, often with the goal of limiting x-ray exposure to a patient (Leahy & Clackdoyle, 2005).

The kilovoltage (kV) of a CT scan refers to the electrical potential applied to an electron as it accelerates through the x-ray tube (Frey, 2014). Another important parameter is the number of x-rays required to obtain an acceptable CT image. This is expressed in milliamperes (mA), the rate at which electrons flow through the x-ray tube. This is generally expressed as mAs, which is combined with time (Frey, 2014).

One of the core principles of x-ray CT visualization is the process of differential attenuation (Beckett & Conlogue, 2020). Attenuation is the reduction of the intensity of an x-ray beam as it passes through matter (McKetty, 1989). The number of photons received by the detector reflects the attenuation that the beam experiences is it passes through the object. The measure of the amount of radiation attenuated by a particular

thickness of an absorbing material is known as the attenuation coefficient, often expressed as μ (McKetty, 1998). Attenuation depends on the penetrating properties of the beam, including the energy of the beam and the number of photons that penetrate the object, as well as the thickness of the object (McKetty, 1998). The most commonly used reconstruction method in CT is known as filtered back-projection which uses the radon transform to generate the image from the attenuation measurements (Leahy & Clackdoyle, 2005).

2.5.2 Paleoradiology

Radiographic imaging methods have been widely applied to the study of archaeological materials; a field known as paleoradiology (Chhem & Brothwell, 2008). Developments in radiographic methods have long been associated with bioarchaeological research. In fact, paleoradiology predates the establishment of radiography as a formalized medical imaging technique. X-rays were discovered in 1895 by Wilhelm Conrad. Less than six months later, German physicist Carl George Walter Koenig conducted the first x-ray examination of mummified remains, imaging a child and a cat from ancient Egypt (Böni et al., 2004; Chhem & Brothwell, 2008 citing Koenig, 1896). The child mummy was re-examined using dual-source CT in 2016 (Zesch et al., 2016). The first radiograph of a Peruvian mummy was taken by Lester Leonard and Stewart Culin in 1897, although the images were never published (Chhem & Brothwell, 2008). The mummy's wrappings were incredibly fragile, making traditional unwrapping and dissection methods impossible without completely destroying the mummy. This illustrated the value of non-destructive examination using x-rays early in the development of this field.

Most of the early studies in paleoradiology sought to examine the internal contents of mummies and expose fake mummies; soon after, physical anthropologists began collecting more sophisticated data to estimate the age and sex of the skeletons and assess skeletal pathology (Beckett & Conlogue, 2009). Chhem and Rühli (2004) outline, what they called at the time, the three major domains of modern paleoradiological research on human skeletons: (1) the use of radiological methods to obtain

osteobiographical information on skeletal remains (e.g., Decker, 2011); (2) the use of CT to examine hominin skulls that are embedded in stone matrices (e.g., Tobias, 2001; Wind, 1984); and (3) the use of radiological examination for the diagnosis of pathological lesions (e.g., Allam et al., 2009; Cramer, 2018; Wade et al., 2011).

Since Chhem and Rühli's (2004) review, a multitude of other approaches have been adopted in paleoradiology. Arguably the most common application of CT in archaeology has been in mummy studies because it is non-invasive and non-destructive. The parallel development of CT and mummy studies follows a similar trajectory as that of the first x-ray images (described above). Lewin and Harwood-Nash (1979) conducted the first CT examination of mummified tissue in 1977 in Toronto, just five years after the invention of the CT scanner (Cosmacini & Piacentini, 2008; Harwood-Nash, 1979). Over the following 40 years, CT has become an integral method in studying mummies from around the world, including Egypt (Allam et al., 2009; Notman, 1986; Thompson et al., 2013; Wade & Nelson, 2013), Peru (Ceruti, 2015; Sutherland, 2019; Wilson et al., 2013), Europe (Colleter et al., 2018; Panzer et al., 2018), and Asia (Kim et al., 2018; Slepchenko et al., 2019). Hughes (2011) notes that one of the key differences in CT scanning mummies versus live patients is that the x-rays are more easily passed through the desiccated tissues of the mummies, resulting in a higher signal-to-noise ratio. Additionally, there are no movement artifacts when scanning mummies (Hughes, 2011).

More recent studies have employed CT in modern archaeological and bioarchaeological research applications, such as the analysis of the internal structure of pottery to compare the modes of production of different ceramic styles, previously unattainable using traditional non-destructive methods (Gomart et al., 2017; Kozatsas et al., 2018; Wauters, 2016). Similarly, Ellis et al. (2017) virtually deconstructed wooden medieval prayer beads using micro-CT to study their method of construction. Additionally, CT has been used to reconstruct mobility patterns in the past by comparing tibial rigidity among Neandertals, Levantine and Upper Palaeolithic *Homo sapiens*, Holocene foragers, and modern varsity swimmers and cross-country runners (Shaw & Stock, 2013). Several studies have also assessed the accuracy of 3D models and their viability in osteological and forensic applications (Colman et al., 2019; Robedizo, 2016).

These studies find that while assessing 3D models is comparable to observing dry bone, standardization remains an issue due to software limitations.

2.5.3 Image segmentation

Image segmentation is the process of separating a digital image into multiple segments, or sets of voxels, that share certain characteristics. Segmentation makes an image more meaningful for specialized analysis and has been applied in various anthropological contexts (Cossu et al. 2004; Friedman et al. 2012; Hati et al., 2020). Cossu and colleagues (2004) present a color image segmentation method with the goal of assisting diagnoses of the state of decay of ancient monuments. Their method segments images according to color and color intensity to create an accurate alternative to the traditional ‘naked eye’ assessment method. It incorporates a histogram threshold and edge detection methods, allowing for automatic segmentation. This article demonstrates the broad applicability of image segmentation techniques.

By segmenting CT volumes of mummies, we can differentiate materials in mummy bundles according to their densities, such as embalming compounds, bones, soft tissues, and burial offerings. For instance, Friedman and colleagues (2012) compare manual, automated threshold-only, and semi-automated dual-energy and threshold-based segmentation strategies for separating bone from tissues, resin, and wrappings of an Egyptian mummy.

A significant pitfall of the traditional manual image segmentation process is how time-consuming it is. For this reason, the recently developed automated segmentation techniques in ORS Dragonfly were considered for segmentation of the fardos examined in this thesis. This required a thorough review of the history of artificial intelligence as well as a summary of the associated concepts and how they function with respect to automated image segmentation and my specific research goals.

2.6 Artificial intelligence, bioarchaeological applications, and deep learning

In his seminal (1950) paper, Alan Turing outlined a theoretical demonstration of how a machine may be able to learn. He argued that because humans use experience and reason to make decisions and solve problems, machines should be able to do the same. The use of micro-CT was not thoroughly investigated until the clinical utility of examining bone was made evident (Feldkamp, 1989; Beckett & Conlogue, 2020). Similarly, the early research on artificial intelligence lacked the proof of concept until breakthroughs in computing technology, particularly memory capacity and the ability to store commands, made computers more accessible (Gugerty, 2006).

The first proof of concept of artificial intelligence was developed in 1957 by Allen Newell, Herbert Simon, and Cliff Shaw who wrote a program designed to mimic human problem solving, called The Logic Theorist (Gugerty, 2006). This program was presented at the Dartmouth Summer Research Project on Artificial Intelligence (DSRPAI) held by John McCarthy in 1956. McCarthy is credited with coining the term "artificial intelligence" in the same year. Many of Newell and Simon's novel ideas about mental representation and problem-solving are still used in modern cognitive psychological research (Gugerty, 2006).

Machine learning is primarily concerned with the development of computer algorithms that can improve automatically. These algorithms use experience and data to develop models by quantifying the relationships between multiple variables and using those relationships to make predictions based on new data (Wernick et al., 2010). This process compiles statistical methods of automated decision-making and predictive modeling, such as regression pattern recognition, and system identification. These are methods that have been used for decades (sometimes centuries) before being applied to automated scenarios involving machine learning. There are three primary categories of machine learning: supervised learning, unsupervised learning, and reinforcement learning (Simeone, 2018). In supervised learning, the machine is given an example and a set of labels or targets associated with that example. The labels help the system sort and

categorize the features. In other words, both inputs and outputs of the examples can be perceived by the machine (Russell & Norvig, 1995). In unsupervised learning, the machine does not have the associated labels or targets and must determine patterns in the data. Reinforcement learning involves goal-oriented algorithms that rely on reward feedback to develop or train a desired behavior. Reinforcement learning is often used for processes that optimize over a series of steps in order to attain a complex goal.

2.6.1 AI in bioarchaeology

The bioarchaeological applications of machine learning are relatively recent; researchers in these early studies have been primarily concerned with assessing methods for automatic estimation of basic osteobiographical information. One of the earliest applications was conducted by Bell and Jantz (2002) who designed an artificial neural network for the classification of both archaeological and modern skeletal remains (according to race, sex, time frame, date of birth, and phase) using osteometric data. Their model was able to accurately categorize the modern skeletal remains, but it was unable to classify the archaeological remains better than chance. This study offered some promising results, but the inability to classify archaeological remains suggests that neural network models require highly accurate archaeological training data, which is not always guaranteed. The training data, and therefore the performance of the model, is only as accurate as our understanding of the archaeological context. In a more recent study, Czibula et al. (2016) tested a deep learning-based approach for estimating anatomical stature. The authors employed artificial neural networks and genetic algorithms (algorithms based on the interactions of genetic processes) to predict the statures of skeletons from the Terry Collection. Several studies have tested systems for the estimation of age-at-death using artificial intelligence as well (Ionescu et al., 2016; Navega et al., 2015; Navega et al., 2018). These studies all found the machine-learning-based systems to be more robust and effective than traditional estimation methods.

Overall, machine learning has made minor contributions in anthropology thus far, most likely because of the considerable amount of time and expertise that is required to develop and train models. Furthermore, the structure of more nuanced architectures, like

deep learning, is highly specific to its intended purpose, limiting broad-scale applicability across research projects.

2.6.2 Deep learning

Deep learning is a specialized type of machine learning by which models are designed based on artificial neural networks. Artificial neural networks are statistical and mathematical models inspired by the biological organization of neurons in the brain (Choy et al., 2018). They are structured with one input layer of neurons, one or more hidden layers, and an output layer. Each hidden layer is made up of neurons that are connected to each of the neurons in the previous layer. The strength of these connections between neurons is assigned its own weight and varies between layers. The goal of the algorithm is to detect patterns in the input data using these weights. The values of the weights are estimated during training (see section 3.4.2 for further details on the training process). If the weights are given suitable values, the network will yield the desired outputs (i.e., correctly detecting features in an image or successfully segmenting densities out of a CT scan) (Choy et al., 2018).

Convolutional neural networks (CNN) are a category of deep learning models in which the hidden layers filter, or convolve, the inputs to extract useful information. A convolution is a mathematical operation that filters the input and produces an activation. Repeated applications of this filter to the input produces a feature map, which is a collection of activations and indicates the locations of a detected feature in the input. Because CNNs take 2- or 3-dimensional shaped inputs and due to the configuration of information in CTs as pixels or voxels, convolutional neural networks have been widely adopted in medical imaging (Choy et al., 2018).

ORS Dragonfly's deep learning engine enables users to apply convolutional neural networks in the software itself. The developers of Dragonfly recently incorporated an automated segmentation tool, Segmentation Wizard, that differentiates materials using textural information in the images (Makovetsky et al., 2018; Piche et al., 2016). Segmentation Wizard provides a framework to develop classifiers. Classifiers are essentially the models by which the images are segmented. One or more types of images

are the input, and a segmented image is the output. The ability to incorporate multiple types of images in this tool offers a significant advantage over traditional radiographic assessments and can save a considerable amount of time. This was the method adopted for this thesis. The next chapter will describe the specific methods of the image segmentation and biodistance analysis.

Chapter 3 Materials and Methods

This chapter will provide an overview of the samples from Pachacamac as well as the comparative samples from Maranga, Ancón, San Jose de Moro, and the Chilean coast. I will summarize the steps taken to examine the scans of the fardos, including a description of the image analysis software (ORS Dragonfly) and the use of deep learning tools to develop and train segmentation models. Because artificial cranial modification is a predominant feature of the samples in this thesis, there will be a summary of the methods used to assess the type and severity of modification and a discussion of the effects of modification on the ability to score nonmetric variants. Finally, this chapter will discuss the statistical methods used for reducing the trait list to account for age, sex, and inter-trait correlations as well as the statistics used in the biodistance analysis.

3.1 Materials

In addition to identifying each individual by site, the data were also grouped into three broad geographic regions: Peru Central Coast, Peru North Coast, and Chile. Table 3.1 lists the sites analyzed in this study, their respective geographic regions, and the sample sizes of each site. The sample sizes of the "Peru Central Coast", "Peru North Coast", and "Chile" groupings were 17, 23, and 33, respectively.

Table 3.1 Summary of sites used in analysis, their geographic regions, and sample sizes.

Site	Region	Sample size	Reference
Pachacamac	Peru Central Coast	5	Baldeos, 2015
Ancon	Peru Central Coast	10	Watson, 2016
Maranga	Peru Central Coast	2	Ordoñez et al., 2015
San Jose de Moro	Peru North Coast	23	Nelson, pers. comm.
Araucanian	Chile	4	Ossenberg, 2013
Arica	Chile	3	Bird, 1943
Coquimbo	Chile	8	Bird, 1943
Junin Grave	Chile	2	Bird, 1943
Iquique	Chile	4	Bird, 1943
Punta Pichalo	Chile	12	Bird, 1943

Table 3.2 lists all of the individuals analyzed in this thesis. The CT-scanned fardos that were eliminated from analysis either contained no skull, were too poorly preserved to be adequately segmented and scored or contained only subadult remains.

Table 3.2 Overview of the individuals analyzed in this thesis (including ID numbers, sites, regions, sex, and general comments). Observations for Pachacamac, Ancón, and Maranga were made by the author. Observations for San Jose de Moro were made by Andrew Nelson in 1999 (pers. comm.). No general observations of the Chilean material were included in the dataset provided by Ossenberg (2013).

ID	Site	Region	Sex	Comments
E76E	Pachacamac	Peru Central Coast	Female	Cranium and mandible intact (articulated). Few cranial bones of a second individual present.
E82C	Pachacamac	Peru Central Coast	Male	Cranium and mandible intact. Dense unknown object placed in right orbit, 'taco' artifact, 5-7 oval-shaped objects (Stones), 1 rectangular object.
E82F	Pachacamac	Peru Central Coast	Male	Cranium and mandible intact. Dense unknown object placed in left orbit, 'half-taco' artifact.
E82S	Pachacamac	Peru Central Coast	Male	Cranium and mandible intact.
E84	Pachacamac	Peru Central Coast	Male	Mandible intact. Frontal bone smashed and right parietal cracked.
PE-0087	Ancon	Peru Central Coast	Male	Cranium scanned separately, intact. Mandible present in fardo with rest of postcrania, few teeth in mandible (AMTL).
PE-0088	Ancon	Peru Central Coast	Male	Base of skull, sphenoid, and parietals smashed. Facial and frontal bones still intact and scorable. Mandible intact.
PE-0089	Ancon	Peru Central Coast	Female	Cranium and mandible intact. Left ramus of mandible blocking view of left facial bones.
PE-0091	Ancon	Peru Central Coast	Male	Cranium and mandible intact.
PE-0093	Ancon	Peru Central Coast	Male	Cranium and mandible intact. Mandible impeding view of face. Teeth clustered in left orbit.
PE-0100	Ancon	Peru Central Coast	Female	Cranium and mandible intact. Large artifact, roughly size of cranium, likely a pottery sherd.
PE-0101	Ancon	Peru Central Coast	Female	Cranium and mandible intact. Rest of fardo contains only a single humerus, radius, ulna, scapula, and clavicle.
PE-0102	Ancon	Peru Central Coast	Female	Cranium and mandible intact.
PE-0103	Ancon	Peru Central Coast	Female	Cranium and mandible intact. Ceramic artifacts in fardo: small vase/pot, round cup, and figurine.
PE-0104	Ancon	Peru Central Coast	Male	Cranium and mandible intact. Spondylus shell in fardo.
JC-AE-2288	Maranga	Peru Central Coast	Female	Fully articulated skeleton. Flexed position. Cranium and mandible intact.
JC-AE-2305	Maranga	Peru Central Coast	Male	Cranium and mandible intact, slightly disarticulated.
SJM-301	San Jose de Moro	Peru North Coast	Female	Face fragmentary, cranium reconstructed. Shell bead bracelet around left wrist
SJM-311	San Jose de Moro	Peru North Coast	Male	Observed in situ, fragmentary, cranium reconstructed. Ceramic vessels, llama bones, and copper stained piece of textile.

SJM-313	San Jose de Moro	Peru North Coast	Female	Cranium mostly complete. Occipital bone fragmentary, foramen magnum is present and part of the occipital artic. with the temporals.
SJM-316	San Jose de Moro	Peru North Coast	Female	Skull fragmentary, but reconstructed.
SJM-319	San Jose de Moro	Peru North Coast	Male	Cranium almost complete, reconstructed.
SJM-320	San Jose de Moro	Peru North Coast	Male	Cranium fragmentary, mostly reconstructed. Facials too fragmentary to reconstruct.
SJM-321	San Jose de Moro	Peru North Coast	Female	Cranium partially complete, but heavily eroded. Partial reconstruction.
SJM-405	San Jose de Moro	Peru North Coast	Female	Cranium mostly complete, parietals in small pieces, central portion of occiptal preserved. Ceramics, chalk and stone beads, copper object.
SJM-412	San Jose de Moro	Peru North Coast	Female	Good preservation, cranium complete. Ochre flakes under face
SJM-413	San Jose de Moro	Peru North Coast	Male	Cranium fragmentary.
SJM-414	San Jose de Moro	Peru North Coast	Male	Fair preservation, cranium fragmentary. Anterior portion of left parietal, orbit, occipital absent.
SJM-415 1	San Jose de Moro	Peru North Coast	Male	Skull only, no postcrania. Good preservation.
SJM-415 2	San Jose de Moro	Peru North Coast	Male	Cranium only, no mandible, no postcrania. Good preservation.
SJM-415 3	San Jose de Moro	Peru North Coast	Male	Cranium only, no mandible, no postcrania. Fair preservation.
SJM-415 4	San Jose de Moro	Peru North Coast	Male	Cranium only, no mandible, no postcrania. Fair preservation.
SJM-415 5	San Jose de Moro	Peru North Coast	Male	Skull only, no postcrania. Good preservation.
SJM-415 6	San Jose de Moro	Peru North Coast	Male	Parts of cranium present. Face and mandible originally together, but two separate individuals.
SJM-418	San Jose de Moro	Peru North Coast	Male	Skull fragmentary, poor preservation.
SJM-501	San Jose de Moro	Peru North Coast	Female	Skull fragmentary, fair preservation.
SJM-502	San Jose de Moro	Peru North Coast	Female	Skull mostly complete, fair preservation, crushed occipital/ basi-cranium.
SJM-503	San Jose de Moro	Peru North Coast	Male	Skull fragmentary, fair preservation.
SJM-509 A	San Jose de Moro	Peru North Coast	Female	Skull fragmentary, reconstruction very approximate. Lots of chalk adhering to bone surfaces.
SJM-512	San Jose de Moro	Peru North Coast	Male	Skull fragmentary, reconstructed.
VL 3299	Araucanian	Chile	Male	
VL 3342	Araucanian	Chile	Male	
VL 3343	Araucanian	Chile	Male	
VL 3344	Araucanian	Chile	Male	
991/717	Arica	Chile	Male	
991/718	Arica	Chile	Male	
VL 258	Arica	Chile	Male	
99/9942	Coquimbo	Chile	Male	
99/9943	Coquimbo	Chile	Male	

99/9944	Coquimbo	Chile	Male	
99/9945	Coquimbo	Chile	Female	
99/9946	Coquimbo	Chile	Male	
99/9947	Coquimbo	Chile	Male	
99/9948	Coquimbo	Chile	Male	
99/9949	Coquimbo	Chile	Male	
991/756	Iquique	Chile	Male	
VL 190	Iquique	Chile	Indeterm.	
VL 199	Iquique	Chile	Male	
VL 277	Iquique	Chile	Female	
991/753	Junin grave 10	Chile	Female	
991/754	Junin grave 15	Chile	Male	
991/720	Punta Pichalo	Chile	Male	
991/729	Punta Pichalo	Chile	Female	
991/731	Punta Pichalo	Chile	Female	
991/732	Punta Pichalo	Chile	Male	
991/735	Punta Pichalo	Chile	Male	
991/736	Punta Pichalo	Chile	Female	
991/739	Punta Pichalo	Chile	Female	
991/740	Punta Pichalo	Chile	Male	
991/741	Punta Pichalo	Chile	Male	
991/742	Punta Pichalo	Chile	Female	
991/745	Punta Pichalo	Chile	Male	
991/749	Punta Pichalo	Chile	Male	

3.1.1 Pachacamac

The sample from Pachacamac was excavated from Sector 3, along the north bank of the sanctuary, between March 4 and May 30, 2015 following the discovery of three funerary contexts found during an archaeological evaluation for the construction of the new Museo Nacional del Perú (Figure 3.1) (Baldeos, 2015). The Archaeological Rescue Project (also known as the MUNA Project), launched to mitigate the effects of the construction, uncovered a pre-Hispanic cemetery containing 138 funerary contexts and 36 cultural features spanning an area of 7,943.36 m^2 (Baldeos, 2015). The site sits on an artificial slope, referred to as *hondonada* by locals (Figure 3.2) produced by modern alterations from the area's use as a quarry for construction material during the 1960s (Baldeos, 2015). The location of the new museum was divided into 4 sectors (100, 200,

Figure 3.1 Overhead view of the boundary of the Pachacamac Sanctuary (yellow) and the region of interest in the 2015 rescue project (red). Photo by Google Earth, labelled by Jhon Baldeos (2015, p. 22).

300, and 400). It is in sector 300 that the pre-Hispanic cemetery was discovered and subsequently excavated to recover any archaeological material.

Sector 300 is divided into three units of excavation (I, II, and III) oriented from the southwest to northeast. Each unit was roughly 23 m long by 30 m wide. Among the three units, the team also identified four major layers, or *capas*, from which materials were recovered; most of the material was recovered from the first layer, roughly 10-15 cm below the surface. The surface of the site was characterized by beige aeolian sands; almost all of the burials in this layer had been disturbed by anthropogenic activity. There are disarticulated human skeletal remains, ceramics, and metal fragments scattered across the surface. Most of the burials were found in layer 1/*capa I*, which was subsequently divided further into four levels. The fardos examined in this study came from level 2 (E-76E, E-82C/F/S, and E-84).

The Rescue Project recovered a total of 72 fardos (Figure 3.3). This cemetery is believed to be associated with the Ychsma culture with some limited influence of the Inca, encompassing the end of the Middle Horizon and Wari influence, the Late Intermediate Period, and the beginning of the Late Horizon most likely between 700 and

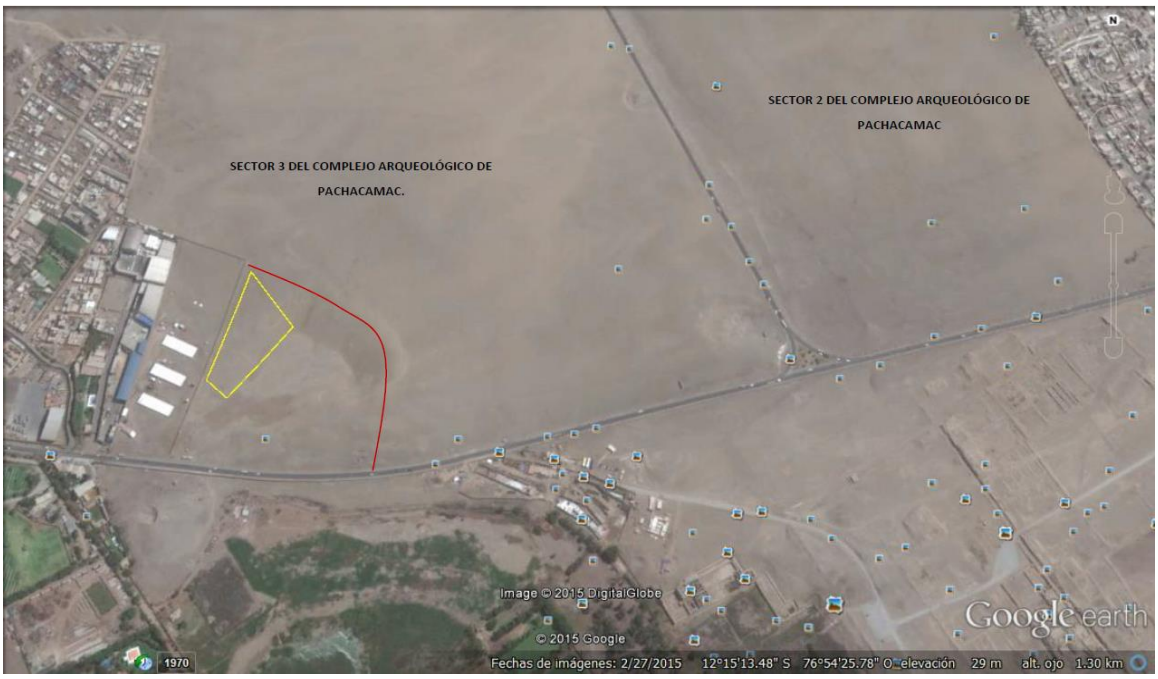

Figure 3.2 Overhead view of the total area excavated in Sector 300 (yellow) and the area of the artificial slope/hondonada (red). Photo by Google Earth, labelled by Jhon Baldeos (2015, p. 23).

1400 A.D. (Baldeos, 2015). This association with the Ychsma culture is evidenced by the fardo preparation and the associated ceramic artifacts (Baldeos, 2015).

Eighteen of the fardos from this sample were CT scanned in July and August 2019 at the Resocentro Clinic in Miraflores, Peru as a part of the collaboration between the Museo Pachacamac and Dr. Nelson's bioarchaeological research project, "Mummies as Microcosms" (Nelson et al., 2021). The goal of the project was to explore the ways in which the fardos from different sites along the Central Coast of Peru at successive time periods are microcosms of the biological and cultural identity of the individuals and of the mortuary program of the society. The researchers addressed this goal by non-destructively studying the evidence of health and disease, the treatment of the body, the structure of the fardo, and the artifacts contained within the bundles. The individuals from Pachacamac-Sector 3 were first visually assessed and x-rayed before being chosen for their state of preservation and ability to be CT scanned. Five of these fardos are used in the biodistance analysis.

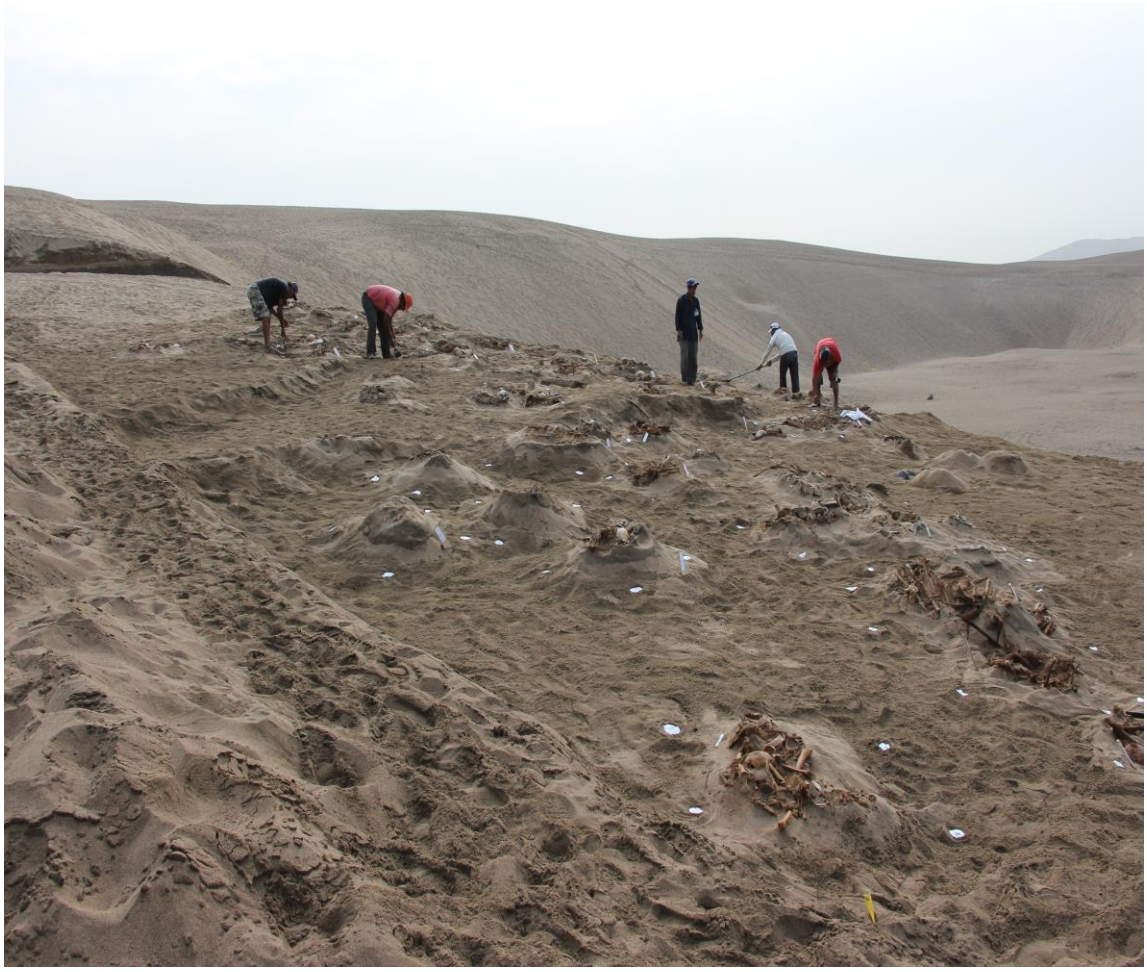

Figure 3.3 View of Area B and disturbed burials close to the surface. Photo by Jhon Baldeos (2015, p. 35).

3.1.2 Maranga

The sample from Maranga was originally excavated in 1925 by the Ecuadorian historian, archaeologist, and politician, Jacinto Jijón y Caamaño, who was the heir to one of the wealthiest families in Quito at the time. Jijón sent 42 fardos back to Quito to be a part of his family's private collection. They are now housed in the Museo Jacinto Jijón y Caamaño which was founded in 1963 on the grounds of the Pontifical Catholic University of Ecuador in Quito (Ordoñez et al., 2015).

The four individuals from this sample were CT scanned as part of a paleoimaging and bioarchaeological investigation of the Peruvian samples from this collection (Ordoñez et al., 2015). Because most of our knowledge of the Maranga culture is based

on the analysis of textiles and ceramics, the primary goal of this project was to non-destructively collect more data on the individuals to complement existing records of the sample. All the bundles were x-rayed in round 1, and four of the mummies from this collection were CT scanned during the second phase of the project in May and June 2013 at the Radiology Center at the AXXIS Hospital in Quito, Ecuador. Two of these mummies were used in the biodistance analysis.

3.1.3 Ancón

The data on the sample from Ancón were generously provided by Dr. Lucia Watson Jiménez (2016, 2019) and were made available for use in this study with the permission of the Horus group. The fardos that were CT scanned were housed at the Museo del Sitio- Ancón in Peru. Twenty-nine individuals from this sample were CT scanned at the Resocentro Clinic in Miraflores, Peru in collaboration with the Horus group for their study of atherosclerosis in ancient populations (Sutherland et al., 2014; Thompson et al., 2013). Ten individuals from this sample were used in the biodistance analysis.

3.1.4 San Jose de Moro

The skulls from the San Jose de Moro sample were catalogued and x-rayed by Drs. Andrew Nelson and Jerry Conlogue from 1995 to 1999; while the x-rays were not accessed in this thesis, the nonmetric trait scores and cranial index measurements taken by Dr. Nelson of 23 individuals (Nelson pers. comm.) were entered to an excel spreadsheet. This sample is believed to be composed of local individuals and was used as an outgroup Peruvian population that was not located on the Central Coast and derived from Mid- and Late Moche and Lambayeque transitional contexts.

3.1.5 Chilean samples

The 33 individuals from Chile are housed at the American Museum of Natural History in New York and the nonmetric trait data were presented in Ossenberg (2013). The sites were labelled as follows: Arica, Araucanian, Coquimbo, Iquique, Junin Grave, and Punta Pichalo. Most of the material from this collection was excavated by Junius

Bird during the 1930s and 40s and the nonmetric traits were scored by Ossenberg sometime between 1963-2003 (Bird, 1943; Ossenberg, 2013). While Ossenberg's (2013) database did not provide any Peruvian samples, the sites in the Chilean sample are coastal and were thus useful for comparison. There is little contextual information on the samples and the dates are not known for these individuals.

3.2 Scanning technique and hardware specifications

The author intended to assist Dr. Nelson in the scanning of additional individuals from Pachacamac during May of 2020. However, the trip was abruptly cancelled in March 2020 in response to the outbreak of the COVID-19 pandemic. Thus, all the CT scans studied in this thesis were conducted prior to the conception of this project. The scans were studied using the image analysis software, Dragonfly (2020.1), developed by Object Research Systems (ORS). The scans were analyzed on the author's Windows desktop computer with 32 GB of RAM and a Nvidia GeForce GTX 1070 graphics card (GPU). Table 3.3 summarizes the scan date, scanner model, and the scan specifications of each of the CT scanned samples observed in this thesis.

Table 3.3 CT scan specifications (including date, model, kVp, pixel spacing, slice thickness, and mA) of the three CT-scanned samples studied in this thesis.

	Pachacamac	**Maranga**	**Ancón**
Scan date	July 21 & August 4, 2019	May 31 & June 1, 2013	April 6, 2013
Scanner	Siemens SOMATOM Definition AS	Philips Brilliance 64-Slice Scanner	Toshiba Aquilion CX 128-Slice CT
kVp	120	120	120
Pixel spacing	0.556\0.556 mm	0.924\0.924 mm	0.881\0.881 mm
Slice thickness	0.75 mm (reconstructed to 0.5 mm)	0.6 mm	0.5 mm
mA	581	430	100

3.3 Cranial modification and cranial index measurement

As previously mentioned, artificial cranial modification was a common practice throughout the prehistory of the Andes (Blom, 2005; Dingwall, 1931). With respect to the expression of nonmetric traits, modification is most frequently associated with an increase in wormian bones along the sutures of the cranial vault (Del Papa & Perez, 2007;

Konigsberg et al., 1993; White, 1996). However, the effects of artificial cranial modification are ultimately considered to be negligible with respect to estimating biodistance via nonmetric traits (Herrera, 2016; Konigsberg et al., 1993).

To assess the extent of modification and characterize the types of modification observed in the sample from Pachacamac, screenshots of each modified skull were taken in Dragonfly, from six anatomical positions (anterior, lateral- left and right, posterior, superior, and inferior). Additionally, measurements of maximum breadth (euryon-euryon) and maximum length (glabella – opisthocranion) were taken on average-intensity projections with a slab thickness of 8 mm (mid sagittal to measure max length and axial to measure breadth). Measurements were taken using the measuring tool in Dragonfly following the standards outlined by Buikstra and Ubelaker (1994), and were used to calculate the cranial index (CI) of each individual. Cranial index ((breadth x 100)/length) quantifies the relationship between the length and breadth of the cranium (Buisktra & Ubelaker, 1994). Non-pathological, non-modified skulls of individuals from the Peruvian coast typically have cranial indices in the mid- to high 80s. Fronto-occipitally modified crania will have a higher CI and annular modified crania will have a lower CI (Mackey & Nelson, 2020, p. 29).

3.4 Deep learning and image segmentation methodology

Traditional image segmentation of CT scans takes a considerable amount of time, especially when analyzing fardos that contain fragmentary remains and other associated artifacts, such as cotton seeds, *spondylus* shells, and ceramics. In 2017, the developers of Dragonfly incorporated artificial-intelligence-guided image segmentation features in their software (Piche et al., 2017). One of the primary goals of this thesis is to determine the applicability of these automated segmentation features in Dragonfly in segmenting the fardos. Before conducting experimentation with automated segmentation, I tested whether the nonmetric variants were indeed visible on clinical CT scans of dry bone. Five dry skulls from Western University's Oddfellows collection were scanned on February 17, 2020 at the Diagnostic Imaging Centre at St. Joseph's Healthcare in London, Ontario on a Canon Aquilion ONE Genesis CT scanner at 120 kVp, and 400 mAs. Comparison of

the original skulls with the 3D models of the skulls suggested that the nonmetric variants were sufficiently visible in the scans (see Figure 3.4).

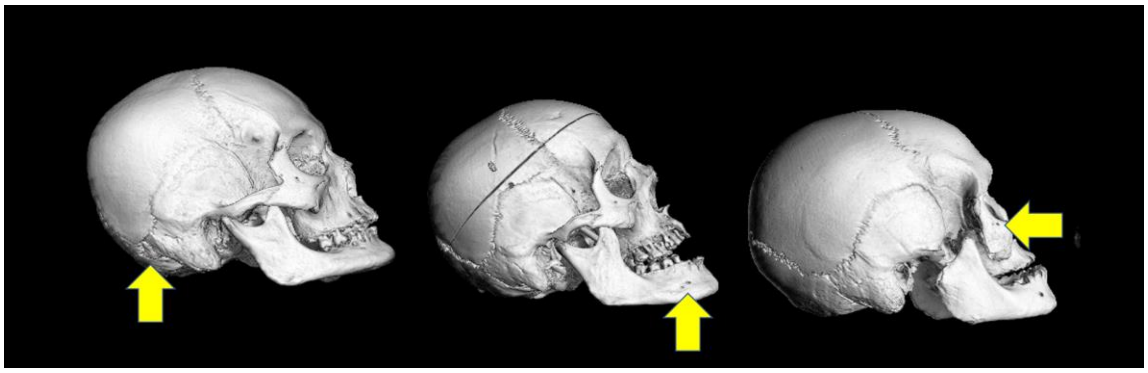

Figure 3.4 CT scans of three of the skulls from the Oddfellow's collection illustrating visible nonmetric variants (From left to right: Extrasutural bone at the asterion, mental foramen double, and accessory infraorbital foramen). Image by Andrew Nelson.

3.4.1 Automated image segmentation tools in Dragonfly

All image analysis in this study, including deep learning experimentation, image segmentation, and scoring the nonmetric traits, was conducted in Dragonfly 2020.0 or 2020.1. In May 2020, I attended virtual tutorials hosted by Mike Marsh, the director of product management at ORS, to learn how to develop and train models using in Dragonfly (https://www.youtube.com/playlist?list=PLbYyniU4wPOtHGT0m68liH5SntwfETKsP) (Object Research Systems, 2020).

Dragonfly's initial generalized machine learning segmentation platform, Segmentation Trainer, automates the image segmentation process by differentiating materials using textural information in the images to automate the image segmentation process (Piche et al., 2017). Segmentation Trainer allows users to develop, train, and implement classifiers for image segmentation procedures. *Classifiers* are the models with which the images are segmented. Piche and colleagues (2017) describe classifiers in this context as a "black box" that can take an input image and produce a segmentation as an output (p. 132). This version of Segmentation Trainer was limited to only machine learning models. Upon subsequent updates, ORS implemented a deep learning engine and enables users to apply convolutional neural networks (CNNs) in the software itself (Makovetsky et al., 2018). As of the Dragonfly 2020.0 update in May 2020,

Segmentation Trainer is now called *Segmentation Wizard*, and will be referred to as *Segmentation Wizard* throughout the rest of this thesis.

The automated segmentation of the fardos required experimentation with the different tools provided in the software. Table 3.4 lists the models tested during this phase. While Dragonfly offers several other architectures, these models were chosen following the recommendations made in the virtual Dragonfly Daily webinar series (Object Research Systems, 2020). As of June 2021, there are three tools in Dragonfly that enable the creation of artificial intelligence (AI) models: Machine Learning Segmentation, Deep Learning Tool, and Segmentation Wizard. Preliminary experimentation with all three tools was conducted to determine the most effective workflow for automated segmentation of the fardos. While advanced users can draft new models and edit features such as the specific nodes of the networks, novice users can simply segment reference slices and use them to train pre-existing models. The latter approach was taken in this study. Because the trained neural networks act like image filters, they are relatively easy to preview, apply to a full image stack, and reuse on further datasets.

Table 3.4 AI models tested for segmentation in Dragonfly.

Model type	Architecture	Reference
Machine learning	Random forest	Breiman, 2001
Deep learning	Autoencoder	Bengio et al., 2006
Deep learning	Sensor 3D	Novikov et al., 2019
Deep learning	U-Net	Ronneberger et al., 2015

The Machine Learning Segmentation tool functions similarly to the Deep Learning tool but incorporates only machine learning models. Due to the effectiveness of deep learning versus machine learning models following the initial experimentation in Dragonfly, the Deep Learning Tool and Segmentation Wizard were chosen as the primary segmentation methods in this study. As previously mentioned, Segmentation Wizard is the updated version of Segmentation Trainer. This platform applies the same capabilities as the deep learning and machine learning segmentation tools but guides the user through a workflow that expedites the process of segmenting reference slices and

enables the training of multiple models, including both deep learning and machine learning models.

In August 2020, Dr. Natalie Reznikov provided a more in-depth tutorial for achieving accurate models and segmentations. Reznikov's method, which I have entitled the "manual abridged stack method", employs the same overall approach as Segmentation Trainer as outlined by Piche et al., (2017), but involves the manual selection and painting of an abridged stack of slices without any guided workflow by the software. First, the entire volume was cropped to encompass only the cranium and mandible. The abridged stack was made up of individual slices taken from the volume at 50-slice intervals to represent the span of 2D images in the 3D volume. The first and last images in the stack were included to encompass the limits of the object of interest (the skull) within the fardo (see Figure 3.5 for a representation of the distribution of training slices across the skull). The abridged stack was then edited using the image processing

Figure 3.5 Visual representation of the distribution of 2D training slices (labelled in orange) throughout the entire clipped skull volume (E82S). Image by Cameron Beason.

panel in Dragonfly to enhance the edge detection and contrast of the image; this enables a more accurate input, or ground truth, from which the model learns and produces the output. This method was used to segment scans on which previously trained models did not adequately segment the image.

3.4.2 Training parameters and terminology

Training is a heuristic process and selecting appropriate parameters and models can be quite challenging. *Ground truth* refers to the data that is assumed to be true or, in other words, the input from which the model learns (Choy et al., 2018). Training data is split into 2-dimmensional data *patches* that are randomly processed as *batches*. The batch size parameter reflects the number of patches in a single batch and a *step* is completed when the model passes over a single batch during training. An *epoch* is a single pass over all the data patches. The *loss function* is optimized during training and represents the difference between the model's output and the desired output or target (Object Research Systems, 2021). However, training was set to stop automatically once the value of the loss function failed to decrease for ten consecutive epochs, following the recommendations given in the Dragonfly webinars. (Figure 3.6). The *Sørensen-Dice Coefficient* measures the amount of overlap between the output of an automated segmentation and the target output specified by the user and can be used to determine the accuracy of a model (Dice, 1945; Sørensen, 1948). *Data augmentation* was also used in this study and involves the reorienting of the input (such as rotating the image or flipping it horizontally or vertically) to produce more training data for the model. *Validation* sets aside a specified percentage of the training data (20% in this study) to validate the models' progress in each epoch.

These training parameters are heavily dependent on the hardware specifications of the computer, particularly the system's memory (RAM) and graphic card (GPU). Dragonfly's artificial intelligence features are limited to CUDA-enabled NVIDIA graphics cards. CUDA is a programming model developed by NVIDIA that enables the use of graphics cards for generalized computing processes, such as decryption in cryptocurrency mining or, in this study, the training of machine learning and deep learning models (Ebersole, 2012).

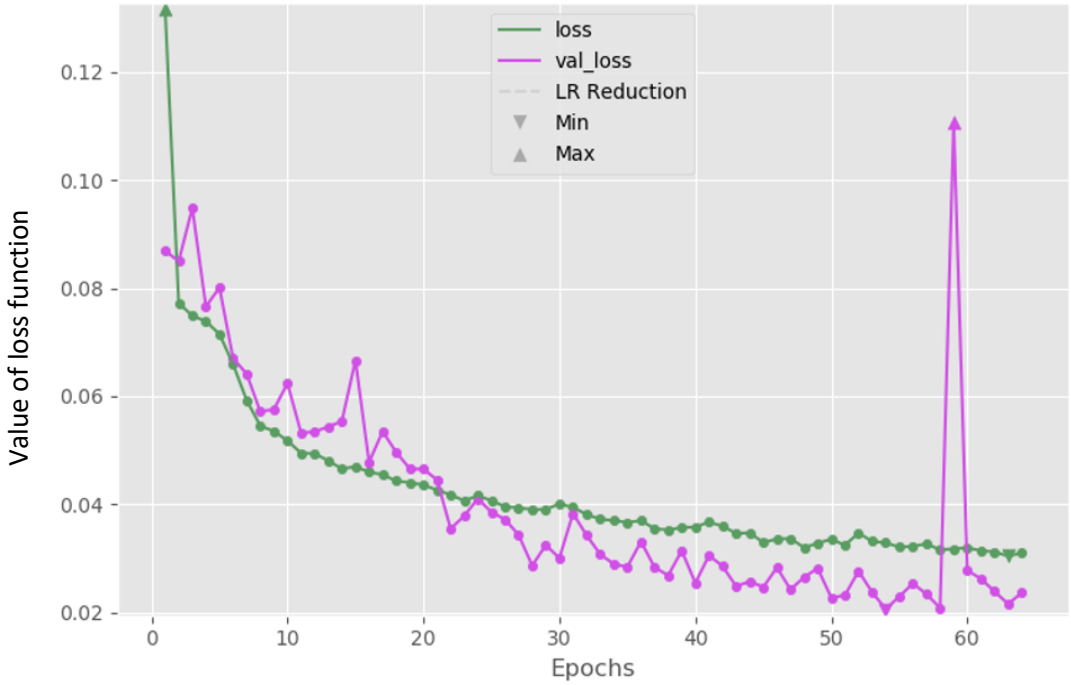

Figure 3.6 Loss function of the training data ('loss', green) and the loss function of the validation data ('val_loss', pink) during training of a U-Net architecture and using fardo E82S as the input. Each point represents the resultant values after each training epoch.

An image segment is formatted as a region of interest (ROI) on the CT scan. ROIs are associated with a specific geometry (the volume or image that is being segmented) and the process of image segmentation involves the assigning of each pixel of that geometry to a specific category, known as a class. This is done using painting tools in Dragonfly and can be conducted on both the 2-dimensional and 3-dimensional views. All the segmentations conducted in this analysis were binary segmentations, or 2-class segmentations. Each pixel of the input image was either considered "Skull" or "ETC." to separate the skulls from the additional contents of the fardos and to minimize the complexity of the segmentation.

3.4.3 Dragonfly semi-automated segmentation procedure

The first step of this process was to import the DICOM image stack into Dragonfly, crop the volume to encompass only the skull, and apply pre-existing U-Net models to gauge their ability to adequately segment the skull from the remaining features of the fardo (including post cranial remains, wrappings, cotton seeds, and various

artifacts). If a new model was needed (i.e., the output did not adequately separate the skull from the fardo contents), Segmentation Wizard was used to develop a new model capable of addressing the specific context of a particular fardo. Training frames were labelled and segmented manually using painting tools in the software and served as the ground truth for the models to use as training. Once the reference frames were manually painted and sufficiently labelled, both new and pre-existing model architectures were loaded into Segmentation Wizard, and the system ran through the training epochs of each model in succession.

Because the samples from Pachacamac, Maranga, and Ancón were scanned on different scanners with different settings (see section 3.2), each scan's intensity profile (window leveling) varies. As a result, a U-Net model used to segment an individual from one site/scanner cannot be used to segment an individual from another site/scanner. Each model was trained on a well-preserved individual who would be representative of the skulls being segmented out of the fardos.

On average, an epoch took about 1 minute to complete depending on the number of slices in the training input image. An entire training session ranged from 90 to 120 minutes to make a new model, produce training data, and run the deep learning training. A single training session in Dragonfly can run a maximum of 100 epochs. The number of epochs varied for each model according to the specifications of the input (total number of slices) and output (quality and amount of training data). Training never reached 100 epochs in a single session in this study, often stopping early after about 70-80 epochs for a new and untrained model. When re-training a model, the early stopping occurred in fewer epochs, sometimes as few as 15 epochs.

In some instances, the resulting models struggled to obtain adequate segmentations; in these cases, the "manual abridged stack method" was used to apply image processing, such as enhanced edge detection, to input image stack. None of the models trained in this study were able to segment the entire skull within a fardo with complete accuracy; this is likely due to the variability in preservation and the presence of artifacts within the bundles. The 'success' of a model was determined using qualitative visual assessment as well the calculation of the Sørensen-Dice Coefficient in Dragonfly

using the Deep Learning Model Evaluation Tool. Models that segmented the majority of the skull from the remaining volume while limiting the number of false positives were considered successful and used on subsequent fardo segmentations. False positives occur when pixels are assigned to the wrong class (“skull” or “ETC.”) (Figure 3.7).

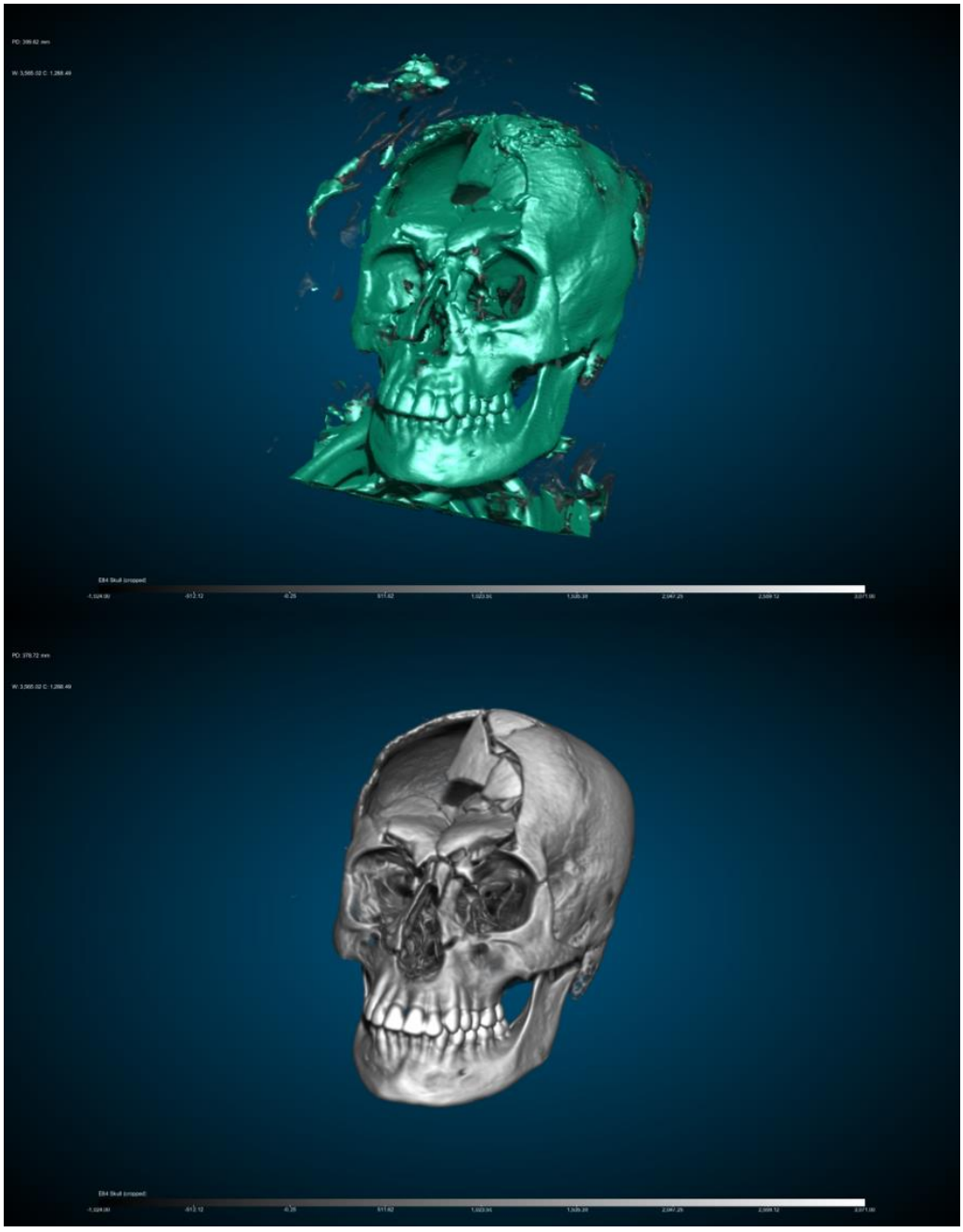

Figure 3.7 Segmentation output of fardo E84 produced by a custom U-Net model (above) and the manually corrected segmentation with coloring removed (below). Image by Cameron Beason.

Finally, once the most successful models were applied to the image, either created in Segmentation Wizard or via the "manual abridged stack method", the segmentations were manually corrected for each individual using the ROI painting tools to enhance the visibility of the nonmetric traits. Most of the fardos from Pachacamac contain thousands of cotton seeds scattered throughout; given their similar density to bone, this presented an unforeseen challenge in the segmentation process as the models frequently included the cotton seeds in the "Skull" ROI. This manual correction was also required for regions of the skull with lower density and/or higher complexity, such as the structures of the sphenoid. Figure 3.7 shows the difference between the segmentation produced by a deep learning model and the subsequent manually-corrected segmentation.

3.5 Nonmetric trait selection

A total of 31 cranial traits and three mandibular traits were analyzed following the procedures outlined by Hauser & De Stefano (1989) and Buikstra & Ubelaker (1994) for the Pachacamac, Maranga, and Ancón samples (Appendix D). The trait list used on the San Jose de Moro sample mostly overlapped with these 34 traits while 17 of the traits used by Ossenberg (2013) overlapped with this list (Table 3.5). These traits make up the full trait list that was used for subsequent data screening (trait list reduction) and biodistance analysis (see Tables 3.5 and 4.2).

It is important to capture the full range of expression observed in each sample. For this reason, the "individual count method" was used for the final scoring of bilateral traits, in which the greatest level of expression of the trait (presence or number of foramina) is noted regardless if the trait is absent or unobservable on the other side (Hauser & De Stefano, 1989). This method assumes that the same genes and/or environmental interactions are responsible for the expression of a nonmetric variant, regardless of side (Sutter & Mertz, 2004; Scott & Turner, 1977). The individual count method is also useful for maximizing sample sizes in relatively small or fragmentary samples. During initial scoring, the side of occurrence of a trait was recorded; the individual count method was applied when recording the frequencies of the traits and when combining the nonmetric trait data from San Jose de Moro and Chile.

Table 3.5 Full nonmetric trait list used in the biodistance analysis with coding, coding used by Ossenberg (2013), criteria for scoring as present, and references with image page numbers from Buikstra & Ubeleker (1994) and Hauser & DeStefano (1989).

Trait name	Coding	Ossenberg Coding	Bilateral?	Present	Source	
Metopic Suture	MSR	METO	N	Complete	Hauser & De Stefano, 1989, p. 41	p. 45, Plate VI
Supraorbital Foramen	SOF L/R	SOF L/R*	Y	Present	Hauser & De Stefano, 1989, p. 50	p. 52, Plate VII
Supraorbital Notch	SON L/R	SOF L/R*	Y	Present	Hauser & De Stefano, 1989, p. 50	p. 52, Plate VII
Tympanic Dehiscence/Foramen of Huschke	FOH L/R	TYM L/R	Y	Present	Hauser & De Stefano, 1989, p. 143	p. 145, Plate XXII
Condylar Canal	CCP L/R	ICC L/R	Y	Open	Hauser & De Stefano, 1989, p. 114	p. 105, Plate XVII
Divided Hypoglossal Canal	DHC L/R	HYP L/R	Y	Complete Division	Hauser & De Stefano, 1989, p. 120	p. 123, Plate XXI
Foramen Ovale Incomplete	FOI L/R	FSP L/R**	Y	Open	Hauser & De Stefano, 1989, p. 149	p. 150, Plate XXIII
Foramen Spinosum Incomplete	FSO L/R	FSP L/R**	Y	Open	Hauser & De Stefano, 1989, p. 149	p. 150, Plate XXIII
Occipito-mastoid Bone	OMB L/R	OMB L/R	Y	Present	Buikstra & Ubelaker, 1994, p. 88	p. 88, Figure 59
Apical Bone	ABP	APIC	N	Present	Buikstra & Ubelaker, 1994, p. 88	p. 88, Figure 59
Asterionic Bone	OAA L/R	AST L/R	Y	Present	Buikstra & Ubelaker, 1994, p. 88	p. 88, Figure 59
Parietal Notch Bone	PNB L/R	PNB L/R	Y	Present	Hauser & De Stefano, 1989, p. 207	p. 200, Plate XXIX
Os Japonicum	OJP L/R	JAP L/R	Y	Present	Hauser & De Stefano, 1989, p. 222	p. 211, Plate XXXI
Inca Bone	IBP	INCA	N	Present	Hauser & De Stefano, 1989, p. 99	p. 100, Plate XVI
Precondylar Tubercle	PCT	PCTB	N	Present	Hauser & De Stefano, 1989, p. 134	p. 119, Plate XX
Infraorbital Suture	IOS L/R	CON L/R	Y	Present	Hauser & De Stefano, 1989, p. 67	p. 71, Plate X
Mylo-hyoid Bridge	MHB L/R	MHB L/R	Y	Present	Hauser & De Stefano, 1989, p. 234	p. 231, Plate XXXIII
Torus Mandibularis	TMP L/R	TMP	Y	Present	Hauser & De Stefano, 1989, p. 182	p. 181, Plate XXVII
Multiple Mental Foramen	MMF L/R	MEN L/R	Y	>1 Present	Hauser & De Stefano, 1989, p. 230	p. 231, Plate XXXIII

*Ossenberg scored the supraorbital foramen and notch as one trait but distinguished between the two forms when scoring. An individual was scored '1' if two or more foramina were present and a '2' if a notch was present. The scores were separated for comparability with the scoring in this thesis.

**Ossenberg scored all variants of the foramen spinosum and ovale as one trait with no further distinction. Therefore, the separate frequencies of open foramen spinosum and ovale were pooled into one trait for the Pachacamac, Maranga, Ancón, and San Jose de Moro samples for comparability with the Ossenberg dataset.

3.5.1 Age and sex

The effects of age and sex on trait expression are frequently disagreed upon in the literature. Hauser and DeStefano (1989) suggest that age and sex have inconsistent effects on the frequency of nonmetric trait expression. For comparability with other biodistance analyses using nonmetrics, the effects of age and sex were considered for the trait list reduction analysis. There is consensus that most of the age effects are associated with subadults and can therefore be eliminated by removing subadults from analysis. Buisktra (1972) and Ossenberg (1969) note that adult material is more stable with respect to age associations.

Some scholars note significant age associations (e.g., Corruccini, 1974; Ossenberg, 1976) while others note little or no association (cf. Berry, 1975; Brasili et al., 1999). Some scholars also note that age correlations vary significantly among samples (Corruccini, 1974; Hauser & DeStefano, 1989; Sjøvold, 1984). Although these disagreements in the appropriate protocol make it difficult to take a precise stance on this subject, age was assessed on all of the scanned fardos (Pachacamac, Maranga, Ancón) using third molar eruption and epiphyseal fusion only to eliminate juvenile skulls from the analysis, in accordance with the guidelines of Buikstra and Ubelaker (1994) for dry bone. This limited the sample size dramatically, especially in the Pachacamac sample, but the removal of subadults is consistent with other studies and allows for greater comparability (e.g., Jahnke, 2009; Sutter & Mertz, 2004; Verano, 1987).

There is also disagreement in the literature regarding the existence of sex-based correlations in trait expression. Berry and Berry (1967) argue that the effects of sex dependent traits are negligible. However, more recent scholars note significant sex correlations in multiple traits (Brasili et al., 1999; Buikstra 1972; Corruccini, 1974). There is consensus regarding the need to identify and control for sex correlations, but the methods by which this is done are not agreed upon. Some scholars suggest that analyzing males and females separately and equalizing demographic distributions is the best approach (Cesnys, 1982; Ossenberg, 1976). This approach is difficult to apply to archaeological samples, however, as it can severely reduce sample size. Alternatively, some scholars recommend pooling all adults from all samples, identifying sex-associated

traits, and eliminating them from analysis (Buisktra, 1972; Jahnke, 2009; Jantz, 1970; Sutter & Mertz, 2004; Verano, 1987). This approach was used in the present study, identifying any sex-correlated traits with a Chi-square test among all adults whose sex could be determined (a single individual from Coquimbo (VL 190) was of indeterminate sex and was excluded from this specific procedure). Sex was estimated by the author on all of the scanned fardos using cranial and pelvic (when visible and intact) morphological characteristics outlined in Buisktra and Ubelaker (1994) for dry bone. Sex estimations were previously recorded for San Jose de Moro and the Chilean samples. Only one individual from Iquique (Chile) was of indeterminate sex and was excluded from the trait list reduction analysis.

3.5.2 Intertrait correlation

Another common source of bias in nonmetric cranial analyses is correlation between traits. A central assumption in biodistance studies is that the traits used for analysis are expressed independently of each other. If trait frequencies are correlated with one another, the values of each trait for the calculation of the MMD will be redundant and may lead to an overestimation or underestimation of distance between groups.

As with biases associated with age and sex, there is disagreement in the literature on both the significance of this correlation as well as the best approach to test for this correlation. Some scholars report little to no significant correlations among traits (e.g., Rothhammer et al., 1984) or low but significant correlations (e.g., Corruccini, 1974). Molto (1980) and Ossenberg (1976) report multiple significant inter-trait correlations. The traits exhibiting correlations vary among these studies, making comparability even more difficult. There are several statistical methods that have been used to test for these correlations, including chi-square (Sutter & Mertz, 2004), Bartlett's test of sphericity (Corrucini, 1974), and the more commonly used *phi* coefficient (Jahnke, 2009; Sjøvold, 1984; Velasco, 2016).

The *phi* coefficient is a modification of the chi-square test that includes the strength of nominal associations between two categorical variables (Thomas, 1976). It is

calculated from a 2x2 contingency table for pairwise comparison of trait frequencies. The formula for finding the phi coefficient is as follows:

$$\Phi = \frac{\mathrm{ab} - \mathrm{bc}}{\sqrt{(\mathrm{a}+\mathrm{b})(\mathrm{a}+\mathrm{c})(\mathrm{b}+\mathrm{d})(\mathrm{c}+\mathrm{d})}}$$

The values *a*, *b*, *c*, and *d* represent the cell frequencies from the contingency table of presence and absence of both traits; *a* represents the frequency of both traits' simultaneous presence, *b* and *c* represent the frequencies of one trait's presence coupled with the other trait's absence, and *d* represents the frequency of both traits' simultaneous absence.

3.6 Statistical analysis

3.6.1 The mean measure of divergence (MMD)

The mean measure of divergence (MMD) converts a battery of trait frequencies into a numerical value that represents the degree of dissimilarity (or divergence) between samples (Harris & Sjøvold, 2004; Irish, 2010). The MMD formula is as follows:

$$MMD = \frac{1}{r}\sum_{i=1}^{r}\left[(\theta_{1i} - \theta_{2i})^2 - (\frac{1}{n_{1i}+0.5} + \frac{1}{n_{2i}+0.5})\right]$$

"where *r* is the number of traits scored, n_{1i} and n_{2i} are the numbers of individuals examined for the *i*th trait in samples one and two respectively, and θ_{1i} and θ_{2i} are the angular transformations of the relative frequencies of the *i*th trait in the two samples, in radians" (Santos, 2018, p. 201; Green et al., 1979).

The statistic was developed in the 1960s by Cedric A.B. Smith, a statistician who developed the measure for use by Grewal (1962) to quantify the biological divergence among mice using nonmetric skeletal traits (Santos, 2018). It was first employed in human divergence studies by Berry and Berry (1967) and quickly became a widely used statistic among biological anthropologists. However, the statistic has come under recent scrutiny, with some calling for its abandonment in biodistance analyses (see Harris, 2008; Konigsberg & Buikstra, 2006).

Over the years, the MMD formula has been modified, often incorrectly, as suggested by Harris and Sjøvold (2004), leading to difficulties in the ability to compare results across multiple studies using variations of the same formula. Irish (2010) argues that MMD has been successfully employed in the past and recommends the methodological advice outlined by Harris and Sjøvold (2004) to accommodate some of the valid criticisms against the measure (such as dichotomization of traits and small sample sizes). One such approach is the application of either Anscombe (1948) or Freeman and Tuckey's (1950) angular transformations to the trait frequencies. Originally applied to the MMD formula by Green and Suchey (1976), these are arc-sine transformations that stabilize the sample variance, which is tied to the frequencies of both presence and absence of a given trait. The Anscombe (1948) transformation is recommended by Harris and Sjøvold (2004) because it is best suited for large sample sizes and can be extended to multistate traits (in which multiple degrees of the expression of the nonmetric traits are recorded). While Harris and Sjøvold (2004) argue that the Anscombe transformation offers a better improvement from the original MMD formula overall, the Freeman and Tuckey transformation is better equipped at handling smaller samples (Freeman & Tuckey, 1950; Irish, 2010). It should also be noted that these two transformations provide similar MMDs (Harris & Sjøvold, 2004; Santos, 2018).

3.6.2 AnthropMMD R package

Once the individuals were fully scored on all traits and groupings were established, the MMDs were calculated using a program in the R Statistical software package, AnthropMMD (Santos, 2018). This package provides a graphical user interface for the calculation of MMD using dichotomous data. The trait frequencies were formatted in a comma-separated values spreadsheet in excel. The data were coded numerically: 0-absent, 1- present, and 9-unobservable. Once the spreadsheet was imported, either the Anscombe (1948) or Freeman and Tuckey (1950) angular transformations of the original MMD formula were selected. Due to the small sample sizes in this study, the Freeman and Tuckey (1950) transformation was used, following Green and Suchey (1976) and Irish (2010). AnthropMMD also enables the user to define a trait reduction strategy. For the sake of transparency and comparability with other studies, no trait reduction strategy

was defined in the package itself and both the full trait list and reduced trait list (using the methods outlined in the previous section) were imported in the package and compared. The R package calculates the significance of the MMDs using a z-test statistic and enables graphical representations of the MMDs with multi-dimensional scaling (MDS) plots and hierarchical clustering analysis to visualize the results.

As previously mentioned, if the Pachacamac sample is comprised of pilgrims, I expect high MMD values when compared with Ancón and Maranga and low MMD values when compared to either the San Jose de Moro or Chilean outgroups. However, it may not cluster closely with any of the comparative samples. For the regional comparison, I expect the Central and North Coasts to cluster more closely with one another than with the Chilean sites on the basis of geographic distribution. The resulting MMDs and visualizations will be discussed in the following chapter.

Chapter 4 Results

This chapter will summarize the results of the CT image analysis and the biodistance analysis. The first section will present the results of the semi-automated image segmentation of the fardos. The second section will summarize the biodistance analysis, including the nonmetric trait list reduction results as well as the trait frequencies of both sample groupings (site and region). Additionally, the analysis using the AnthropMMD R package includes the mean measure of divergence (MMD) and two proximity visualization methods, multidimensional scaling (MDS) plots and hierarchical clustering.

4.1 Deep learning and image segmentation of CT Scans

4.1.1 Deep learning model evaluation

Throughout the course of this study, ORS released several substantial software updates to Dragonfly. These frequent changes in Dragonfly's image analysis toolkit and the exploratory methodological aims of this thesis resulted in an experimental approach to determine the most effective procedure for the segmentation of the fardos for the scoring of nonmetric cranial traits.

Initial experimentation sought to determine whether machine learning or deep learning architectures were preferred for segmenting the fardos. Segmentation Wizard was used in this phase and determined that the deep learning architecture, U-Net, designed for biomedical image segmentation (Ronneberger et al., 2015), was the most successful in segmenting images of the crania from the fardos. Figures 4.1 and 4.2 illustrate the difference in segmentation output between a random forest model (Figure 4.1) and a U-Net model (Figure 4.2). While the other deep learning architectures, Autoencoder and Sensor-3D, achieved results similar to U-Net, they were slightly outperformed by U-Net, according to the visual assessment done by the author. This was expected, as U-Net was designed specifically for biomedical image segmentation and to be trained with very little data (Ronneberger et al., 2015).

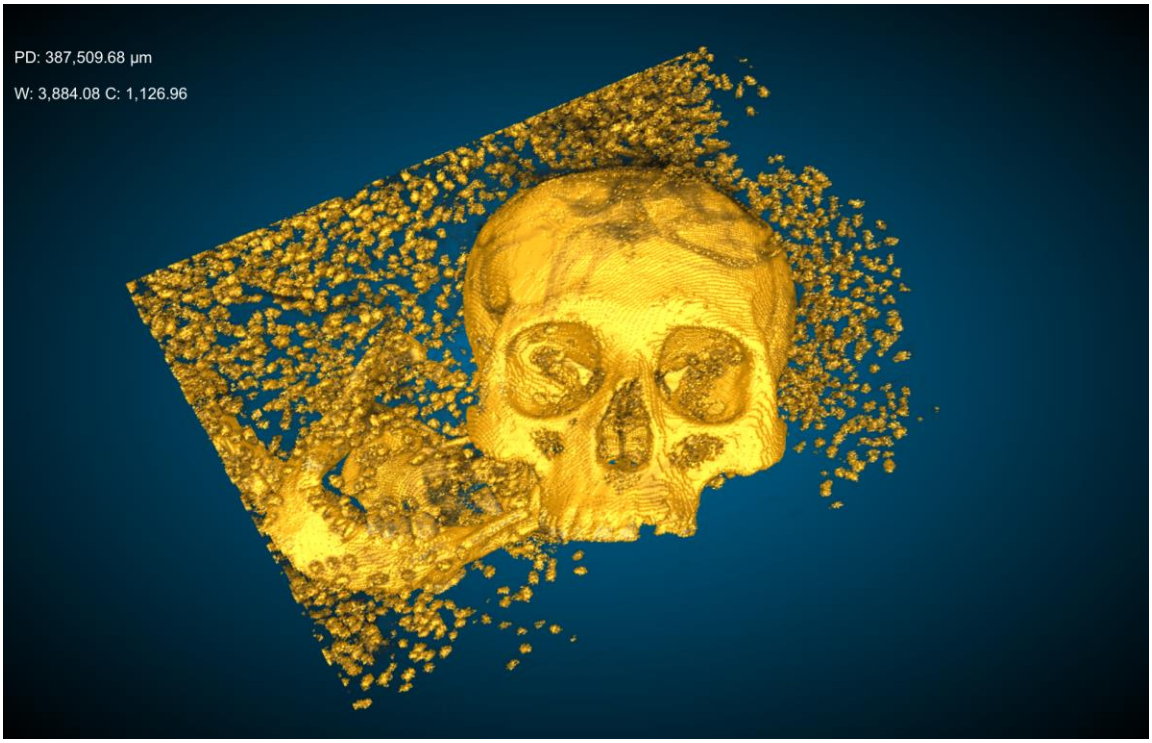

Figure 4.1 Test segmentations of fardo E82S using a random forest model generated in Segmentation Wizard.

Figure 4.2 illustrates the results of the manual correction of the output segmentations after training. While this segmentation method was not fully automated, as intended by the original goals of the study, it was consistently quicker than a full manual segmentation by several hours. Traditional manual segmentation of a single fardo took roughly 4-5 hours to complete, whereas the semi-automated approach tested in this thesis took roughly 2-3 hours to segment and manually correct an entire skull.

4.1.2 Visualization for nonmetric trait scoring

The scanning technique varied across the samples, making visualization of the nonmetric variants on the 3D rendering of the skull difficult. Additionally, the fardos vary in their preservation status and the concentration and orientation of wrappings and cotton seeds (see Figure 4.1). These conditions required the adjustment of 3D visualization and lighting settings (e.g., anti-aliasing, edge contrast, and focus) in Dragonfly to adequately score the traits on each skull. Dragonfly comes with several 3D presets that offer different combinations of these parameters and were useful in

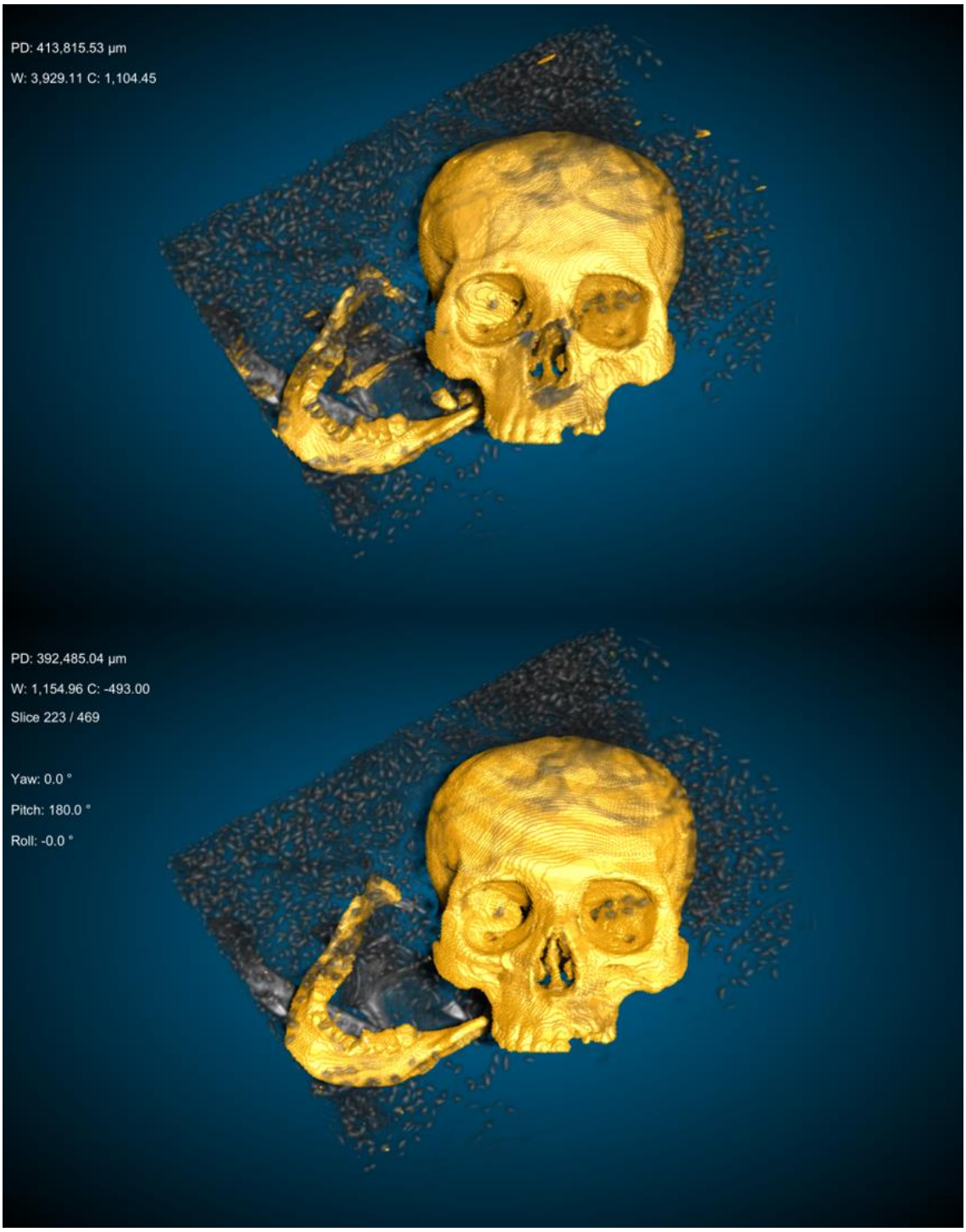

Figure 4.2 Test segmentation (top) with false positives scattered throughout the volume and subsequent manual correction (bottom) of E82S using a U-Net model generated in Segmentation Wizard. Note the 'clutter' (yellow) present in the top image (above the cranium) and surrounding the mandible.

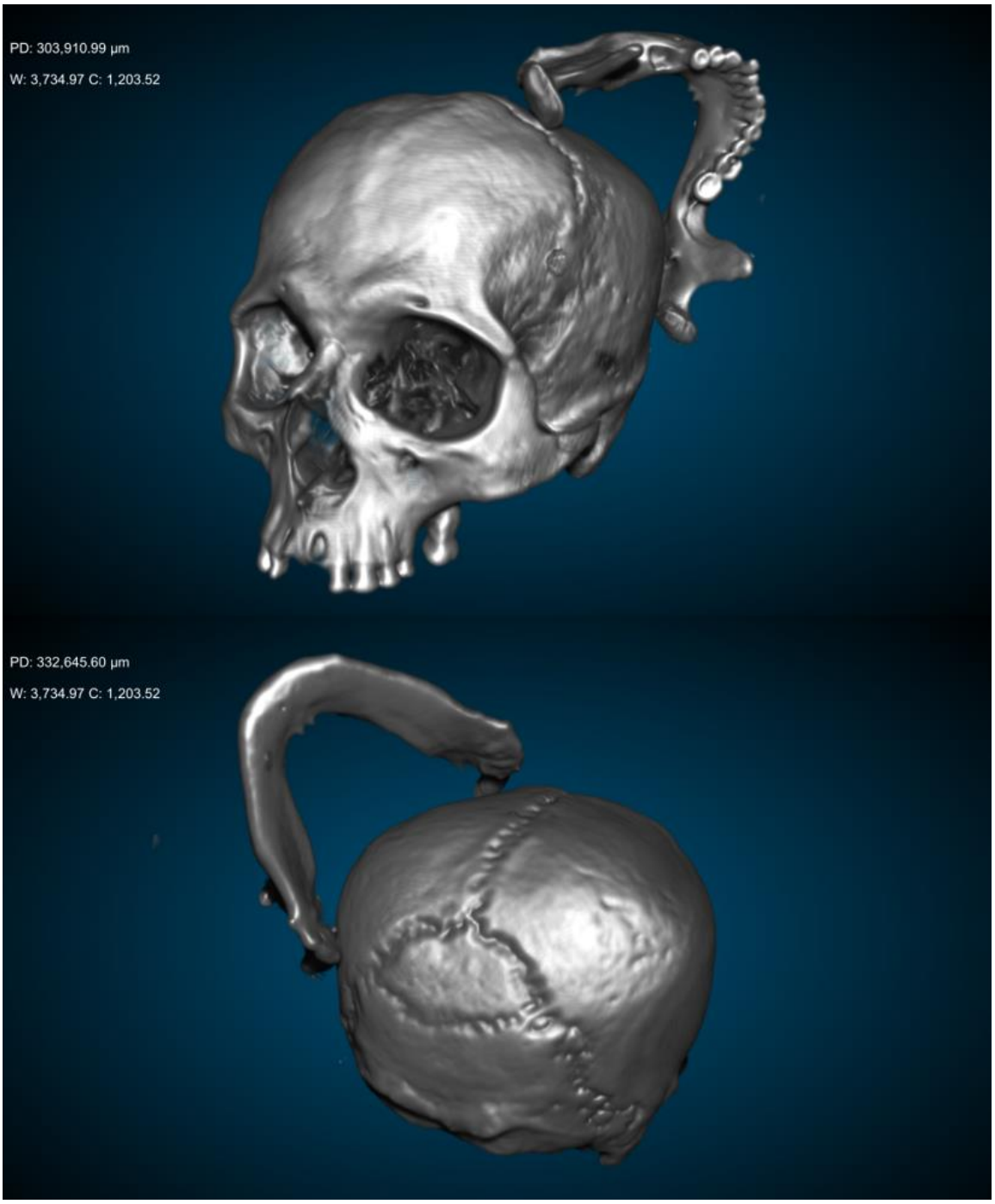

Figure 4.3 Fully segmented scan (E82C) with nonmetric traits (IBP, SOF, OAT, GEP) visible (see Table 3.5 for trait abbreviations).

navigating the skulls for scoring. Furthermore, the presets allow comparability between users analyzing the same images on different computers. It was also beneficial to consult the 3D view and 2D views to ensure accuracy during scoring. This was especially relevant for assessing the presence of extrasutural bones and the completeness of foramina closure. Figure 4.3 shows an example of the final segmentation of a skull (E82C) and the presence of nonmetric traits.

4.2 Data screening and trait list reduction results

4.2.1 Cranial index

The maximum cranial length and breadth measurements as well as the cranial index calculations are presented in Table 4.1. All of the individuals from Pachacamac, nine out of ten individuals from Ancón, and one of the two individuals from Maranga exhibit some cranial modification. Of the 23 individuals from San Jose de Moro, 19 were able to be measured. Nine of these individuals exhibit cranial modification. Cranial modification in the Pachacamac, Ancón, and Maranga samples was assess visually in Dragonfly. Modification was recorded for San Jose de Moro and Chile based on the observer's comments.

Table 4.1 Maximum cranial breadth and length measurements and cranial index of Peruvian samples observed in this study.

Individual	Site	Breadth	Length	Cranial Index	Modified?
E76E	Pachacamac	130	155	83.8	Y
E82C	Pachacamac	152	158	96.2	Y
E82F	Pachacamac	153	176	86.9	Y
E82S	Pachacamac	155	144	107.6	Y
E84	Pachacamac	147	132	111.4	Y
PE-0087	Ancon	152	169	89.9	Y
PE-0089	Ancon	148	155	95.5	Y
PE-0091	Ancon	146	169	86.4	Y
PE-0093	Ancon	142	169	84.0	N
PE-0100	Ancon	141	159	88.6	Y
PE-0101	Ancon	140	147	95.2	Y
PE-0102	Ancon	143	166	86.1	Y
PE-0103	Ancon	146	151	96.7	Y
PE-0104	Ancon	166	174	95.4	Y
JC-AE-2288	Maranga	132	173	76.3	N
JC-AE-2305	Maranga	144	169	85.2	Y

SJM-313	San Jose de Moro	160	165	96.9	Y
SJM-316	San Jose de Moro	140	165	85	Y
SJM-319	San Jose de Moro	163	169	96.4	Y
SJM-320	San Jose de Moro	148	171	86.55	Y
SJM-405	San Jose de Moro	125	175	71.4	N
SJM-412	San Jose de Moro	147	157	93.6	Y
SJM-413	San Jose de Moro	146	188	77.7	N
SJM-415 1	San Jose de Moro	153	161	95	Y
SJM-415 2	San Jose de Moro	143	164	87.2	N
SJM-415 3	San Jose de Moro	144	165	87.3	Y
SJM-415 4	San Jose de Moro	129	188	68.6	Y
SJM-415 5	San Jose de Moro	142	171	83	N
SJM-415 6	San Jose de Moro	139	178	78.1	N
SJM-418	San Jose de Moro	131	152	86.2	Y
SJM-501	San Jose de Moro	156	129	120.9	Y
SJM-502	San Jose de Moro	154	148	104.1	Y
SJM-503	San Jose de Moro	160	165	97	Y
SJM-509 A	San Jose de Moro	166	206	80.6	N
SJM-512	San Jose de Moro	156	170	91.7	Y

4.2.2 Trait frequencies and bilateral expression of traits

Table 4.2 presents the frequencies of traits after the individual count method was applied to all sites. The number of individuals with each trait present *n* is divided by the total number of observable individuals for a site to obtain the frequency. The fardos that were analyzed in Dragonfly were scored for the traits that are listed in Table 3.5.

Upon accessing the Ossenberg (2013) dataset and determining its comparability with the Peruvian samples, the trait list was reduced to include only those traits that overlapped with Ossenberg's analysis, leading to a total of 30 traits. When applying the individual count method to the bilateral traits, the resulting trait list contained 17 traits (Table 4.2). The traits SOF and SON (labelled SOF by Ossenberg, see Table 3.5 for trait abbreviations) were scored as one trait together but differentiated by Ossenberg; these traits were made into two discrete traits for multivariate analysis. Additionally, Ossenberg treats FOI and FSO (labelled FSP by Ossenberg) as one trait. The frequencies of these traits in the Peruvian samples were combined into one category for subsequent analysis.

Table 4.2 Nonmetric trait frequencies of adults from all sites with the full trait list (individual count method). Sexes are pooled. See Table 3.5 for trait abbreviations.

	Pachacamac		Ancon		Maranga		San Jose de Moro		Araucanian		Arica		Coquimbo		Iquique		Junin Grave		Punta Pichalo	
Trait	**n**	**%**	**n**	**%**	**n**	**%**	**n**	**%**	**n**	**%**	**n**	**%**	**n**	**%**	**n**	**%**	**n**	**%**	**n**	**%**
MSR	0	0.0%	0	0.0%	0	0.0%	4	21.1%	0	0.0%	1	33.3%	0	0.0%	0	0.0%	1	50.0%	0	0.0%
SOF	3	75.0%	5	50.0%	2	100.0%	9	56.3%	3	75.0%	3	100.0%	5	62.5%	3	75.0%	1	50.0%	3	25.0%
SON	2	50.0%	8	80.0%	2	100.0%	11	68.8%	1	25.0%	2	66.7%	3	37.5%	0	0.0%	0	0.0%	0	0.0%
FOH	3	60.0%	3	30.0%	0	0.0%	10	58.8%	2	50.0%	2	66.7%	4	66.7%	2	50.0%	1	50.0%	6	50.0%
CCP	2	40.0%	1	10.0%	0	0.0%	2	33.3%	2	50.0%	2	66.7%	2	40.0%	3	75.0%	1	100.0%	10	83.3%
DHC	0	0.0%	4	40.0%	0	0.0%	4	50.0%	2	50.0%	2	66.7%	2	28.6%	0	0.0%	1	100.0%	6	50.0%
FOI	1	20.0%	4	40.0%	1	50.0%	2	28.6%	4	100.0%	3	100.0%	0	0.0%	2	50.0%	0	0.0%	4	33.3%
OMB	0	0.0%	6	75.0%	0	0.0%	3	20.0%	3	75.0%	0	0.0%	5	71.4%	1	33.3%	1	50.0%	3	27.3%
ABP	1	20.0%	3	33.3%	0	0.0%	3	20.0%	0	0.0%	1	33.3%	3	37.5%	1	25.0%	0	0.0%	1	9.1%
OAA	4	80.0%	9	90.0%	1	50.0%	3	18.8%	2	50.0%	0	0.0%	5	71.4%	2	50.0%	0	0.0%	2	18.2%
PNB	1	50.0%	2	28.6%	1	50.0%	3	23.1%	0	0.0%	3	100.0%	1	14.3%	3	75.0%	1	50.0%	6	54.5%
OJP	0	0.0%	0	0.0%	0	0.0%	2	20.0%	1	25.0%	0	0.0%	0	0.0%	3	75.0%	1	50.0%	1	9.1%
IBP	1	20.0%	2	22.2%	0	0.0%	1	5.6%	0	0.0%	0	0.0%	1	14.3%	0	0.0%	0	0.0%	1	9.1%
PCT	0	0.0%	0	0.0%	0	0.0%	1	14.3%	1	25.0%	0	0.0%	0	0.0%	0	0.0%	0	0.0%	0	0.0%
IOS	0	0.0%	1	10.0%	0	0.0%	1	100.0%	0	0.0%	1	33.3%	0	0.0%	0	0.0%	0	0.0%	0	0.0%
MHB	1	25.0%	4	44.4%	0	0.0%	3	21.4%	0	*	0	0.0%	1	16.7%	0	0.0%	1	50.0%	2	22.2%
MMF	0	0.0%	1	11.1%	0	0.0%	3	25.0%	0	0.0%	0	0.0%	1	16.7%	0	0.0%	1	50.0%	5	55.6%

*Trait was unobservable for this sample.

4.2.3 Elimination of rare and frequently unobservable traits

Using the trait list in Table 4.2, rare traits and frequently unobservable traits were assessed and removed from analysis, following Sjøvold (1977). Traits that were present in less than 5% of the sample were removed, as they would have no power to detect differences between individuals. The precondylar tubercle (PCT) was the only trait in this analysis with such a low frequency. Traits that were observable in less than 25% of the sample were also removed as well. This resulted in the elimination of four traits: condylar canal (CCP), infraorbital suture (IOS), mylohyoid bridge (MHB), and multiple mental foramina (MMF).

4.2.4 Sex-based correlations

Sex was estimated in the CT-scanned fardos by the author for the purpose of eliminating any traits with sex-based correlations. Table 4.3 shows the results of this analysis, including the frequencies of traits between sexes, their chi-square values, and

Table 4.3 Trait frequencies grouped by sex showing Chi-square and significance. See Table 3.5 for trait abbreviations.

	Males		**Females**			
Trait	**n**	**%**	**n**	**%**	**χ2**	**p-value**
MSR	4/45	8.9%	2/22	9.1%	0.001	0.978
SOF	23/42	54.8%	13/22	59.1%	0.110	0.740
SON	20/42	47.6%	9/22	40.9%	0.262	0.609
FOH	19/42	45.2%	13/22	59.1%	1.108	0.293
CCP	16/36	44.4%	8/14	57.1%	0.651	0.420
DHC	15/39	38.5%	6/16	37.5%	0.004	0.947
FOI	14/38	36.8%	6/17	35.3%	0.012	0.912
OMB	14/40	35.0%	7/17	41.2%	0.196	0.658
ABP	8/43	18.6%	5/19	26.3%	0.473	0.492
OAA	20/43	46.5%	7/20	35.0%	0.739	0.390
PNB	12/38	31.6%	8/16	50.0%	1.638	0.201
OJP	5/40	12.5%	3/17	17.7%	0.262	0.609
IBP	5/42	11.9%	1/22	4.6%	0.920	0.337
PCT	1/39	2.6%	1/15	6.7%	0.511	0.475
IOS	2/32	6.3%	1/16	6.3%	0.000	1.000
MHB	4/27	14.8%	8/20	40.0%	3.833	0.0503
MMF	6/27	22.2%	5/19	22.2%	0.103	0.749

associated p-values. None of the traits demonstrated significant sex correlations at $p < 0.05$; therefore, no traits were eliminated from analysis on this basis

4.2.5 Intertrait correlations

All adults were pooled for all possible pairs of the 30 traits analyzed between the Peruvian and Chilean samples to test for intertrait correlations. Table 4.4 summarizes the results for each of the trait pairs, showing the *phi* coefficients and their associated p-value. Traits that demonstrated significant correlations with more than one trait were eliminated. Additionally, traits with significant correlations at $p < 0.05$ were eliminated if only one significant pairwise correlation was observed, following Harris and Sjøvold (2004). This led to the exclusion of the metopic suture (MET), apical bone (ABP), os japonicum (OJP), Inca bone (IBP), and precondylar tubercle (PCT).

4.2.3 Final reduced trait list

With the combination of bilateral traits using the individual count method and the elimination of rare traits, frequently unobservable traits, and intertrait correlations, the final trait list was reduced to eight nonmetric variants: supraorbital foramen (SOF), supraorbital notch (SON), foramen of Huschke (FOH), divided hypoglossal canal (DHC), foramen ovale incomplete (FOI), occipto-mastoid bone (OMB), asterionic bone (OAA), and parietal notch bone (PNB). The frequencies for all adults grouped by site can be found in Table 4.5. The R package offers selection of a trait exclusion strategy, but there is little information regarding best practices for this selection as the specific trait reduction strategy will vary according to the structure of the data. The methods used for trait list reduction (mentioned above) offer greater comparability to similar studies; therefore, no exclusion strategy was used in the R package itself.

4.3 Biological distance results

4.3.1 Mean measure of divergence

The MMD values for samples grouped by site using the reduced trait list can be found in Table 4.6. It is common for MMDs to yield negative values when sample sizes are too small or the distance between samples is too small. Following Harris and Sjøvold

Table 4.4 Inter-trait correlation using the full trait list. The upper triangle contains the phi coefficients, the lower triangle contains the p-values. See Table 3.5 for trait abbreviations.

	MSR	SOF	SON	FOH	CCP	DHC	FOI	OMB	ABP	OAA	PNB	OJP	IBP	PCT	IOS	MHB	MMF
MSR		0.031	0.024	0.003	0.004	0.058	0.058	0.055	0.139*	0.028	0.054	0.175*	0.202*	0.233*	0.215*	0.117	0.124
SOF	0.608		0.004	0.001	0.001	0.009	0.009	0.008	0.021	0.004	0.008	0.027	0.031	0.035	0.032	0.017	0.018
SON	0.690	0.952		0.000	0.001	0.007	0.007	0.007	0.017	0.003	0.006	0.021	0.024	0.027	0.025	0.013	0.014
FOH	0.955	0.993	0.995		0.000	0.001	0.001	0.001	0.002	0.000	0.001	0.003	0.003	0.215*	0.004	0.002	0.002
CCP	0.945	0.992	0.994	0.999		0.001	0.002	0.001	0.003	0.001	0.001	0.004	0.004	0.005	0.005	0.003	0.003
DHC	0.365	0.892	0.916	0.988	0.986		0.016	0.015	0.039	0.008	0.015	0.049	0.057	0.066	0.060	0.032	0.034
FOI	0.365	0.892	0.916	0.988	0.986	0.812		0.015	0.039	0.008	0.015	0.049	0.057	0.066	0.060	0.032	0.034
OMB	0.379	0.895	0.918	0.988	0.986	0.817	0.817		0.037	0.008	0.014	0.047	0.055	0.063	0.058	0.031	0.033
ABP	**0.024**	0.733	0.791	0.970	0.964	0.550	0.550	0.561		0.019	0.037	0.119	0.137*	0.158*	0.146*	0.078	0.083
OAA	0.644	0.944	0.957	0.994	0.993	0.903	0.903	0.906	0.759		0.007	0.024	0.028	0.032	0.029	0.016	0.017
PNB	0.394	0.899	0.921	0.989	0.986	0.823	0.823	0.828	0.574	0.909		0.046	0.054	0.062	0.057	0.030	0.033
OJP	**0.005**	0.676	0.745	0.963	0.955	0.459	0.459	0.472	0.064	0.707	0.486		0.173**	0.203**	0.187**	0.100	0.107
IBP	**0.001**	0.617	0.698	0.956	0.946	0.377	0.377	0.391	**0.028**	0.653	0.406	**0.007**		0.231*	0.214*	0.115	0.123
PCT	**0.000**	0.584	0.671	**0.003**	0.940	0.327	0.327	0.342	**0.015**	0.623	0.356	**0.002**	**0.000**		0.256*	0.137	0.146*
IOS	**0.001**	0.626	0.705	0.956	0.946	0.381	0.381	0.397	**0.029**	0.661	0.409	**0.006**	**0.001**	**0.000**		0.126	0.135
MHB	0.076	0.794	0.839	0.977	0.972	0.642	0.642	0.652	0.243	0.814	0.662	0.144	0.083	0.050	0.078		0.071
MMF	0.060	0.782	0.830	0.976	0.970	0.622	0.622	0.633	0.216	0.803	0.643	0.121	0.066	**0.037**	0.061	0.326	

**Significant at $p < 0.05$*

Table 4.5 Trait frequencies of adults from all sites using the reduced trait list. Sexes are pooled. See Table 3.5 for trait abbreviations.

	Pachacamac		Ancon		Maranga		San Jose de Moro		Araucanian		Arica		Coquimbo		Iquique		Junin Grave		Punta Pichalo	
Trait	**n**	**%**	**n**	**%**	**n**	**%**	**n**	**%**	**n**	**%**	**n**	**%**	**n**	**%**	**n**	**%**	**n**	**%**	**n**	**%**
SOF	3	75.0%	5	50.0%	2	100.0%	9	56.3%	3	75.0%	3	100.0%	5	62.5%	3	75.0%	1	50.0%	3	25.0%
SON	2	50.0%	8	80.0%	2	100.0%	11	68.8%	1	25.0%	2	66.7%	3	37.5%	0	0.0%	0	0.0%	0	0.0%
FOH	3	60.0%	3	30.0%	0	0.0%	10	58.8%	2	50.0%	2	66.7%	4	66.7%	2	50.0%	1	50.0%	6	50.0%
DHC	0	0.0%	4	40.0%	0	0.0%	4	50.0%	2	50.0%	2	66.7%	2	28.6%	0	0.0%	1	100.0%	6	50.0%
FOI	1	20.0%	4	40.0%	1	50.0%	2	28.6%	4	100.0%	3	100.0%	0	0.0%	2	50.0%	0	0.0%	4	33.3%
OMB	0	0.0%	6	75.0%	0	0.0%	3	20.0%	3	75.0%	0	0.0%	5	71.4%	1	33.3%	1	50.0%	3	27.3%
OAA	4	80.0%	9	90.0%	1	50.0%	3	18.8%	2	50.0%	0	0.0%	5	71.4%	2	50.0%	0	0.0%	2	18.2%
PNB	1	50.0%	2	28.6%	1	50.0%	3	23.1%	0	0.0%	3	100.0%	1	14.3%	3	75.0%	1	50.0%	6	54.5%

Table 4.6 Mean Measure of Divergence of all adults grouped by site with reduced trait list. Sexes are pooled. MMDs are located in the upper triangle, standard deviations are located in the lower triangle.

	Ancon	**Araucanian**	**Arica**	**Coquimbo**	**Iquique**	**Junin grave**	**Maranga**	**Pachacamac**	**Punta Pichalo**	**San Jose de Moro**
Ancon		0.727*	0.234	0.199	0.071	0.353	0.005	0.000	0.341*	0.130*
Araucanian	0.161		0.068	0.534*	0.082	0.406	0.556*	0.736*	0.597*	0.551*
Arica	0.193	0.254		0.261	0.083	0.000	0.000	0.180	0.105	0.188
Coquimbo	0.117	0.178	0.210		0.000	0.168	0.000	0.000	0.314*	0.283*
Iquique	0.169	0.231	0.262	0.187		0.021	0.000	0.000	0.142	0.000
Junin grave	0.270	0.331	0.362	0.287	0.340		0.240	0.080	0.000	0.063
Maranga	0.270	0.331	0.362	0.287	0.340	0.442		0.000	0.312	0.012
Pachacamac	0.132	0.193	0.225	0.149	0.202	0.302	0.302		0.169	0.000
Punta Pichalo	0.091	0.152	0.184	0.108	0.161	0.261	0.261	0.123		0.197*
San Jose de Moro	0.101	0.161	0.193	0.117	0.170	0.272	0.272	0.132	0.092	

*Significant at $p < 0.05$

Table 4.7 Mean Measure of Divergence of all adults grouped by site with full trait list ('individual count method'). Sexes are pooled. MMDs are located in the upper triangle, standard deviations are located in the lower triangle.

	Ancon	**Araucanian**	**Arica**	**Coquimbo**	**Iquique**	**Junin Grave**	**Maranga**	**Pachacamac**	**Punta Pichalo**	**San Jose de Moro**
Ancon		0.146	0.571*	0.000	0.377*	0.299	0.000	0.000	0.495*	0.267*
Araucanian	0.139		0.271	0.206	0.000	0.000	0.000	0.153	0.226	0.143
Arica	0.166	0.217		0.675*	0.100	0.052	0.000	0.066	0.375	0.106
Coquimbo	0.099	0.150	0.177		0.232	0.000	0.073	0.000	0.256*	0.153
Iquique	0.141	0.192	0.219	0.153		0.000	0.000	0.000	0.009	0.144
Junin grave	0.214	0.265	0.292	0.226	0.268		0.000	0.000	0.000	0.000
Maranga	0.214	0.265	0.292	0.226	0.268	0.341		0.000	0.186	0.000
Pachacamac	0.142	0.191	0.218	0.152	0.194	0.267	0.267		0.093	0.000
Punta Pichalo	0.080	0.130	0.158	0.091	0.133	0.206	0.206	0.133		0.203*
San Jose de Moro	0.075	0.125	0.152	0.086	0.128	0.201	0.201	0.128	0.067	

*Significant at $p < 0.05$

(2004), negative MMDs are entered as zeroes in the MMD matrix. The most frequent negative MMD values are found between Pachacamac, Maranga, and the Junin Grave, likely due to their small sample sizes. The reduced trait list produced the greatest significant MMDs between sites. These occur between Pachacamac and Araucanian (0.736) as well as Ancón and Araucanian (0.727). The MMDs using the full trait list can be found in Table 4.7. Using both trait lists, Pachacamac, Maranga, and the Junin Grave demonstrate mostly negative contributions to the MMD. This is likely a result of the small sample sizes. The highest significant MMDs are found between Arica and Coquimbo (0.675).

Generally, a pair of samples is considered significantly different if their MMD is greater than twice its standard deviation (Green & Suchey, 1976). The values that are significantly different from each other at $p < 0.05$ are marked with an *; however, these results should not be overemphasized as assessing the significance of the MMD is not straightforward (Jahnke, 2009; Sjøvold, 1977). A non-significant MMD does not necessarily mean the two samples are from the same group, but that the samples cannot be differentiated with the data provided because of the trait selection or sample size (Harris & Sjøvold, 2004).

MMDs for the samples grouped by geographical region using the reduced trait list can be found in Table 4.8. The MMDs using the full trait list can be found in Table 4.9. All the MMDs in both tables are significant. The MMD values in Table 4.8 (reduced trait list) suggest that the greatest divergence exists between the Chilean and Central Coast samples (0.186) while Table 4.9 (full trait list) suggests the greatest divergence exists between the Central Coast and North Coast of Peru (0.278).

Table 4.8 Mean Measure of Divergence of all adults grouped by region with reduced trait list. Sexes are pooled. MMDs are located in the upper triangle, standard deviations are located in the lower triangle.

	Peru Central Coast	**Peru North Coast**	**Chile**
Peru Central Coast		0.123*	0.186*
Peru North Coast	0.080		0.143*
Chile	0.044	0.067	

**Significant at p < 0.05*

Table 4.9 Mean Measure of Divergence of all adults grouped by region with full trait list ('individual count method'). Sexes are pooled. MMDs are located in the upper triangle, standard deviations are located in the lower triangle.

	Peru Central Coast	**Peru North Coast**	**Chile**
Peru Central Coast		0.278*	0.192*
Peru North Coast	0.078		0.217*
Chile	0.033	0.071	

**Significant at $p < 0.05$*

4.3.2 Multidimensional scaling

Multidimensional scaling (MDS) plots are frequently used to uncover the underlying structure of a relational system and, in the case of this study, to help visualize the dissimilarity between samples (Irish, 2010; Jahnke, 2009; Sutter & Mertz, 2004). MDS calculates the Euclidean distances between samples in *n*-dimensional space, often scaling the data to two or three dimensions. The distances in the MMD matrix are assigned to arbitrary coordinates in as many dimensions as necessary to obtain the most concise fit possible (Irish, 2010). The values on the axes of the plots represent the two dimensions by which the points on the plot are dissimilar from each other. They do not reveal anything about the variables themselves. The relative position of the points on the plot indicates the relatedness between groups. Stress majorization of a complicated function (SMACOF) is a software package used to implement multidimensional scaling into R (De Leeuw & Mair, 2009). The AnthropMMD R package enables the use of the four main methods or types of multidimensional scaling (Classical/metric MDS, SMACOF interval type, SMACOF ratio type, and SMACOF ordinal (nonmetric) MDS). The ordinal (nonmetric) MDS was used because of its comparability with similar studies (e.g., Jahnke, 2009; Irish, 2010; Sutter & Mertz, 2004).

Figure 4.4 shows the MDS plot for all ten sites using the reduced trait list. Figure 4.5 shows the MDS plot for all sites using the full trait list. Figure 4.6 shows the MDS plot for the samples grouped into geographic region using the reduced trait list. Figure 4.7 shows the MDS plot for geographical regions using the full trait list. Each plot provides the Spearman's rho and stress values. Spearman's rho indicates the correlation coefficient between the MMDs and the distances observed in the MDS plot. A value close to 1

indicates indicates a perfect fit. The stress value provides the quality of fit by a least squares criterion, in which the value of an excellent fit is less than 0.01 (Kruskal, 1964).

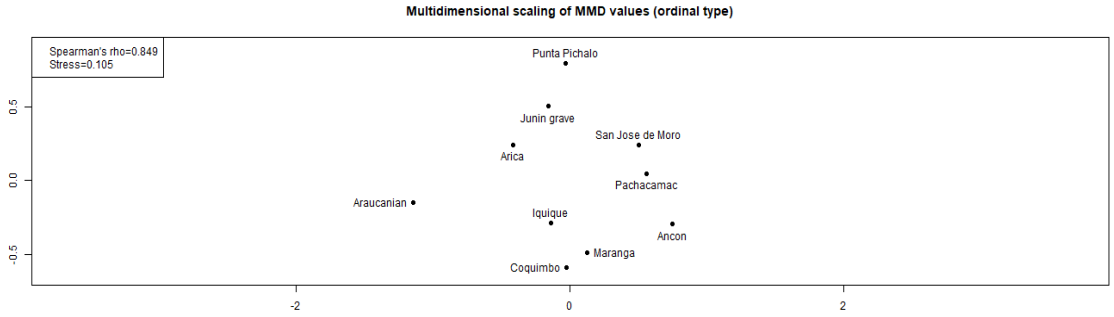

Figure 4.4 Plot of MMD values among all sites with reduced traits list.

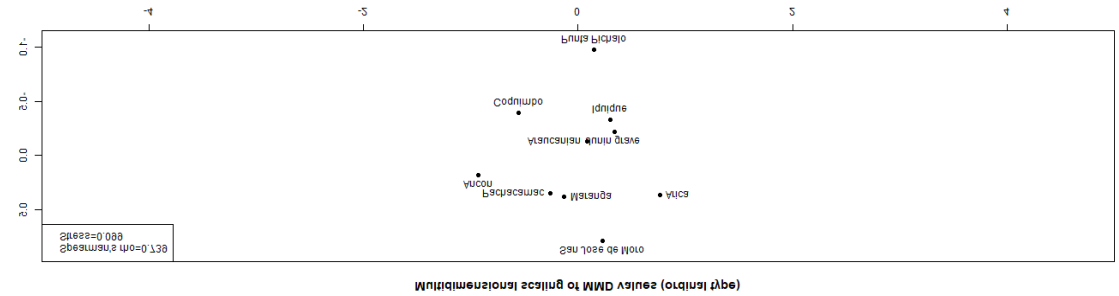

Figure 4.5 MDS Plot of MMD values among all sites with full trait list (‘individual count method’).

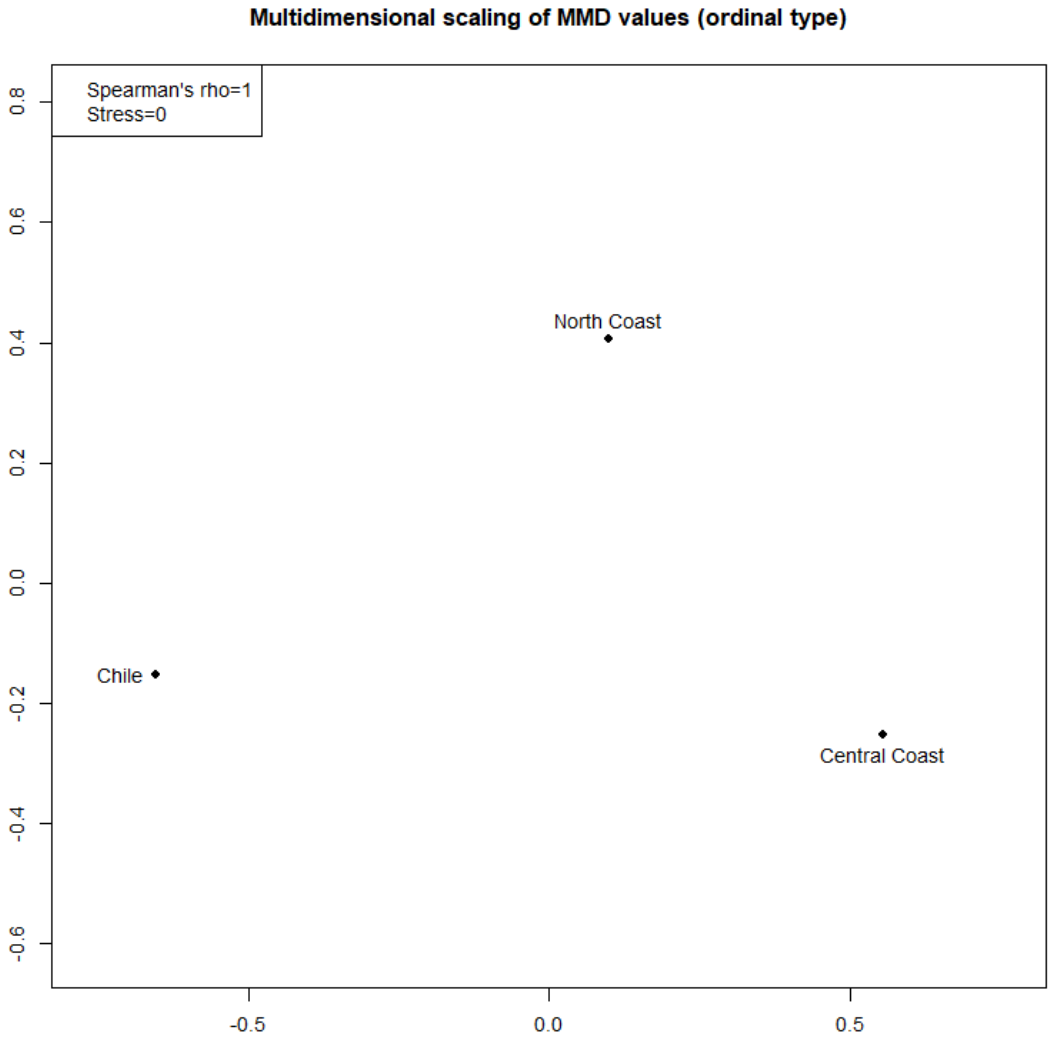

Figure 4.6 MDS plot of MMD values of all regions with reduced trait list.

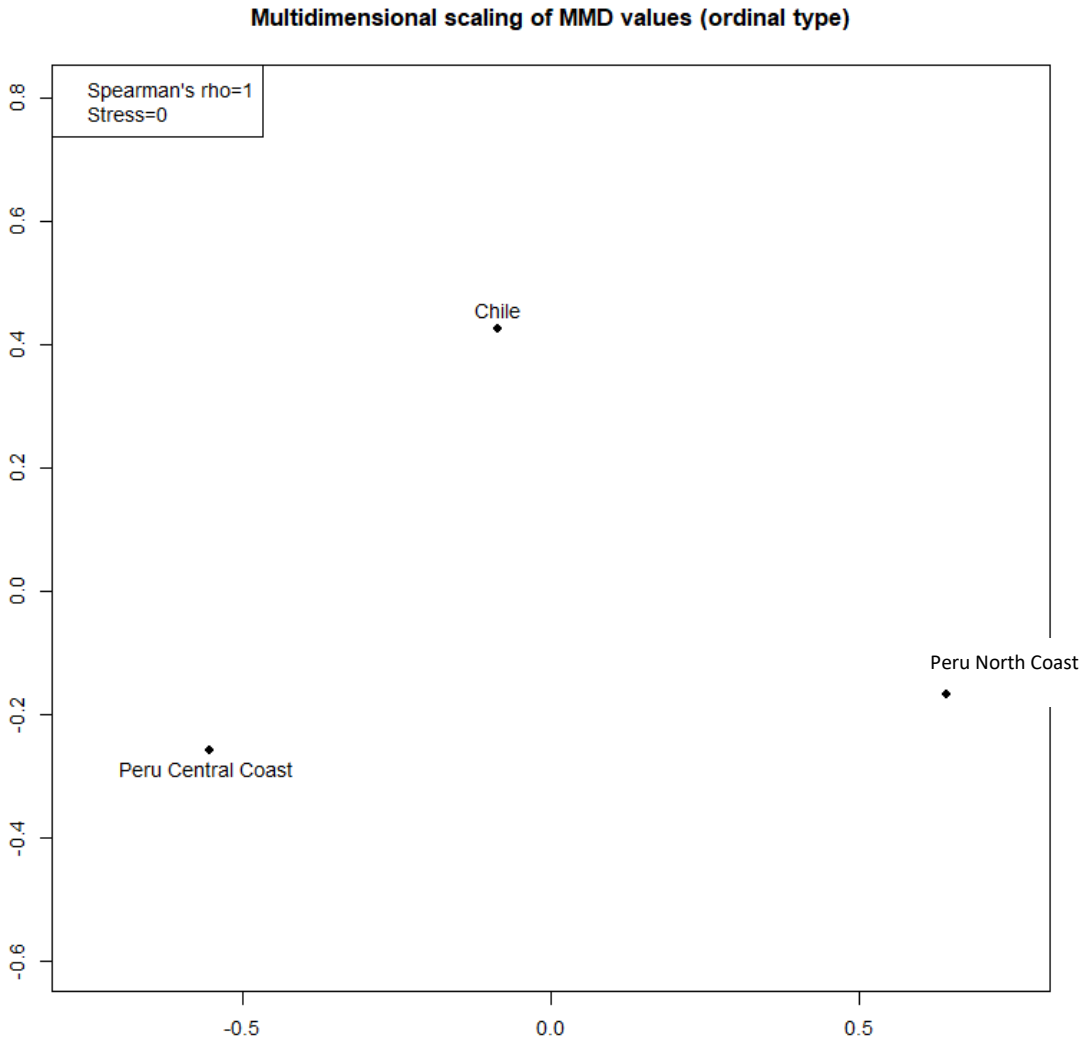

Figure 4.7 MDS Plot of MMD values among all regions with full trait list ('individual count method').

4.3.4 Hierarchical clustering

The AnthropMMD R package enables the use of hierarchical clustering methods to visualize the relationships between samples. The goal of cluster analysis is to identify underlying patterns in the groupings of various datasets (Aldenderfer & Blashfield, 1984). The R package allows the selection of four agglomeration methods: Ward's method (squared distances), single linkage, complete linkage, and average linkage. Each of these methods employ different algorithms to determine which samples are included in which cluster. For instance, the single linkage method requires only a single linkage in order to group two samples (or cases) into the same cluster. Ward's method minimizes the variance between samples and attempts to create equal-sized clusters when possible (Aldenderfer & Blashfield, 1984). To determine the most appropriate agglomeration method, all four methods were applied to each grouping method (Site, geographic region, reduced trait list, full trait list). The agglomeration methods that maintained the most similarities among clusters were used as they indicate replicability (Aldenderfer & Blashfield, 1984).

Ward's method was used for all grouping methods. Figure 4.8 shows the clustering of all sites using the reduced trait list. Figure 4.9 shows the clustering of sites using the full trait list. Both Figures 4.8 and 4.9 demonstrate a two-cluster solution but differ substantially with respect to the further divisions. Figure 4.8 groups most of the Peruvian sites together, including Pachacamac and Ancón which cluster closely to one another. Figure 4.9 produces an unexpected clustering of sites, separating all the Peruvian sites from each other. Figure 4.10 shows the clustering of geographic regions using the reduced trait list while Figure 4.11 shows the clustering of geographic regions using the full trait list. Figure 4.10 follows the expected clustering, with Chile being separate from the two coasts of Peru. This is not the case in Figure 4.11, which clusters Chile and the Central Coast closely while the North Coast is separate.

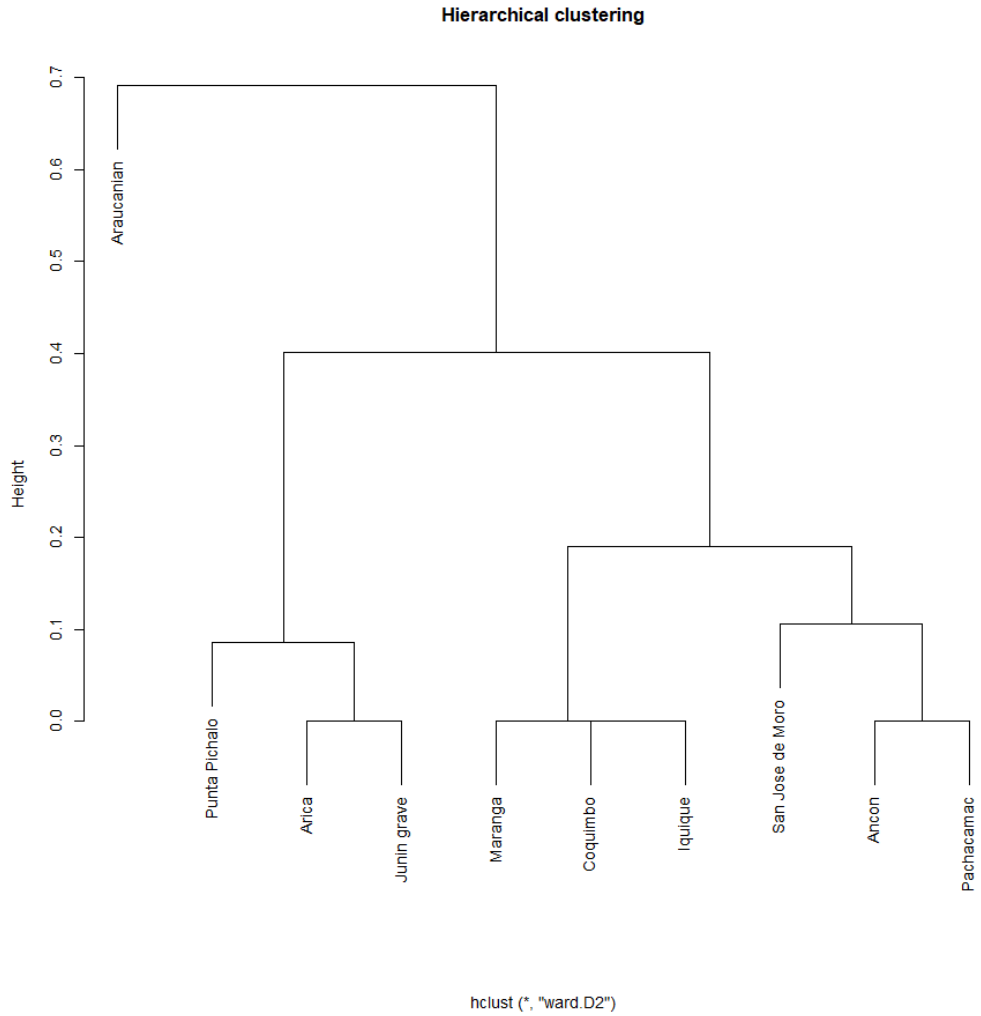

Figure 4.8 Hierarchical clustering (Ward's Method) of all sites with reduced trait list.

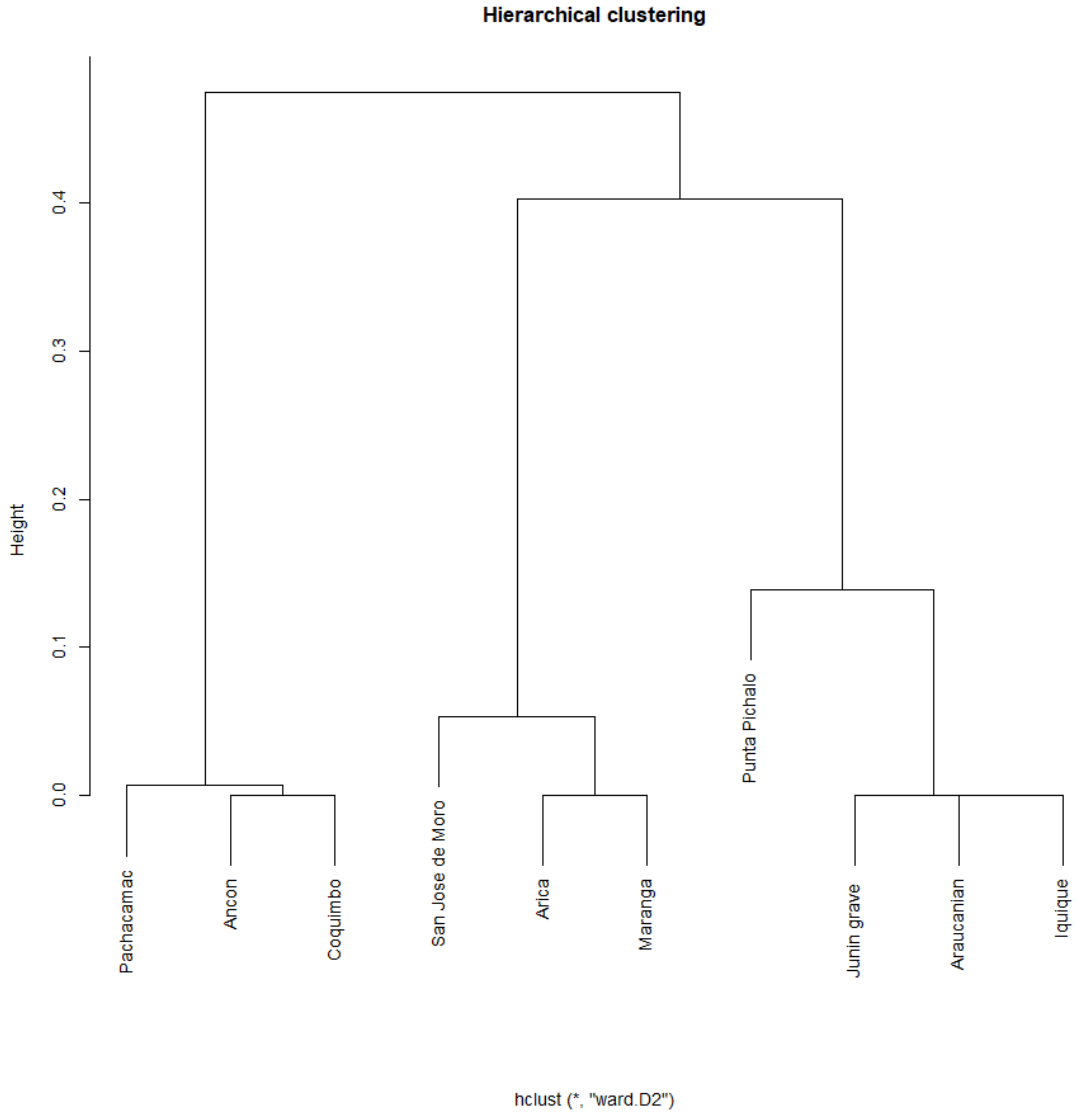

Figure 4.9 Hierarchical clustering (Ward's Method) of all sites with full trait list ('individual count method').

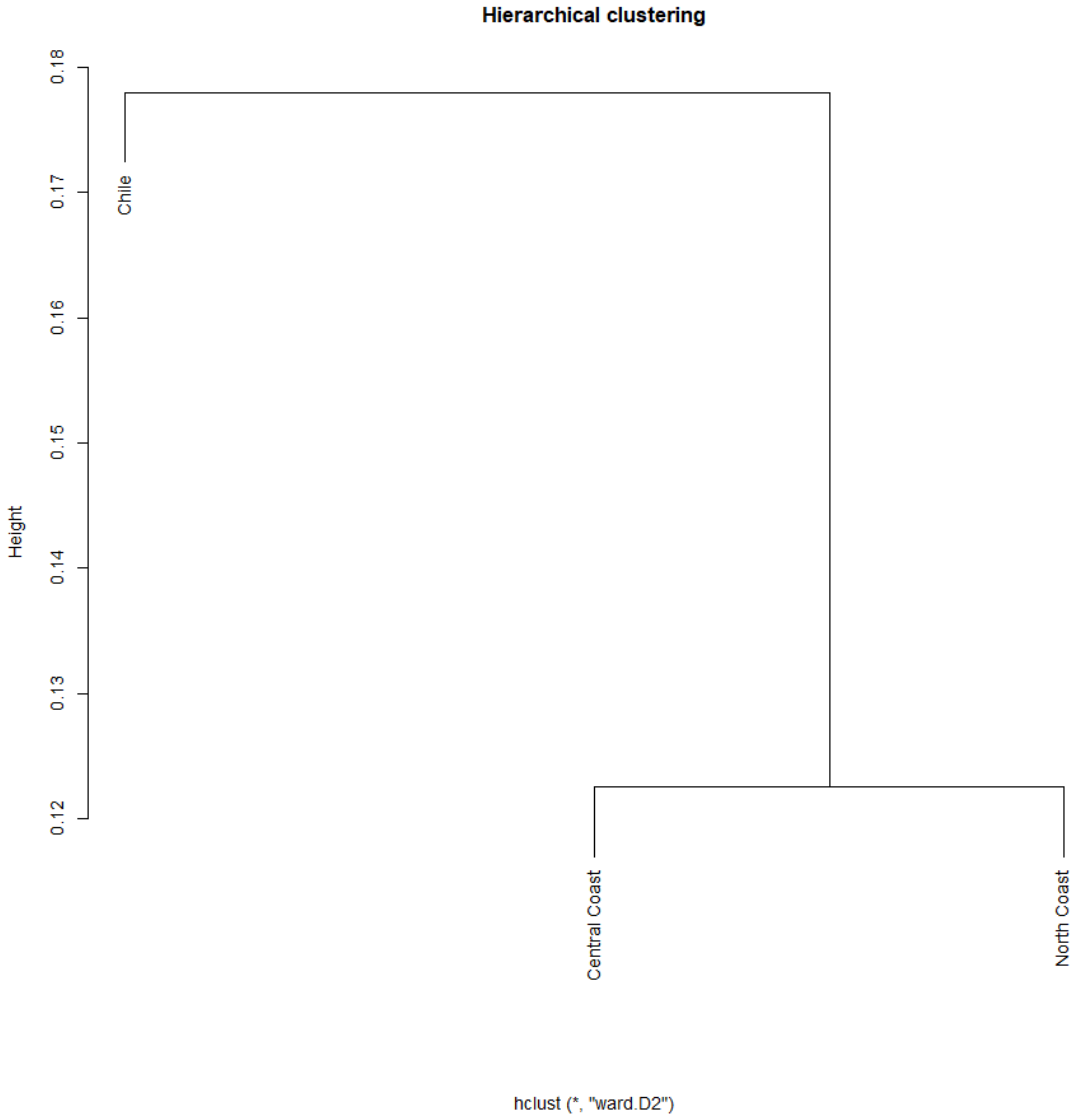

Figure 4.10 Hierarchical clustering (Ward's Method) of all regions with reduced trait list.

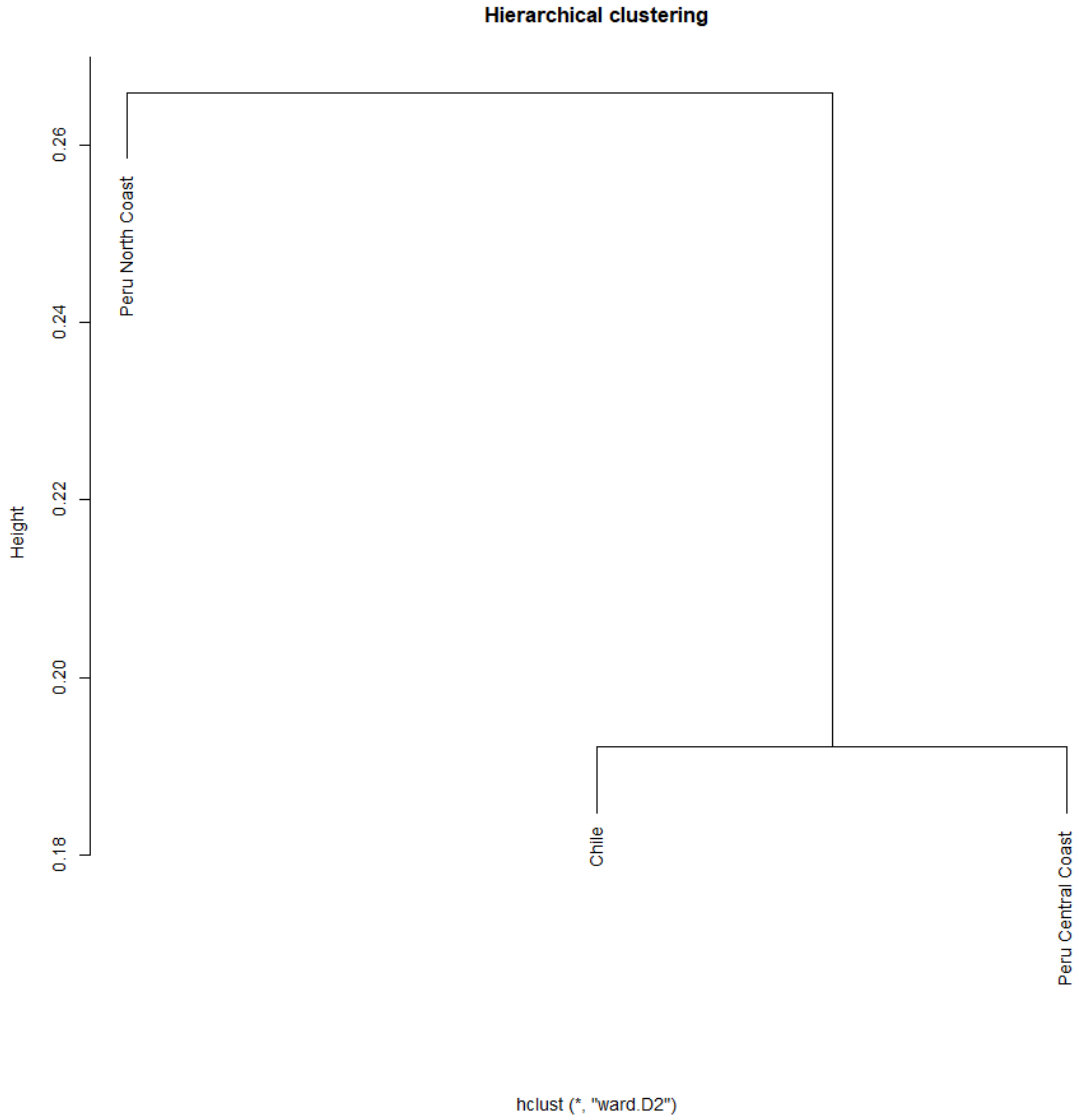

Figure 4.11 Hierarchical clustering (Ward's Method) of all regions with full trait list ('individual count method').

4.4 Summary

Overall, this thesis sought to explore the applicability of a new method of analysis on CT scans of mummy bundles; biodistance analysis using cranial nonmetric variants by conducting automated segmentation of the skulls from the remaining content of the fardos. It is clear that it is possible to obtain scorable images of the skull from these scans using not fully automated, but semi-automated segmentation techniques. The small sample sizes across all sites led to a grouping of the individuals analyzed in this thesis by their broader geographic region. The following chapters will discuss these results and make considerations for future applications of this methodology.

Chapter 5 Discussion

This chapter will discuss the semi-automated image segmentation process, including how specific U-Net models were selected and the approaches to visualizing and accurately scoring the nonmetric traits. It will also discuss the results of the biodistance analysis with respect to the original hypotheses with specific considerations of trait reduction strategies, sample sizes, and groupings of the data. Most of the inter-site comparisons are inadequate to make any definitive conclusions regarding their relatedness among each other, likely due to the small sample sizes.

5.1 Image segmentation using deep learning

The thesis sought to address several methodological questions regarding the analysis of CT images of the fardos: (1) Can nonmetric cranial data be collected from the CT scans? (2) Can this be done using manual image segmentation techniques? (3) Can the traditional (manual) process be automated using the recently implemented deep learning architecture in ORS Dragonfly? (4) If the fardos can be segmented automatically, is this quicker than the traditional method and can it produce a model of the skull suitable for scoring the nonmetric variants in both the two- and three-dimensional views?

5.1.1 Deep learning model selection in Dragonfly

Several model architectures were trained in this study to test the applicability of automated segmentation tools in the image analysis software, Dragonfly (Table 3.4). The models tested included both machine learning and deep learning architectures. The deep learning architecture, U-Net, was chosen for the subsequent biodistance analysis because of its relative success in segmentation the fardos and its frequent use in biomedical image segmentation. Other models, such as Autoencoder and Sensor3D, were also successful in their ability to segment the bundles. However, U-Net was found to be the most consistent and enabled greater comparability to other automated image segmentation studies.

The segmentation of CT scans of mummy bundles, especially those from Peru, is a challenging task due to the inconsistent contents and distribution of materials within the

bundle. The individuals wrapped inside the fardos are often found in a fragmentary state, in a variety of flexed positions, and sometimes with elements of multiple individuals. Each fardo offered a unique challenge with respect to image segmentation. Traditional manual segmentation methods are very time-consuming and biodistance analysis requires relatively large sample sizes, which can be difficult to obtain when working with mummified remains. The deep learning segmentation tools in Dragonfly adequately addressed these issues and enabled quicker segmentation of the fardos. Compared to fully manual segmentation, the semi-automated method tested in this thesis saved roughly 2 hours per bundle.

5.1.2 Visualization and nonmetric trait scoring

The outputs of the segmentations consist of regions of interest (ROIs) in which pixels corresponding to different objects (skull, cotton seeds, postcranial bones, miscellaneous bundle contents) are assigned to a class. This allows the user to isolate and visualize specific objects within the fardos (the skull and mandible in this case). After experimenting with multiple approaches to training segmentation models (outlined in Chapter 3), several patterns were observed. It became evident that the models would not be able to fully automatically segment the images with sufficient accuracy or completeness for scoring the nonmetric traits (Figure 4.2). Every segmentation output from a trained U-Net model produced some false positives (including pixels in the ‘cranium’ class that did not correspond with the skull or mandible) and false negatives (including pixels in the ‘ETC’ class that corresponded with the skull and mandible). This necessitated the manual correction of the ROI. The corrections were conducted on every slice using the 2D ROI painting tool. If there were large and continuous sections including a single class of pixel, the 3D painting tool was used to save time.

Furthermore, it became clear that, because the samples from Pachacamac, Maranga, and Ancón were scanned on different scanners with different settings (see Table 3.3), the models trained on individuals from one site could not adequately segment the samples from others (Figure 5.1). In other words, the applicability of the models

across individual fardos was dependent on the scanning specifications. This applied to models trained on individuals from Pachacamac, Maranga, and Ancón.

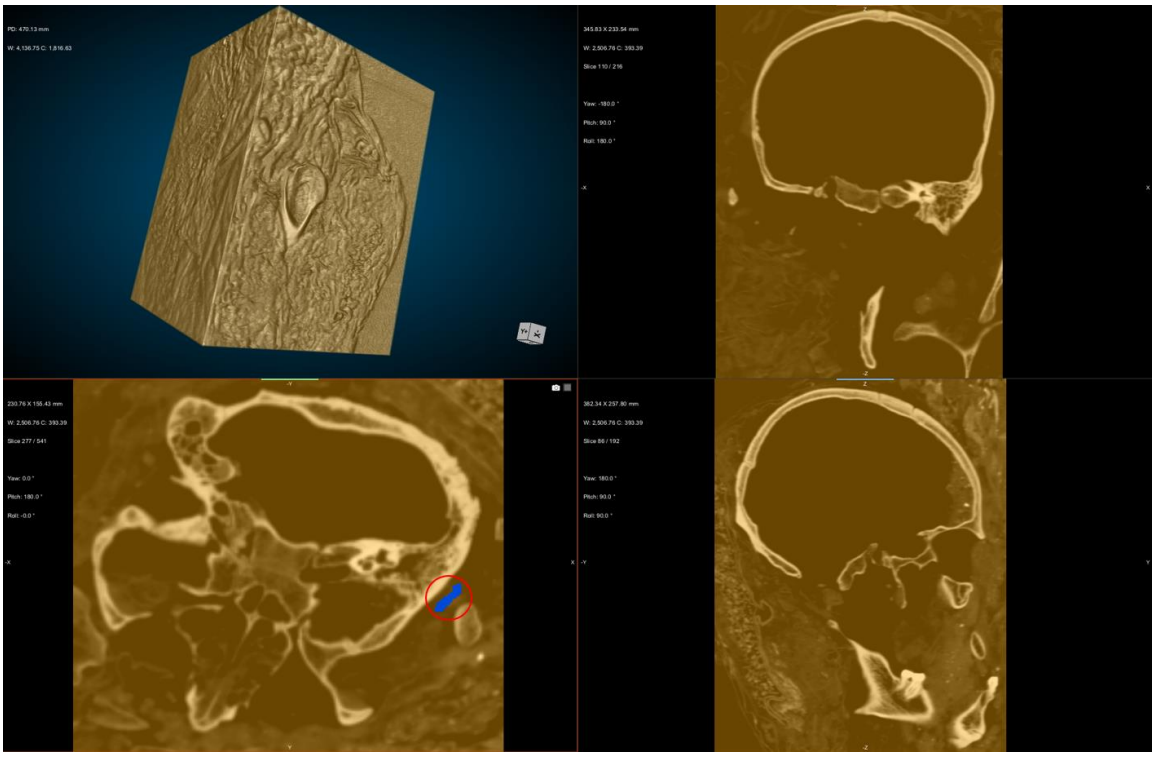

Figure 5.1 Low-accuracy segmentation (high frequency of false positives) output on cranium of fardo PE-0091 (Ancón) using a U-Net model trained on fardo E82S (Pachacamac). Pixels that were assigned to the 'Cranium' class are labelled in yellow (throughout). Pixels assigned to the 'ETC' class are labelled in blue (bottom left frame, circled). Note that only the bones of the cranium and mandible should be colored yellow while the remaining matter (air, postcrania, wrappings) should be colored in blue (hence the label, 'ETC').

Scoring of the nonmetric traits on an individual began when the finalized, manually corrected segmentation was achieved. Scoring was primarily conducted on the 3D view of the entire segmented cranium. When scoring the presence of sutural bones and foramina, it was necessary to reference the 2D cross-sections to ensure accuracy in scoring and limit false positives due to visualization or user errors. When examining the skull for the nonmetric traits, it was beneficial to experiment with the various lighting settings and 3D presets in Dragonfly to adequately visualize the features of the skulls. For example, presets with high specular light and shininess helped visualize the shape of cranial sutures, creating more contrast between the flat surface of the cranium and the grooves of the sutures.

5.1.3 Replicability for future applications

Based on the results of the deep learning experimentation, automated or semi-automated image segmentation of CT scans will most likely save time compared to traditional methods. It took a considerable amount of time to learn how to use Dragonfly, especially the ROI tools used for segmentation, and to learn how to appropriately create training data for a model and assess and adjust the output for additional training. However, this process was exploratory and required some experimentation. Now, with an outline of the necessary steps to automatically or semi-automatically segment CT volumes (see Appendix A), future applications may be more efficient.

The rapid rise in the use of artificial intelligence allows non-imaging specialists to develop unique tools that automate various steps in their research process. One advantage of this increasing accessibility is the ability to export and share pre-existing models. Although, as shown in Figure 5.1, it is evident that there may be some scanner and scanning technique dependence among specific U-Net models when segmenting mummy bundles. This may hinder the comparability among individual mummies scanned on different machines or with different specifications, but the workflow is relatively easy to learn and tailor to the sample under investigation.

5.2 Biodistance on the Andean coast

5.2.1 Considerations of the full trait list versus the reduced trait list

The differences in results between the reduced trait list and the full trait list illustrate how the selection of traits can significantly impact the results of the biodistance analysis. Harris and Sjøvold (2004) argue that including as many traits as possible can more thoroughly sample the battery of potentially meaningful traits and limit the influence of only one or a few traits. They suggest this approach reduces biases in trait selection, making the phenetic distances between groups more objective and thus more comparable. However, many researchers argue that including as many traits as possible can lead to several traits being nondiscriminatory and that using a reduced trait list, as long as the traits are not correlated, can produce more robust statistics (Irish, 2010; Ishida

& Dodo, 1993; Nikita, 2015; Sutter & Mertz, 2004; Velasco, 2018). Therefore, sections 5.2.3 and 5.2.4 will focus primarily on the results from the reduced trait list for each of the two grouping strategies (sites and regions, respectively).

5.2.2 Data screening and trait list reduction considerations

Biodistance analyses using nonmetric traits require a cautious approach to data screening procedures and sampling strategies. The criteria by which the presence of a trait is scored also varies among practitioners. Most researchers refer to Buikstra and Ubelaker (1994) and Hauser and De Stefano (1989) to obtain trait lists and scoring criteria. However, as noted with the Ossenberg dataset (see Table 3.5), specific scoring differences arose and had to be adjusted accordingly when comparing the Chilean samples to those scored in this thesis.

The scoring of bilateral traits dichotomously (present/absent) or on a multilevel system (various degrees of expression) can contribute to different results among studies. Carson (2006) conducted a maximum-likelihood variance components analysis on the heritabilities of both dichotomous and multilevel trait frequencies in the skeletal series in Hallstatt, Austria. Although Carson found uniformly low heritabilities among both scoring systems, she reports slightly higher heritabilities for the dichotomous traits.

Additionally, different treatments of bilateral traits result in various cranial and/or side incidences and can hinder comparability between studies. Hauser and De Stefano (1989) outline the various approaches to bilateral expression: (1) scoring the two sides separately, identifying asymmetry and providing both cranial and side incidences (e.g., Dodo & Ishida, 1987; Ossenberg, 1981); (2) scoring the two sides separately, but summing their frequencies regardless of side and dividing by two (e.g., Berry & Berry, 1967; Corruccini, 1974); and (3) using the individual count method, ignoring the side of occurrence and only indicating whether the individual shows the trait (e.g., Buisktra, 1972; Sutter & Mertz, 2004; Scott & Turner, 1977). The decision to use any of these methods may also be influenced by the state of fragmentation of the study sample. As noted previously, the individual count method was used in this thesis to obtain a greater

sample size and for comparability to other nonmetric trait analyses conducted in the Andes (Herrera, 2016; Jahnke, 2009; Sutter & Mertz, 2004).

Although it is common for researchers conducting biodistance analysis to emphasize comparability when determining mortuary samples, trait selection, scoring criteria, and statistical analyses, there is still a considerable amount of methodological variability throughout the literature and various biodistance studies conducted on the same samples produce different results. For instance, several biodistance analyses of Azapa Valley, Chile samples have been conducted using nonmetric dental traits (Sutter, 2000), craniometrics (Rothhammer & Santoro, 2002; Rothhammer & Silva, 1989; Rothhammer et al., 1982, 1984) and cranial nonmetric traits (Sutter & Mertz, 2004). While Sutter and Mertz (2004) strive for comparability with their own previous studies, they highlight the difficulty of summarizing and comparing previous studies done by other researchers because of the differences in combinations of variables, samples, and statistical procedures.

The individuals in this analysis were originally grouped by site. Most of the samples examined in this thesis contained sample sizes that were inadequate for substantial statistical analysis (n<10 individuals). For this reason, the sites were also grouped into broader geographical regions to obtain sample sizes of at least ten in each group.

5.2.3 Inter-site variability

The effects of small sample sizes are obviously more prevalent when examining inter-site variability than the regional grouping method (see Tables 4.6 and 4.7). Negative MMD values often occur when sample sizes are too small, therefore not being representative of the entire population, or when samples are drawn from populations that do not differ biologically. The former is most likely the case in the present study, as most groups (Arica, Araucanian, Coquimbo, Iquique, Junin Grave, Maranga, and Pachacamac) contain fewer than ten individuals.

Overall, the MMD matrix using the reduced trait list (Table 4.6) produces 12 out of 44 pairwise comparisons resulting in a negative MMD value (these values are

automatically adjusted to zero by AnthropMMD, following Harris and Sjøvold (2004)). Significant MMD values occur in 11 pairwise comparisons. The greatest divergences (i.e., the significant MMD values closest to 1) occur among the Araucanian-Pachacamac and Araucanian-Ancón comparisons with MMD values of 0.736 and 0.727, respectively. The smallest divergence occurs between San Jose de Moro and Ancón with an MMD of 0.130, suggesting these two samples are the most closely related.

None of the samples from Peru produced a non-zero or a significant MMD value when compared with Pachacamac using either trait list. While the Pachacamac-Peruvian sample comparisons were expected to result in lower MMD values than the Pachacamac-Chilean sample comparisons, it is not possible to reach a conclusion regarding the relatedness of these groups due to the small sample sizes and nonsignificant p-values. Furthermore, as previously mentioned, non-significant MMD values do not necessarily suggest that two samples are from the same group, but that they cannot be differentiated with the data provided. As such, the significance of the MMD values should not be overemphasized.

There are a few discernible patterns between the MDS plots for the inter-site comparisons. In the MDS plot for the reduced trait list (Figure 4.4), the Peruvian sites scale positively along the x-axis while the Chilean sites scale negatively. This pattern seems to loosely resemble the broad geographic differentiation between Peruvian and Chilean sites, although the plot places Ancón and Pachacamac further “north” than San Jose de Moro. Figure 4.4 suggests a fairly strong correlation between the distances in the MDS plots and the real dissimilarity values (MMD), indicated by the Spearman’s rho value of 0.849. Again, it is difficult to make any conclusions about the dissimilarity between these groups due to the low sample sizes and negative MMD values in the matrix. It would be useful to further test the extent to which the inter-sample variation is related to their geographic distribution. This could be tested with other types of data, such as isotopic analysis or a comparison of associated artifact styles.

With respect to the hierarchical clustering results, both trait lists resulted in a two-cluster solution, but the further divisions of the clusters differ greatly. The reduced trait list (Figure 4.8) results in a separate cluster for three of the four Peruvian sites (San

Jose de Moro, Ancón, and Pachacamac), with Ancón and Pachacamac clustering together and San Jose de Moro diverging from them as might be expected by their geographic distribution. The initial division of the Araucanian site from the rest of the sites indicates a substantial difference, although the exact cause of the divergence is unclear.

5.2.4 Regional variability

The samples analyzed in this thesis were also grouped by their geographic region to obtain the most robust sample size possible. San Jose de Moro makes up the Peru North Coast group (n=23); Pachacamac, Ancón, and Maranga make up the Peru Central Coast group (n=17); and Araucanian, Arica, Coquimbo, Iquique, Junin Grave, and Punta Pichalo make up the Chile group (n=33). This limits the scope of the biodistance analysis to only broad patterns among regions of the Andes, but this is necessary considering the high prevalence of negative MMD values when comparing individual sites.

The MMD values among the three regions are relatively low and similar to one another ranging from 0.123 to 0.186 (Table 4.8). This is most likely because of the mixture of sites included in the Peru Central Coast and Chile groupings. The greatest divergence occurs between the Peruvian Central Coast and Chile (which was unexpected) while the most closely related regions are the Central and North Coasts of Peru (as expected).

The MDS plot (Figure 4.6) reflects this pattern well, indicated by the stress value of 0 and a Spearman's rho value of 1. This suggests an excellent fit and correlation between MMD and the distances between points. Given the MDS test statistics and significant MMD values overall, the cause of this pattern of divergence may be geographical.

The regional hierarchical clustering (Figure 4.10) produces a two-cluster solution. The result shown in Figure 4.10 was expected on the basis of geography, with the Chilean samples separated from the Peruvian coastal samples. This is also consistent with the higher spatial distribution of sites from Chile.

5.2.5 Pilgrimage and hypotheses revisited

Previous archaeological studies have confirmed the use of Pachacamac as an important ritual centre that attracted pilgrims throughout the region (Eeckhout, 2003, 2013; Menzel et al., 1964; Pozzi-Escot & Uceda, 2019; Uhle, 1903). However, given the small number of individuals from this cemetery at Pachacamac that were usable for the inter-site biodistance analysis, it is not possible to determine whether this sample was composed of pilgrims or local individuals on the basis of the MMD values obtained in this thesis. Furthermore, the lack of temporal context for some samples (e.g., Chilean samples) as well as the wide temporal distribution of other samples (e.g., San Jose de Moro, which includes individuals from the Moche, Transitional, and Lambayeque periods) made it difficult to determine what specific factors contributed to the divergences observed between the groups.

Some of the trends observed in the MDS plots and hierarchical clustering for both the sites and regions may reflect the geographic distribution between samples. The MMD values in Table 4.8 (regional comparison using the reduced trait list), although they are relatively low, suggest that the Central and North Coast sites are the most similar to each other. The hierarchical clustering solution (Figure 4.10) is the most consistent with the expected patterns laid out in Chapter 1. The Chilean sites form an outgroup that is separate from the Peruvian coastal sites. This is also consistent with Sutter's (2009) findings of dental nonmetric trait frequencies between these regions.

As mentioned previously, there is a substantial body of ethnohistoric and archaeological evidence suggesting the importance of features of the landscape (e.g., Cieza de Leon, 1941 [1553]; Contreras, 2010; Rostworowski, 1972). To fully understand the dynamics between groups in the Andes more broadly, it would be useful to compare the coastal samples with samples from other ecological zones (see Figure 2.4). This would help elucidate the role of geographic and climatic variation in patterns of biological affiliation throughout the Andes. Potentially identifying the regions from which pilgrims travelled to Pachacamac would contribute to our understanding of the range of phenomenological experiences of traversing the landscape to reach Pachacamac. The following chapter will summarize the conclusions of this thesis with respect to the

original aims of the project and will suggest future directions for both automated segmentation of CT scans and archaeological analyses of the sample from Pachacamac.

Chapter 6 Summary & Conclusions

6.1 Summary

6.1.1 Image segmentation of mummy bundles

The adoption of deep learning solutions has rapidly increased across many domains of scientific inquiry. This has also led to frequent performance improvements of deep learning models as more researchers are discovering the benefits of automated workflows. With respect to image processing tasks, the developers of Dragonfly have incorporated the popular deep learning engine, TensorFlow, to incorporate user-friendly deep learning features in the software (Makovetsy et al., 2018). These features, particularly Segmentation Wizard and the Deep Learning Tool, have been one of the primary foci of Dragonfly's recent patch and update schedule, offering regular updates and improvements. With respect to deep learning algorithm design and development, these tools are designed for microscopists and image scientists of all skill levels.

6.1.2 Biodistance analysis on mummified remains

Paleoradiological methods have developed alongside radiography for over a century (Chhem, 2008). Paleoradiographic imaging is traditionally used to observe archaeological materials that are difficult to visualize in a non-invasive or non-destructive manner, such as the internal contents of mummies or the production method of an artifact (e.g., Ellis et al., 2017; Wade & Nelson, 2013). Bioarchaeological applications of CT have primarily been interested in osteobiographical assessment of skeletal remains and identification of pathological lesions (e.g., Decker, 2011; Thompson et al., 2013; Wade et al., 2011). One of the central aims of this thesis was to test the potential for a more nuanced analysis of mummified remains: biodistance analysis using cranial nonmetric traits. This approach was applied to test whether the sample of fardos from a recently discovered cemetery at the ritual centre, Pachacamac, composed of pilgrims coming from non-local regions or local individuals with similar nonmetric trait frequencies as a known sample of local individuals from the coastal site of Ancón.

6.2 Conclusions

The original aims of this thesis were twofold: the primary methodological objective was to determine whether the CT scans of mummy bundles (fardos) could be segmented automatically using artificial intelligence segmentation tools such that the images could be visualized for the scoring of nonmetric traits. After experimentation with various tools implemented in the image analysis software, ORS Dragonfly, it became clear that while fully automated segmentation may not yet be possible, semi-automated segmentation still proved to be more time-efficient than the traditional, fully manual method of image segmentation and was able to visualize the crania such that the nonmetric traits were scorable on the scans.

This methodological approach was then applied to an anthropological objective: a biodistance analysis of nonmetric cranial traits to determine whether the fardos from a recently discovered cemetery at Pachacamac comprised a sample of pilgrims, as expected based on the history of archaeological studies on Pachacamac, or a sample of local individuals. This was done using comparative samples from sites along the north and central coasts of Peru as well as nonmetric trait scoring published online by Ossenberg (2013) on Chilean samples from the American Museum of Natural History. The list of traits to be used for biodistance analysis was screened using various statistical methods to test for rare traits, sex correlations, and inter-trait correlations. Both the full trait list and reduced trait list frequencies were then formatted to be entered into the AnthropMMD R package for the calculation of Smith's Mean Measure of Divergence (Santos, 2018).

The findings of this study suggest that the sample sizes were too small to make any conclusions about inter-site variability with respect to the evidence of pilgrimage among the sample from Pachacamac, as indicated by the negative MMDs between Pachacamac and the other Peruvian sites. Broader regional analysis suggests there are significant biological differences between geographical regions. The Central Coast samples (Pachacamac, Maranga, and Ancón) were more closely related to San Jose de Moro (which makes up the North Coast group) than the Chilean sites. The exact nature of these differences, whether they are related to geographic or temporal distribution, should

be further investigated to understand the population dynamics along the Andean coast more accurately.

6.3 Future directions

There are several potential areas of improvement in this thesis that can be addressed in future studies. With respect to automated image segmentation of archaeological materials, and, in fact, most image processing tasks, the tools required to address specific research questions will vary according to a variety of conditions. In paleoradiological analysis, this may entail various states of preservation, materials and material densities, hardware accessibility, and scanner specifications. Image segmentation is only one of many image processing tasks that can be automated using deep learning. For instance, deep learning in Dragonfly can be used for denoising and super-resolution, which may require different architectures than the ones tested in this thesis. The specific details of these image processing tasks are beyond the scope of this analysis, but can be explored further with the help of the tutorials provided by ORS and may be beneficial for addressing future visualization issues with other samples or research objectives (https://www.theobjects.com/dragonfly/deep-learning-getting-started.html).

There are several considerations for future analysis on the sample from Pachacamac as well. The most obvious is to CT scan all 72 fardos recovered from the MUNA Project and survey the full collection to increase the available sample size for biodistance analysis. Another possible direction would be to compare the sample of fardos with other individuals (both mummified and skeletal) from a variety of samples from Pachacamac. For instance, there is skeletal material from the cemetery excavated by the MUNA project that could provide further information on the sample (Baldeos, 2015). This would increase the sample size from Pachacamac and allow for a comparison or classification of individuals based on associated artifacts.

DNA analysis would be the most effective for elucidating genetic relatedness of the individuals in this sample. To increase sample size, dental nonmetric traits should also be considered because the number of available samples is much greater for teeth than

crania. Several studies have illustrated utility of dental nonmetrics in biodistance analyses (e.g., Corruccini & Shimada, 2002; Sutter, 2000; Sutter & Verano, 2007). However, this would likely require a high-resolution imaging solution (micro-CT) in order to adequately visualize the features of the individual teeth (Nelson & Kogon, 2021). Biodistance analysis using craniometrics can also be performed in Dragonfly, but this is not recommended due to the high prevalence of artificial cranial modification. This has been shown to significantly impact craniofacial measurements (Anton, 1989; Cheverud et al., 1992).

Overall, bioarchaeological analysis of mummified material using CT presents a unique set of challenges and requires exploratory approaches to traditional methodologies. Future improvements in our ability to automate image processing tasks will enable more efficient analyses of even larger samples. With more resources available to practitioners who are not computer science or imaging specialists coupled with increased access to archaeological samples via online databases, such as the IMPACT database (Nelson & Wade, 2015), paleoradiological analyses will likely begin to explore more complex research questions addressing materials that have been historically difficult or tedious to study non-destructively.

References

Aldenderfer, M. S. (1999). The Pleistocene/Holocene transition in Peru and its effects upon human use of the landscape. *Quaternary International 53/54*, 11–19.

Aldenderfer, M., & Blashfield, R. (1984). *Cluster analysis*. Sage Publications, Inc.

Allam, A. H., Thompson, R.C., Miyamoto, M. I., & Gregory S Thomas, G.S. (2009). Computed tomographic assessment of atherosclerosis in ancient Egyptian mummies. *Jama,* 302, 2091–2094. https://doi.org/10.1001/jama.2009.1641

Anscombe, F.J. (1948). The transformation of Poisson, binomial and negative-binomial data. *Biometrika, 35*(3-4), 246-254.

Anton, S. C. (1989). Intentional cranial vault deformation and induced changes of the cranial base and face. *American Journal of Physical Anthropology*, *79*(2), 253–267. https://doi.org/10.1002/ajpa.1330790213

Armelagos, G. J., & Gerven, D. P. Van. (2003). A century of skeletal biology and paleopathology: Contrasts, contradictions, and conflicts. *American Anthropologist*, *105*(1), 53–64. https://doi.org/10.1525/aa.2003.105.1.53

Armelagos, G. J., Carlson, D. S., & Van Gerven, D. P. (1982). The theoretical foundations and development of skeletal biology. In F. Spencer (Ed.), *A history of American physical anthropology* (pp. 305-328). Academic Press.

Baldeos Terrones, J, A. (2015). *Proyecto de rescate arqueológico en el sitio monumental de Pachacamac – Sector 3. Informe de proyecto de rescate arqueológico para la construcción del Museo Nacional del Perú "Muna".* Museo de Sitio – Pachacamac.

Barberena, R., Durán, V. A., Novellino, P., Winocur, D., Benítez, A., Tessone, A., Quiroga, M. N., Marsh, E. J., Gasco, A., Cortegoso, V., Lucero, G., Llano, C., & Knudson, K. J. (2017). Scale of human mobility in the southern Andes (Argentina and Chile): A new framework based on strontium isotopes. *American Journal of Physical Anthropology*, *164*(2), 305–320. https://doi.org/10.1002/ajpa.23270

Bauer, D. E. (2007). The reinvention of tradition: An Ethnographic study of spondylus use in coastal Ecuador. *Journal of Anthropological Research*, *63*(1), 33–50. https://doi.org/10.3998/jar.0521004.0063.104

Bauer, Brian S., & Stanish, C. (2001). *Ritual and pilgrimage in the ancient Andes: The Islands of the sun and the moon.* University of Texas Press.

Beckett, R. G., & Conlogue, G. J. (2009). *Paleoimaging: Field applications for cultural remains and artifacts*. Taylor & Francis Group.

Beckett, R. G., & Conlogue, G. J. (2020). *Advances in paleoimaging. Applications for paleoanthropology, bioarchaeology, forensics, and cultural artefacts*. CRC Press.

Bell, S., & Jantz, R. (2002). Neural network classification of skeletal remains. In G. Burenhult & J. Arvidsson (Eds.), *Archaeological informatics: Pushing the envelope. CAA2001. Computer Applications and Quantitative Methods in Archaeology. Proceedings of the 29th Conference, Gotland, April 2001*. Archaeopress.

Bengio, Y., Lamblin, P., Popovici, D., & Larochelle, H. (2006). Greedy layer-wise training of deep networks. In *Proceedings of the 19th International Conference on Neural Information Processing Systems (NIPS'06)*. MIT Press.

Berger, S. L., Kouzarides, T., Shiekhattar, R., & Shilatifard, A. (2009). An operational definition of epigenetics. *Genes and Development*, *23*(7), 781–783. https://doi.org/10.1101/gad.1787609

Berry, A. C. (1975). Factors affecting the incidence of non-metrical skeletal variants. *Journal of Anatomy*, *120*(3), 519–535. https://www.ncbi.nlm.nih.gov/pmc/articles/PMC1231693/

Berry, A. C., & Berry, R. J. (1967). Epigenetic variation in the human cranium. *Journal of Anatomy*, *101*(2), 361–379.

Besom, T., 2009. *Of summits and sacrifice: An ethnohistory study of Inka religious practices.* University of Texas Press.

Binford, M. W., Kolata, A. L., Brenner, M., Janusek, J. W., Seddon, M. T., Abbott, M., & Curtis, J. H. (1997). Climate variation and the rise and fall of an Andean civilization. *Quaternary Research*, *47*(2), 235–248. https://doi.org/10.1006/qres.1997.1882

Bird, J. B. (1943). *Excavations in northern Chile* (Vol. 38). Anthropological Papers of the American Museum of Natural History.

Blom, D. E. (2005). Embodying borders: Human body modification and diversity in Tiwanaku society. *Journal of Anthropological Archaeology*, *24*(1), 1–24. https://doi.org/10.1016/j.jaa.2004.10.001

Blom, D. E., & Knudson, K. J. (2014). Tracing Tiwanaku childhoods: A bioarchaeological study of age and social identities in Tiwanaku society. In J. L. Thompson, M. P. Alfonso-Durruty, & J. J. Crandall (Eds.), *Tracing childhood: Bioarchaeological investigations of early lives in antiquity*, (pp. 228–245).

Blom, D. E., Lozada, M. C., Hallgrímsson, B., Keng, L., & Buikstra, J. E. (1998). Tiwanaku 'colonization': Bioarchaeological implications for migration in the Moquegua Valley, Peru. *World Archaeology*, *30*(2), 238–261. https://doi.org/10.1080/00438243.1998.9980409

Böni, T., Rühli, F. J., & Chhem, R. K. (2004). History of paleoradiology: Early published literature, 1896-1921. *Canadian Association of Radiologists Journal*, *55*(4), 203–210. https://pubmed.ncbi.nlm.nih.gov/15362342/

Boston, C. E., Smith, D., Ubeda, C., Chandia, M., & Gonzalez, M. (2015). Examining the effects of artificial cranial modification on craniofacial metrics. *Chungara*, *47*(2), 331–341. https://doi.org/10.4067/s0717-73562015005000028

Brasili, P., Zaccagni, L., & Gualdi-Russo, E. (1999). Scoring of nonmetric cranial traits: a population study. *American Journal of Anatomy*, *195*(4), 551–562. https://doi.org/10.1046/j.1469-7580.1999.19540551.x

Breiman, L. (2001). Random forests. *Machine Learning*, *45*, 5–32. https://doi.org/10.1023/A:1010933404324

Bueno Mendoza, A. (1974). Cajamarquilla y Pachacamac: Dos ciudades de la Costa Central del Perú. *Boletín Bibliográfico de Antropología Americana*, *37*(46), 171–201.

Buikstra, J.E. (1972). *Hopewell in the Lower Illinois River Valley: A regional approach to the study of biological variability and mortuary activity* [Doctoral dissertation]. The University of Chicago.

Buikstra J.E., & Ubelaker, D. (1994). *Standards for data collection from human skeletal remains.* Arkansas Archaeological Survey Press.

Buikstra, J. E., Frankenberg, S. R., & Konigsberg, L. W. (1990). Skeletal biological distance studies in American Physical Anthropology: Recent trends. *American Journal of Physical Anthropology*, *82*(1), 1–7. https://doi.org/10.1002/ajpa.1330820102

Burger, R. L. (1988). Unity and heterogeneity within the Chavín Horizon. In R.W. Keatinge (Ed.) *Peruvian prehistory* (pp. 99-144). Cambridge University Press.

Burger, R. L. (1992). *Chavin and the origins of Andean civilization.* Thames and Hudson.

Burger, R., & Salazar, L. (2014). ¿Centro de qué? Los sitios con arquitectura pública de la cultura Manchay en la costa central del Perú. *Senri Ethnological Studies*, *89*, 291–313.

Carson, E. A. (2006). Maximum-likelihood variance vomponents analysis of heritabilities of cranial nonmetric traits. *Human Biology*, *78*(4), 383–402. 10.1353/hub.2006.0054

Castillo, L. J. (2012). *San José de Moro y el fin de los Mochicas en el Valle de Jequetepeque, Costa Norte del Perú*. [Doctoral dissertation, University of California Los Angeles] ProQuest Dissertations Publishing. https://escholarship.org/uc/item/0th2s0ss

Castillo, L. J., & Quilter, J. (2010). Many Moche models: An overview of past and current theories and research on Moche political organization. In J. Quilter & L. J. Castillo (Eds.). *New perspectives on Moche political organization* (pp. 1–16). Dumbarton Oaks.

Cavalli, G., & Heard, E. (2019). Advances in epigenetics link genetics to the environment and disease. *Nature*, *571*(7766), 489–499. https://doi.org/10.1038/s41586-019-1411-0

Ceruti, M.C., (2015). Frozen mummies from Andean mountaintop shrines: Bioarchaeology and ethnohistory of Inca human sacrifice. *BioMed Research International*, pp.1–12. https://doi.org/10.1155/2015/439428

Cesnys G. 1982. Side difference of non-metric cranial traits in the lst-2nd millenia A.D. Lithuanian materials. *Homo, 33*, 201-210.

Cheverud, J.M., & Buikstra, J.E. (1981a) Quantitative genetics of skeletal non-metrics in the rhesus macaques on Cayo Santiago II. Phenotypic, genetic, and environmental correlations between traits. *American Journal of Physical Anthropology, 54*:51-58.

Cheverud J.M., & Buikstra, J.E. (1981b). Quantitative genetics of skeletal nonmetric traits in the rhesus macaques on Cayo Santiago. I. Single trait heritabilities. *American Journal of Physical Anthropology, 54*(l):43-49.

Cheverud, J. M., Kohn, L. A. P., Konigsberg L. W., Leigh, S. R. (1992). Effects of fronto-occipital artificial cranial vault modification on the cranial base and face. *American Journal of Physical Anthropology, 88*, 323-345.

Chhem, R. K., & Brothwell, D. R. (2008). *Paleoradiology: Imaging Mummies and Fossils*. Springer Berlin Heidelberg.

Chhem, R. K., & Rühli, F. J. (2004). Paleoradiology: Current status and future challenges. *Canadian Association of Radiologists Journal*, *55*(4), 198–199.

Choy, G., Khalilzadeh, O., Michalski, M., Do, S., Samir, A. E., Pianykh, O. S., Geis, J. R., Pandharipande, P. V., Brink, J. A., & Dreyer, K. J. (2018). Current applications and future impact of machine learning in radiology. *Radiology*, *288*(2), 318–328. https://doi.org/10.1148/radiol.2018171820

Cieza de León, P. de. (1984). *La crónica del Perú.* (M. Ballesteros, Trans.). Historia 16, Madrid. (Original work published ca. 1553).

Cobo, B. (1979). *History of the Inca empire: An account of the indians' customs and their origin together with a treatise on Inca legends, history, and social institutions.* (R. Hamilton, Ed., Trans.). University of Texas Press. (Original work published ca. 1653).

Coleman, S. & Elsner, J. (1994). The pilgrim's process: Art, architecture and ritual movement at Sinai. *World Archaeology, 26*(1): 73–89.

Colleter, R., Dedouit, F., Duchesne, S., Gérard, P., Dercle, L., Poilpré, P., Gendrot, V., Rousseau, H., Crubézy, É., Telmon, N., Mokrane, F. Z. (2018). Study of a seventeenth-century French artificial mummy: autopsical, native, and contrast-injected CT investigations. *International Journal of Legal Medicine*, *132*(5), 1405–1413. https://doi.org/10.1007/s00414-018-1830-8

Colman, K. L., de Boer, H. H., Dobbe, J. G. G., Liberton, N. P. T. J., Stull, K. E., van Eijnatten, M., Streekstra, G. J., Oostra, R. J., van Rijn, R. R., & van der Merwe, A. E. (2019). Virtual forensic anthropology: The accuracy of osteometric analysis of 3D bone models derived from clinical computed tomography (CT) scans. *Forensic Science International*, *304*(2019), 1-10. https://doi.org/10.1016/j.forsciint.2019.109963

Conklin, W. J., & Moseley, M. E. (1988). The patterns of art and power in the Early Intermediate Period. In R. W. Keatinge (Ed.), *Peruvian Prehistory* (pp.145-165). Cambridge University Press.

Conlogue, G. J., & Nelson, A. J. (1999). Polaroid imaging at an archaeological site in Peru. *Radiologic Technology*, *70*(3), 244–250.

Contreras, D. A. (2010). Landscape and environment: Insights from the prehispanic central Andes. *Journal of Archaeological Research*, *18*(3), 241–288. https://doi.org/10.1007/s10814-010-9038-6

Contreras, D. A. (2017). (Re)constructing the sacred: Landscape geoarchaeology at Chavín de Huántar, Peru. *Archaeological and Anthropological Sciences*, *9*(6), 1045–1057. https://doi.org/10.1007/s12520-014-0207-2

Cormack, A. M. (1963). Representation of a function by its line integrals, with some radiological applications. *Journal of Applied Physics*, *34*(9), 2722–2727. https://doi.org/10.1063/1.1713127

Cormack, A. M. (1964). Representation of a function by its line integrals, with some radiological applications. II." *Journal of Applied Physics, 35*, 2908-2913. https://doi.org/10.1063/1.1713127

Corruccini, R. S. (1974). An examination of the meaning of cranial discrete traits for human skeletal biological studies. *American Journal of Physical Anthropology*, *40*(3), 425–446. https://doi.org/10.1002/ajpa.1330400315

Corruccini, R. S., & Shimada, I. (2002). Dental relatedness corresponding to mortuary patterning at Huaca Loro, Peru. *American Journal of Physical Anthropology*, *117*(2), 113–121. https://doi.org/10.1002/ajpa.10020

Cosmacini, P., & Piacentini, P. (2008). Notes on the history of the radiological study of Egyptian mummies: from X-rays to new imaging techniques. *Radiologia Medica*, *113*(5): 615–626. https://doi.org/10.1007/s11547-008-0280-7

Cossu, R., & Chiappini, L. (2004). A color image segmentation method as used in the study of ancient monument decay. *Journal of Cultural Heritage*, *5*(4), 385-391. https://doi.org/10.1016/j.culher.2004.03.005

Covey, R. A. (2006). Chronology, succession, and sovereignty: The politics of Inka historiography and its modern interpretation. *Comparative Studies in Society and History*, *48*(1), 169–199. https://doi.org/10.1017/S0010417506000077

Covey, R. A. (2008). Multiregional perspectives on the archaeology of the Andes during the Late Intermediate Period (c. A.D. 1000-1400). *Journal of Archaeological Research*, *16*(3), 287–338. https://doi.org/10.1007/s10814-008-9021-7

Covey, R. A. (2018). Archaeology and Inka origins. *Journal of Archaeological Research*, *26*(3), 253–304. https://doi.org/10.1007/s10814-017-9110-6

Cramer, L., Brix, A., Matin, E., Rühli, F., and Hussein, K. (2018). Computed tomography–detected paleopathologies in ancient Egyptian mummies. *Current Problems in Diagnostic Radiology*, *47*: 225–32. https://doi.org/10.1067/j.cpradiol.2017.06.012

Czibula, G., Ionescu, V., Miholca, D., & Mircea, I. (2016). Machine learning-based approaches for predicting stature from archaeological skeletal Remains using long bone lengths. *Journal of Archaeological Science* 69: 85–99. https://doi.org/10.1016/j.jas.2016.04.004

Davis, C., & Coningham, R. (2018). Pilgrimage and procession: temporary gatherings and journeys between the tangible and intangible through the archaeology of South Asia. *World Archaeology*, *50*(2), 347–363. https://doi.org/10.1080/00438243.2018.1490199

Decker, S. J., Davy-Jow, S. L., Ford, J. M., & Hilbelink, D. R. (2011). Virtual determination of sex: Metric and nonmetric traits of the adult pelvis from 3D computed tomography models. *Journal of Forensic Sciences*, *56*(5), 1107–1114. https://doi.org/10.1111/j.1556-4029.2011.01803

De Leeuw, J., & Mair, P. (2009). Multidimensional scaling using majorization: SMACOF in R. *Journal of Statistical Software*, *31*(3), 1–30. https://doi.org/10.18637/jss.v031.i03

Del Papa, M., & Perez, S. I. (2007). The influence of artificial cranial vault deformation on the expression of cranial nonmetric traits: Its importance in the study of evolutionary relationships. *American Journal of Physical Anthropology*, *134*, 251–262. https://doi.org/10.1002/ajpa

De Molina, C. (2011). *Account of the fables and rites of the Incas*. (B. S. Bauer, V. Smith-Oka, G. E. Cantarutti, Trans., Eds.). University of Texas Press. (Original Work Published ca. 1575).

Dice, L. R. (1945). Measures of the amount of ecologic association between species. *Ecology*, *26*(3), 297–302.

Dillehay, T. D., Eling, H. H., & Rossen, J. (2005). Preceramic irrigation canals in the Peruvian Andes. *Proceedings of the National Academy of Sciences of the United States of America*, *102*(47), 17241–17244. https://doi.org/10.1073/pnas.0508583102

Earle, T. K. (1972). Lurin Valley, Peru: Early Intermediate Period settlement development. *American Antiquity*, *37*(4), 467–477.

Ebersole, M. (2012, September). *What is CUDA?* NVIDIA. https://blogs.nvidia.com/blog/2012/09/10/what-is-cuda-2/

Eeckhout, P. (1999). The palaces of the lords of Ychsma: An archaeological reappraisal of the function of Pyramids with Ramps at Pachacamac, Central Coast of Peru. *Revista de Arqueología Americana*, 217–254. http://dx.doi.org/10.1016/j.jaci.2012.05.050

Eeckhout, P. (2003). Ancient monuments and patterns of power at Pachacamac, Central Coast of Peru. *Beiträge Zur Allgemeine Und Vergleichenden Archäologie*, *23*, 139-182.

Eeckhout, P. (2004a). La sombra de Ychsma. *Bulletin de l'Institut Français d'études Andines*, *33 (3)*, 403–423. https://doi.org/10.4000/bifea.5047

Eeckhout, P. (2004b). Pachacamac y el Proyecto Ychsma (1999-2003). *Bulletin de l'Institut Français d'études Andines*, *33*(33 (3)), 425–448. https://doi.org/10.4000/bifea.5049
Eeckhout, P. (2013). Change and permanency on the coast of ancient Peru: The religious site of Pachacamac. *World Archaeology*, *45*(1), 137–160. https://doi.org/10.1080/00438243.2012.759516

Eeckhout, P. (2013). Change and permanency on the coast of ancient Peru: The religious site of Pachacamac. *World Archaeology*, *45*(1), 137–160. https://doi.org/10.1080/00438243.2012.759516

Ellis, L., Suda, A., Martin, R.M., Moffatt, E., Poulin, J., and Nelson, A.J. 2017. The virtual deconstruction of a prayer bead in the Thomson Collection at the Art Gallery of Ontario with micro-CT scanning and advanced 3D analysis software. In E. Wetter & F. Scholten (eds), Prayer-nuts, private devotion and early modern art collecting (pp. 209–217). Abegg-Siftung.

Epstein, C. L. (2007). A basic model for tomography. In C. L. Epstien (Ed.), *Introduction to the Mathematics of Medical Imaging* (pp. 53–90). https://doi.org/10.1137/1.9780898717792.ch3

Feldkamp, L. A., S. A., Parfitt, M.A., Jesion, G., & Kleerekoper, M. (1989). The direct examination of three-dimensional bone architecture in vitro by computed tomography. *Journal of Bone and Mineral Research*, *4*(1), 3–11. https://doi.org/10.1002/jbmr.5650040103

Fleming, S. (1986). The mummies of Pachacamac: An exceptional legacy from Uhle's 1896 excavations in Peru. *Expedition*, *28*(3), 39–45.

Flores, G. M. (2019). The cultural trajectory of the Central Peruvian Coast, the territory and its people in the valleys of pre-Hispanic Lima. In E. A. Engel (Ed.), *A companion to early modern Lima* (pp. 25–45). https://doi.org/10.1163/9789004335363

Franco Jordan, R. (1988). *La Pirámide con Rampa n°2 de Pachacamac. Excavaciones y nuevas interpretaciones.*

Freeman, M. F., & Tukey, J. W. (1950). Transformations related to the angular and the square root. *The Annals of Mathematical Statistics, 21*(4), 607–611. https://doi.org/10.1214/aoms/1177729756

Frey, G. D. (2014). Basic CT parameters. *American Journal of Roentgenology*, *203*(2), 126–127. https://doi.org/10.2214/AJR.13.10994

Friedman, S. N., Nguyen, N., Nelson, A. J., Granton, P. V., MacDonald, D. B., Hibbert, R., Cunningham, I. A. (2012). Computed tomography (CT) bone segmentation of an ancient Egyptian mummy a comparison of automated and semiautomated threshold and dual-energy techniques. *Journal of Computer Assisted Tomography*, *36*(5), 616–622. https://doi.org/10.1097/RCT.0b013e31826739f5

Gomart, L., Weiner, A., Gabriele, M., Durrenmath, G., Sorin, S., Angeli, L., Colombo, M., Fabbri, C., Maggi, R., Panelli, C., Pisani, D. F., Radi, G., Tozzi, C., & Binder, D. (2017). Spiralled patchwork in pottery manufacture and the introduction of farming to Southern Europe. *Antiquity*, *91*(360), 1501–1514. https://doi.org/10.15184/aqy.2017.187

Green, R. F., & Suchey, J. M. (1976). The use of inverse sine transformations in the analysis of non-metric cranial data. *American Journal of Physical Anthropology*, *45*(1), 61–68. https://doi.org/10.1002/ajpa.1330450108

Green, R. F., Suchey, J. M., & Gokhale, D. V. (1979). The statistical treatment of correlated bilateral traits in the analysis of cranial material. *American Journal of Physical Anthropology*, *50*(4), 629–634. https://doi.org/10.1002/ajpa.1330500414

Grewal, M. S. (1962). The rate of genetic divergence of sublines in the C57BL strain of mice. *Genetics Research*, *3*(2), 226–237. https://doi.org/10.1017/S0016672300035011

Grüneberg H. (1952). Genetical studies on the skeleton of the mouse. IV. Quasicontinuous variation. *Journal of Genetics, 51*:95-114.

Gugerty, L. (2006). Newell and Simon's Logic Theorist: Historical background and impact on cognitive modeling. *Proceedings of the Human Factors and Ergonomics Society*, 880–84. https://doi.org/10.1037/e577632012-004

Harris E.F. (2008). Statistical applications in dental anthropology. In J. D. Irish & G. C. Nelson (Eds.), *Technique and application in dental anthropology* (pp. 35-67). Cambridge University.

Harris, E. F., & Sjøvold, T. (2004). Calculation of Smith's Mean Measure of Divergence for intergroup comparisons using nonmetric data. *Dental Anthropology Journal*, 17(3), 83–93. https://doi.org/10.26575/daj.v17i3.152

Harrison-Buck, E., Runggaldier, A., & Gantos, A. (2018). It's the journey not the destination: Maya New Year's pilgrimage and self-sacrifice as regenerative power. *Journal of Social Archaeology*, *18*(3), 325–347. https://doi.org/10.1177/1469605318764138

Hati, A., Bustreo, M., Sona, D., Murino, V., & Del Bue, A. (2020). *Weakly Supervised Geodesic Segmentation of Egyptian Mummy CT Scans*. http://arxiv.org/abs/2004.08270

Hauser, V., & De Stefano, R. (1989). *Epigenetic variants of the human skull*. Stuttgart: E. Schewizerbartsche Verlagsbuchhandlung.

Hefner, J. T., Pilloud M. A., Buikstra J. E., Vogelsberg, C. C. M. (2016). A brief history of biological distance analysis. In M. A. Pilloud & J. T. Hefner (Eds.) *Biological distance analysis: Forensic and bioarchaeological perspectives* (pp. 3-22). Academic Press.

Herrera, B., Hanihara, T., & Godde, K. (2014). Comparability of multiple data types from the bering strait region: Cranial and dental metrics and nonmetrics, mtDNA, and Y-chromosome DNA. *American Journal of Physical Anthropology, 154*(3), 334–348. https://doi.org/10.1002/ajpa.22513

Herrera, S. (2016). *Death and the family: Testing Andean lineage tombs through cranial non-metrics* (Publication No. 10240371) [Masters thesis]. Colorado State University.

Higuchi, R., Bowman, B., Freiberger, M., Ryder, O. A., Wilson, A. C. (1984). DNA sequences from the quagga, an extinct member of the horse family. *Nature, 312*, 282–284. https://doi.org/10.1038/312282a0

Howells, W. W. (1973). *Cranial variation in man: A study by multivariate analysis of patterns of difference among recent human populations* (Vol. 67). Peabody museum of archaeology and ethnology.

Huffman, T. N., & Earley, F. L. (2019). The smell of power: The Apishapa pilgrimage trail. *Time and Mind, 12*(4), 267–286. https://doi.org/10.1080/1751696X.2019.1681745

Hughes, S. (2011). CT scanning in archaeology. In L. Saba (Ed.), *Computed Tomography-Special Applications* (pp. 57–70). https://doi.org/10.5772/22741

Hyslop, J. (1990). *Inka settlement planning.* University of Texas Press.

Ionescu, V., Teletin, M., & E. Voiculescu, E. (2016). Machine learning techniques for age at death estimation from long bone lengths. *2016 IEEE 11th International Symposium on Applied Computational Intelligence and Informatics (SACI),* 2016, pp. 457-462, 10.1109/SACI.2016.7507421

Irish, J. D. (2010). The mean measure of divergence: Its utility in model-free and model-bound analyses relative to the Mahalanobis D^2 distance for nonmetric traits. *American Journal of Human Biology*, *22*(3), 378–395. https://doi.org/10.1002/ajhb.21010

Ishida, H., & Dodo, Y. (1993). Nonmetric cranial variation and the populational affinities of the Pacific peoples. *American Journal of Physical Anthropology*, *90*(1), 49–57. https://doi.org/10.1002/ajpa.1330900104

Jahnke, L. M. (2009). *Human biological variation and cemetery distribution in the Huaura Valley, Peru* [Doctoral dissertation]. Tulane University.

Jantz, R.L. (1970). *Change and variation in skeletal populations of Arikara Indians* [Doctoral dissertation]. University of Kansas.

Jennings, J. (2008). Catastrophe, revitalization and religious change on the prehispanic North Coast of Peru. *Cambridge Archaeological Journal, 18*, 177–194. https://doi.org/10.1017/S0959774308000243

Johnson, A. W. (2014). El poder de los huesos: Peregrinaje e identidad en ixcateopan de cuauhtémoc, guerrero. *Anales de Antropología*, *48*(2), 119–149. https://doi.org/10.1016/s0185-1225(14)70246-2

Keatinge, R. W. (1978). The Pacatnamu textiles. *Archaeology, 31*, 30-41.

Kim, Y. S., Hong, J. H., Oh, C. S., Kim, M. J., Cha, S. C., Park, J. B., Lee, I. S., Yoo, D. S., & Shin, D. H. (2018). Post-factum autopsy to confirm cardiac structures visible on computed tomography images of Korean mummies: The radiological basis of paleocardiology. *Anthropologischer Anzeiger*, *75*(4), 339–350. https://doi.org/10.1127/anthranz/2018/0924

Knudson, K. J., & Stojanowski, C. M. (2009). The bioarchaeology of identity. In K. J. Knudson & C. M. Stojanowski (Eds.) *Bioarchaeology and Identity in the Americas* (pp. 1–23).

Knudson, K. J., & Tung, T. A. (2011). Investigating regional mobility in the southern hinterland of the Wari empire: Biogeochemistry at the site of Beringa, Peru. *American Journal of Physical Anthropology*, *145*(2), 299–310. https://doi.org/10.1002/ajpa.21494

Kolata, A. L. (2000). Environmental thresholds and the 'natural history' of an Andean civilization. In G. Bawden & R. M. Reycraft (Eds.), *Environmental disaster and the archeology of human response* (pp. 163–178). University of New Mexico Press.

Konigsberg L, Buikstra J. (2006). Population structure analysis from prehistoric skeletal material. *American Journal of Physical Anthropology, 42*, 115.

Konigsberg, L. W., Kohn, L. A. P., & Cheverud, J. M. (1993). Cranial deformation and nonmetric trait variation. *American Journal of Physical Anthropology*, *90*(1), 35–48. https://doi.org/10.1002/ajpa.1330900103

Kozatsas, J., Kotsakis, K., Sagris, D., & David, K. (2018). Inside out: Assessing pottery forming techniques with micro-CT scanning. An example from Middle Neolithic Thessaly. *Journal of Archaeological Science*, *100*(2018), 102–119. https://doi.org/10.1016/j.jas.2018.10.007

Kruskal, J. B. (1964). Nonmetric multidimensional scaling: A numerical method. *Psychometrika*, *29*(2), 115–129. https://doi.org/10.1007/BF02289565

Lane, R. A., & Sublett, A. J. (1972). Osteology of social organization: Residence pattern. *American Antiquity*, *37*(2), 186–201. https://doi.org/10.2307/278205

Lanning, E. P. (1963). An early ceramic style from Ancon, Central Coast of Peru. *Ñawpa Pacha, 1*(1), 47–59. https://doi.org/10.1179/naw.1963.1.1.006

Las Casas, B. d. (1967). *Apologética historia sumaria*. Edited by Edmundo O'Gorman. México, D.F.: Universidad Nacional Autónoma de México, Instituto de Investigaciones Históricas. (Original work published ca. 1552-1561).

Lash, R. (2018). Enchantments of stone: Confronting other-than-human agency in Irish pilgrimage practices. *Journal of Social Archaeology*, *18*(3), 284–305. https://doi.org/10.1177/1469605318762816

Leahy, R M, and R Clackdoyle. 2005. Computed tomography. In A. Bovik (Ed.), *Handbook of Image and Video Processing*, (pp. 1155–1172). Academic Press.

Lewin, P.K., & Harwood-Nash, D.C. (1979). X-ray computed axial tomography of an ancient Egyptian brain. *IRCS Medical Science: Anatomy and Human Biology: Biomedical Technology: Nervous System*, 5(78).

Locker, M. (2015). *Landscapes of pilgrimage in medieval Britain.* Archaeopress.

Lucero, L. J., & Kinkella, A. (2015). Pilgrimage to the edge of the watery underworld: An ancient Maya water temple at Cara Blanca, Belize. *Cambridge Archaeological Journal*, *25*(1), 163–185. https://doi.org/10.1017/S0959774314000730

Lymer, K. (2004). Rags and rock art: The landscapes of holy site pilgrimage in the Republic of Kazakhstan. *World Archaeology*, *36*(1): 158–172.

Mac Kay, M., & Santa Cruz, R. (2000). Las excavaciones del Proyecto Arqueológico Huaca 20 (1999 y 2001). *Boletín de Arqueología PUCP*, *4*, 583–595.

Mackey, C. J., & Nelson, A. J. (2020). *Life, death and burial practices during the Inka occupation of Farfán, on Perú's North Coast* (M. Barnes & R. A. Phillips, Eds.). Andean Past Monographs.

Makovetsky, R., Piche, N., & Marsh, M. (2018). Dragonfly as a platform for easy image-based deep learning applications. *Microscopy and Microanalysis*, *24*(1), 532–533. https://doi.org/10.1017/s143192761800315x

Martin, D. L., Harrod, R. P., & Pérez V. R. (2015). *Bioarchaeology: An integrated approach to working with human remains*. Berlin: Springer.

Matos Mar, J., & Mendoza, J. P. (1964). *El valle de Lurín y el pueblo de Pachacamac: Cambios sociales y culturales*. Universidad Nacional Mayor de San Marcos, Departamento de Antropología.

Matsumoto, G. (2005). *Pachacamac GIS Project: A practical application of geographic information systems and remote sensing techniques in Andean archaeology*. [Masters thesis]. Southern Illinois University at Carbondale.

McKetty, M. H. (1998). The AAPM/RSNA physics tutorial for residents: X-ray attenuation. *Radiographics*, *18*(1), 151–163. https://doi.org/10.1148/radiographics.18.1.9460114

Menzel, D., Rowe, J. H., & Dawson, L. E. (1964). *The Paracas pottery of Ica; a study in style and time*. University of California Press.

Michczyński, A., Eeckhout, P., & Pazdur, A. (2003). ^{14}C absolute chronology of Pyramid III and the dynastic model at Pachacamac, Peru. *Radiocarbon*, *45*(1), 59–73. https://doi.org/10.1017/S0033822200032392

Molto, J. E. (1980). *Biological relationships of southern Ontario woodland peoples* [Doctoral dissertation, University of Toronto]. University of Ottawa Press. https://doi.org/10.2307/j.ctv170sj

Moore, J. D. (2005). *Cultural landscapes in the ancient Andes*. University Press of Florida.

Moseley, M. E. (2001). The Incas and their ancestors: The archaeology of Peru (Rev. ed.). Thames & Hudson.

Murra, J. V. (1980). *The economic organization of the Inka state*. JAI Press.

Navega, D., Coelho, J. d. O., Cunha, E., & Curate, F. (2018). DXAGE: A new method for age at death estimation based on femoral bone mineral density and artificial neural networks. *Journal of Forensic Sciences*, *63*(2), 497–503. https://doi.org/10.1111/1556-4029.13582

Navega, D., Vicente, R., Vieira, D. N., Ross, A. H., & Cunha, E. (2015). Sex estimation from the tarsal bones in a Portuguese sample: a machine learning approach. *International Journal of Legal Medicine*, *129*(3), 651–659. https://doi.org/10.1007/s00414-014-1070-5

Nelson, A. J., & Kogon, S. (2021). Teeth: Plane radiography (film); Clinical CT; MicroCT. In R. G. Beckett, G. J. Conlogue, A. J. Nelson, (Eds.), *Case studies for advances in paleoimaging and other non-clinical applications* (pp. 99-110). CRC Press.

Nelson, A. J., & Wade, A. D. (2015). Impact: Development of a radiological mummy database. *Anatomical Record*, *298*(6), 941–948. https://doi.org/10.1002/ar.23130

Nelson, A. J., Nelson, C. S., Castillo, L. J., & Mackey, C. (2000). Osteobiography of a Pre-Columbian spinner: The woman behind the mask. *Iconos*, *4*, 30–43.

Nelson, A. J., Watson, L., Williams, J., Gauld, S., Motley, J., Poeta, L., Seston, D., Gómez, E., Baldeos, J., Fuentes, S., & Pozzi-Escot, D. (2021). Análisis de los fardos funerarios de Pachacamac: Aplicación sistemática de Rayos X y tomografía computarizada en un contexto arqueológico. *Actas Del VI Congreso Nacional de Arqueología*, *1-2*, 293–308.

Nikita, E. (2015). A critical review of the mean measure of divergence and Mahalanobis distances using artificial data and new approaches to the estimation of biodistances employing nonmetric traits. *American Journal of Physical Anthropology*, *157*(2), 284–294. https://doi.org/10.1002/ajpa.22708

Notman, D. N., Tashjian, J., Aufderheide, A. C., Cass, O. W., Shane, O. C., Berquist, T. H., Grey, J. E., Gedgaudas, E. (1986). Modern imaging and endoscopic biopsy techniques in Egyptian mummies. *American Journal of Roentgenology*, *146*(1), 93–96. https://doi.org/10.2214/ajr.146.1.93

Novikov, A. A., Major, D., Wimmer, M., Lenis, D., & Buhler, K. (2019). Deep sequential segmentation of organs in volumetric medical scans. *IEEE Transactions on Medical Imaging*, *38*(5), 1207–1215. https://doi.org/10.1109/TMI.2018.2881678

Object Research Systems (ORS). (2020). *Dragonfly Daily* [Video]. YouTube. https://www.youtube.com/playlist?list=PLbYyniU4wPOtHGT0m68liH5SntwfETKsP

Object Research Systems (ORS). (2021). *Deep Learning FAQS*. Dragonfly Deep Learning Tool. http://www.theobjects.com/dragonfly/deep-learning-faq.html

O'Loughlin, V. D. (2004). Effects of different kinds of cranial deformation on the incidence of wormian bones. *American Journal of Physical Anthropology*, *123*(2), 146–155. https://doi.org/10.1002/ajpa.10304

Ordoñez, M. P., Beckett, R. G., Nelson, A. J., Conlogue, G. Paleoimagen y análisis bioantropológico de la colección Maranga del Museo Jancinto Jijon y Caamaño. *Antropología Cuadernos de Investigación*, *15*(2015), 63-79. https://doi.org/10.26807/ant.v0i15.37

Osborn, A. (1977). Strandloopers, mermaids, and other fairy tales: Ecological determinants of marine resource utilization-the Peruvian case. In L. R. Binford (Ed.), *For theory building in archaeology* (pp. 157–203). Academic Press.

Ossenberg, N.S. (1969). *Discontinuous morphological variation in the human cranium* [Doctoral dissertation]. University of Toronto.

Ossenberg, N. S. (1976). Within and between race distances in population studies based on discrete traits of the human skull. *American Journal of Physical Anthropology*, *45*(3), 701–716. https://doi.org/10.1002/ajpa.1330450337

Ossenberg, N S. (1981). An argument for the use of total side frequencies of bilateral nonmetric skeletal traits in population distance analysis: The regression of symmetry on incidence. *American Journal of Physical Anthropology*, *54*(4), 471-479.

Ossenberg, N. S. (2013). Brief communication: Cranial nonmetric trait database on the internet. *American Journal of Physical Anthropology*, *152*(4), 551–553. https://doi.org/10.1002/ajpa.22377

Panzer, S., Thompson, R. C., Hergan, K., Zink, A. R., & Piombino-Mascali, D. (2018). Evidence of aortic dissection and Marfan syndrome in a mummy from the Capuchin Catacombs of Palermo, Sicily. *International Journal of Paleopathology*, *22*(2018), 78–85. https://doi.org/10.1016/j.ijpp.2018.05.002

Parsons, M. H. (1970). Preceramic subsistence on the Peruvian coast. *American Antiquity*, *35*, 292–304.

Patterson, T. C. (1966). *Pattern and process in the Early Intermediate Period pottery of the Central Coast of Peru 3*. University of California Press.

Paulsen, A. C. (1974). The thorny oyster and the voice of god: Spondylus and strombus in Andean prehistory. *American Antiquity*, *39*(4), 597–607. https://doi.org/10.2307/278907

Paulsen, A. C. (1976). Environment and empire: Climatic factors in prehistoric Andean culture change. *World Archaeology*, *8*,121–132.

Piche, N., Bouchard, I., & Marsh, M. (2017). Dragonfly Segmentation Trainer- A general and user-friendly machine learning image segmentation solution. *Microscopy and Microanalysis*, *23*(1), 132–133. https://doi.org/10.1017/s1431927617001349

Pietrusewsky, M., Buckley, H., Anson, D., & Douglas, M. T. (2014). Polynesian origins: a biodistance study of mandibles from the Late Lapita site of Reber-Rakival (SAC), Watom Island, Bismarck Archipelago. *Journal of Pacific Archaeology*, *5*(1), 1–20.

Pink, C. M., Maier, C., Pilloud, M. A., Hefner, J. T. (2016). Cranial nonmetric and morphoscopic data sets. In M. A. Pilloud & J. T. Hefner (Eds.) *Biological distance analysis: Forensic and bioarchaeological perspectives* (pp. 91-108). Academic Press.

Pomeroy, E., Stock, J. T., Zakrzewski, S. R., & Lahr, M. M. (2010). A metric study of three types of artificial cranial modification from north-central Peru. *International Journal of Osteoarchaeology*, *20*(3), 317–334. https://doi.org/10.1002/oa.1044

Pozzi-Escot, D., & Uceda, C. R. (2019). El Museo Pachacamac en el siglo xxi. *Chungará Revista de Antropología Chilena*, *51*, 253–269. https://doi.org/10.4067/s0717-73562019005001404

Pulgar Vidal, J. (2014). Las ocho regiones naturales del Perú. *Terra Brasilis (Nova Série)*, *3*. (Original work published 1987). https://doi.org/10.4000/terrabrasilis.1027

Ramos, A. (2013). Max Uhle - Julio Tello: Una polémica académico-política en la conformación de la Arqueología peruana. *RUNA*, *34*(2), 197–214. https://doi.org/10.34096/runa.v34i2.643

Reinhard, J., & Ceruti, C. (2005). Sacred mountains, ceremonial sites, and human sacrifice among the Incas. *Archaeoastronomy*, *18*, 1–43.

Relethford, J., & Blangero, J. (1990). Detection of differential gene flow from patterns of quantitative variation. *Human Biology*, *62*(1), 5–25.

Ricaut, F. X., Auriol, V., Von Cramon-Taubadel, N., Keyser, C., Murail, P., Ludes, B., & Crubézy, E. (2010). Comparison between morphological and genetic data to estimate biological relationship: The case of the Egyin Gol necropolis (Mongolia). *American Journal of Physical Anthropology*, *143*(3), 355–364. https://doi.org/10.1002/ajpa.21322

Richtsmeier, J. T., & McGrath, J. W. (1986). Quantitative genetics of cranial nonmetric traits in randombred mice: Heritability and etiology. *American Journal of Physical Anthropology*, *69*(1), 51–58. https://doi.org/10.1002/ajpa.1330690107

Richtsmeier, J. T., Cheverud, J. M., & Buikstra, J. E. (1984). The relationship between cranial metric and nonmetric traits in the rhesus macaques from Cayo Santiago. *American Journal of Physical Anthropology*, *64*(3), 213–222. https://doi.org/10.1002/ajpa.1330640303

Robedizo, B. P. (2016). *The identifiability of osteological traits on 3D models of human skeletal remains* [Masters thesis] Lunds Universitet.

Ronneberger, O., Fischer, P., & Brox, T. (2015). U-net: Convolutional networks for biomedical image segmentation. *Lecture Notes in Computer Science (Including Subseries Lecture Notes in Artificial Intelligence and Lecture Notes in Bioinformatics)*, *9351*, 234–241. https://doi.org/10.1007/978-3-319-24574-4_28

Ross, A., Ubelaker, D., & Guillén, S. (2008). Craniometric patterning within ancient Peru. *Latin American Antiquity*, *19*(2), 158–166. https://doi.org/10.2307/25478221

Rostworowski de Diez Canseco, M. (1972). Breve informe sobre el señorío de Ychma o Ychima. *Arqueología PUC, 13*, 37-51. Instituto Riva-Agüero, Pontificia Universidad Católica del Perú.

Rostworowski de Diez Canseco, M. (1977). *Etnía y sociedad: Costa Peruana prehispánica.* Instituto de Estudios Peruanos.

Rothhammer F., & Santoro, C.M. (2002). El desarrollo cultural en el valle de Azapa, extremo norte de Chile y su vinculación con los desplazamientos poblacionales altiplánicos. *Latin American Antiquity*, *12*, 59–66.

Rothhammer, F., & Silva, C. (1989). Peopling of Andean South America. *American Journal of Physical Anthropology*, *78*(3), 403–410. https://doi.org/10.1002/ajpa.1330780308.

Rothhammer, F., Llop, E., Cocilovo, J. A., & Quevedo, S. (1982). Microevolution in prehistoric Andean populations: I. Chronologic craniometric variation. *American Journal of Physical Anthropology*, *58*(4), 391–396. https://doi.org/10.1002/ajpa.1330580406

Rothhammer, F., Quevedo, S., Cocilovo, J. A., & Llop, E. (1984). Microevolution in prehistoric Andean populations: Chronologic nonmetrical cranial variation in northern Chile.

American Journal of Physical Anthropology, *65*(2), 157–162. https://doi.org/10.1002/ajpa.1330650207

Sandweiss, D., & Richardson, J. (2008). Central Andean Environments. In *The handbook of South American archaeology* (pp. 93–104). https://doi.org/10.1007/978-0-387-74907-5

Rowe, J. H. (1962). Stages and Periods in Archaeological Interpretation. *Southwestern Journal of Anthropology*, *18*(1), 40–54. https://doi.org/10.1086/soutjanth.18.1.3629122

Russell, S., & Norvig, P. (1995). *Artificial intelligence: A modern approach*. Prentice Hall.

Santos, F. (2018). AnthropMMD: An R package with a graphical user interface for the mean measure of divergence. *American Journal of Physical Anthropology*, *165*(1), 200–205. https://doi.org/10.1002/ajpa.23336

Scott G.R., & Turner, C.G. (1997). *The anthropology of modern human teeth: Dental morphology and its variation in recent human populations.* Cambridge: Cambridge University Press. https://doi.org/10.1017/CBO9781316529843

Shady, R., & Ruiz, A. (1979). Evidence for Interregional Relationships during the Middle Horizon on the North- Central Coast of Peru. *American Antiquity*, *44*(4), 676–684.

Shaw, C. N., & Stock, J. T. (2013). Extreme mobility in the Late Pleistocene? Comparing limb biomechanics among fossil Homo, varsity athletes and Holocene foragers. *Journal of Human Evolution*, *64*(4), 242–249. https://doi.org/10.1016/j.jhevol.2013.01.004

Shimada, I. (1991). Pachacamac archaeology: Retrospect and prospect. In M. Uhle & I. Shimada (Eds.) *Pachacamac: A reprint of the 1903 edition.* University Museum of Archaeology and Anthropology, University of Pennsylvania.

Shimada, M., & Shimada, I. (1985). Prehistoric llama breeding and herding on the North Coast of Peru. *American Antiquity*, *50*(1), 3-26.

Shimada, I., Segura Llanos, R., Rostworowski De Diez Canseco, M., & Watanabe, H. (2004). Una nueva evaluación de la Plaza de los Peregrinos de Pachacamac: Aportes de la primera campaña 2003 del Proyecto Arqueólogico Pachacamac. *Bulletin de l'Institut Français d'études Andines*, *33*(3), 507–538. https://doi.org/10.4000/bifea.5106

Silverman, H. (2004). Introduction: Space and time in the central Andes. In H. Silverman (Ed.), *Andean Archaeology* (pp. 1–15). Blackwell.

Simeone, O. (2018). *A brief introduction to machine learning for engineers*. Foundations and Trends in Signal Processing.

Sjøvold, T. (1977). Nonmetrical divergence between skeletal populations. *Ossa*, *4*(1), 1–133.

Sjøvold, T. (1984). Multivariate Statistical Methods in Physical Anthropology. *Multivariate Statistical Methods in Physical Anthropology*. https://doi.org/10.1007/978-94-009-6357-3

Skousen, B. J. (2018). Rethinking archaeologies of pilgrimage. *Journal of Social Archaeology*, *18*(3), 261–283. https://doi.org/10.1177/1469605318763626

Slepchenko, S. M., Gusev, A. V., Svyatova, E. O., Hong, J. H., Oh, C. S., Lim, D. S., & Shin, D. H. (2019). Medieval mummies of Zeleny Yar burial ground in the Arctic Zone of Western Siberia. *PLoS ONE*, *14*(1), 1–23. https://doi.org/10.1371/journal.pone.0210718

Slovak, N. M. (2020). Reassembling the mortuary assemblage: New investigations into the Field Museum's osteological and artifact collections from Ancón, Peru. *Ñawpa Pacha*, *40*(1): 1–19. https://doi.org/10.1080/00776297.2019.1710365

Slovak, N. M., Paytan, A., & Wiegand, B. A. (2009). Reconstructing Middle Horizon mobility patterns on the coast of Peru through strontium isotope analysis. *Journal of Archaeological Science*, *36*(1), 157–165. https://doi.org/10.1016/j.jas.2008.08.004

Sørensen, T. (1948). *A method of establishing groups of equal amplitude in plant sociology based on similarity of species content and its application to analyses of the vegetation on Danish commons* (Vol. 1, Issue 3). I kommission hos E. Munksgaard. https://doi.org/10.1007/BF02852438

Stojanowski, C. & Buikstra, J. (2004). Biodistance analysis, a biocultural enterprise: A rejoinder to Armelagos and Van Gerven (2003). *American Anthropologist*, *106*(2), 430–431. https://doi.org/10.1525/aa.2004.106.2.430

Stojanowski, C., & Schillaci, M. (2006). Phenotypic approaches for understanding patterns of intracemetery biological variation. *Yearbook of Physical Anthropology*, *49*, 49–88. https://doi.org/10.1002/ajpa

Stone, Jessica H., Kristen Chew, Ann H. Ross, and John W. Verano. 2015. "Craniofacial Plasticity in Ancient Peru." Anthropologischer Anzeiger 72 (2): 169–83. https://doi.org/10.1127/anthranz/2015/0458

Sutherland, M. L. (2019). Use of computed tomography scanning in a 'virtual' bioarchaeology of care analysis of a Central Coast Peruvian mummy bundle. *International Journal of Paleopathology*, 25, 129–138. https://doi.org/10.1016/j.ijpp.2018.12.006

Sutherland, M. L., Cox, S. L., Lombardi, G. P., Watson, L., Valladolid, C. M., Finch, C. E., Zink, A., Frohlich, B., Kaplan, H. S., Michalik, D. E., Miyamoto, M. I., Allam, A. H., Thompson, R. C., Wann, L. S., Narula, J., Thomas, G. S., & Sutherland, J. D. (2014). Funerary artifacts, social status, and atherosclerosis in ancient Peruvian mummy bundles. *Global Heart*, *9*(2), 219–228. https://doi.org/10.1016/j.gheart.2014.04.004

Sutter, R. C. (2000). Prehistoric genetic and culture change: A bioarchaeological search for Pre-Inka altiplano colonies in the coastal valleys of Moquegua, Peru, and Azapa, Chile. *Latin American Antiquity*, *11*(1), 43–70. https://doi.org/10.2307/1571670

Sutter, R. C. (2005). A bioarchaeological assessment of prehistoric ethnicity among early Late Intermediate Period populations of the coastal Azapa Valley, Chile. In R. Reycraft (Ed.), *Us and Them: The Assignation of Ethnicity in the Andean Region, Methodological Approaches*, (pp. 183–205).

Sutter, R. C. (2009) Prehistoric population dynamics in the Peruvian Andes. In P. R. Williams & C. Stanish (Eds.) *The foundations of south highland Andean civilization: Papers in honor of Michael E. Moseley* (pp. 9-38). The Cotsen Institute of Archaeology, UCLA.

Sutter, R. C., & Castillo, L. J. (2015). Population structure during the demise of the Moche (550–850 AD). *Current Anthropology*, *56*(5), 762–771. https://doi.org/10.1086/683269.

Sutter, R. C., & Chhatiawala, T. (2016). Population structure during the collapse of the Moche (AD 200-850): A comparison of results derived from deciduous and permanent tooth trait data from San José de Moro, Jequetepeque Valley, Perú. In M. A. Pilloud & J. T. Hefner

(Eds.) *Biological distance analysis: Forensic and bioarchaeological perspectives* (pp. 349-362). Academic Press.

Sutter, R. C., & Mertz, L. (2004). Nonmetric cranial trait variation and prehistoric biocultural change in the Azapa Valley, Chile. *American Journal of Physical Anthropology*, *123*(2), 130–145. https://doi.org/10.1002/ajpa.10311.

Sutter, R. C., & Verano, J. (2007). Biodistance analysis of the Moche sacrificial victims from Huaca de la Luna Plaza 3C: Matrix method test of their origins. *American Journal of Physical Anthropology*, *132*, 193–206. https://doi.org/10.1002/ajpa.

Szpak, P., Millaire, J. F., White, C. D., & Longstaffe, F. J. (2014). Small scale camelid husbandry on the north coast of Peru (Viru´ Valley): Insight from stable isotope analysis. *Journal of Anthropological Archaeology*, *36*, 110–129. https://doi.org/10.1016/j.jaa.2014.08.005

Szpak, P., Millaire, J. F., White, C. D., Lau, G. F., Surette, F., & Longstaffe, F. J. (2015). Reports: Origins of prehispanic camelid wool textiles from the North and Central Coasts of Peru traced by carbon and nitrogen isotopic analyses. *Current Anthropology*, *56*(3), 449–459. https://doi.org/10.1086/680873

Takigami, M. K., Shimada, I., Segura, R., Muno, S., Matsuzaki, H., Tokanai, F., Kato, K., Mukai, H., Takayuki, O., & Yoneda, M. (2014). Assessing the chronology and rewrapping of funerary bundles at the prehispanic religious center of Pachacamac, Peru. *Latin American Antiquity*, *25*(3), 322–343. https://doi.org/10.7183/1045-6635.25.3.322

Tello, J. C. (1930). Andean civilization: Some problems of Peruvian archaeology. In *Proceedings of the Twenty-Third International Congress of Americanists* (pp. 259–290). Science Press.

Tello, J. C. (1943). Discovery of the Chavin Culture in Peru. *American Antiquity*, *9*(1), 135–160. https://doi.org/10.2307/275457

Thomas, D. H. (1976). *Figuring anthropology: First principles of probability and statistics.* Holt, Rinehart and Winston.

Thompson, R. C., Allam, A. H., Lombardi, G. P., Wann, L. S., Sutherland, M. L., Sutherland, J. D., Soliman, M. A. T., Frohlich, B., Mininberg, D. T., Monge, J. M., Vallodolid, C. M., Cox, S. L., Abd El-Maksoud, G., Badr, I., Miyamoto, M. I., El-Halim Nur El-Din, A., Narula, J., Finch, C. E., & Thomas, G. S. (2013). Atherosclerosis across 4000 years of human history: The Horus study of four ancient populations. *The Lancet*, *381*(9873), 1211–1222. https://doi.org/10.1016/S0140-6736(13)60598-X

Toft, P. (1996). *The Radon Transform- Theory and implementation*. [Doctoral dissertation]. Technical University of Denmark.

Torres, J. B., Stone, A. C., & Kittles, R. (2013). An anthropological genetic perspective on creolization in the anglophone Caribbean. *American Journal of Physical Anthropology*, *151*(1), 135–143. https://doi.org/10.1002/ajpa.22261

Torres-Rouff, C. (2019). Cranial modification and the shapes of heads across the Andes. *International Journal of Paleopathology*, 1–8. https://doi.org/10.1016/j.ijpp.2019.06.007

Torres-Rouff, C., Knudson, K. J., & Hubbe, M. (2013). Issues of affinity: Exploring population structure in the middle and regional developments periods of San Pedro de Atacama,

Chile. *American Journal of Physical Anthropology*, *152*(3), 370–382. https://doi.org/10.1002/ajpa.22361

Toyne, J. M., Church, W. B., Luis Coronado Tello, J., & Morales Gamarra, R. (2017). Exploring imperial expansion using an isotopic analysis of paleodietary and paleomobility indicators in Chachapoyas, Peru. *American Journal of Physical Anthropology*, *162*(1), 51–72. https://doi.org/10.1002/ajpa.23085

Tronick, E., & Hunter, R. G. (2016). Waddington, dynamic systems, and epigenetics. *Frontiers in Behavioral Neuroscience*, *10*(107), 1–6. https://doi.org/10.3389/fnbeh.2016.00107

Turing, A.M. (1950). Computing machinery and intelligence. *Mind*, *59*(236), 433-460. https://doi.org/10.1093/mind/lix.236.433

Turner, B. L., Klaus, H. D., Livengood, S. V., Brown, L. E., Saldaña, F., & Wester, C. (2013). The variable roads to sacrifice: Isotopic investigations of human remains from Chotuna-Huaca de los Sacrificios, Lambayeque, Peru. *American Journal of Physical Anthropology*, *151*(1), 22–37. https://doi.org/10.1002/ajpa.22238

Turner, C.G., Nichol, C.R., Scott, G.R. (1991). Scoring procedures for key morphological traits of the permanent dentition: the Arizona State University Dental Anthropological System. In M.A. Kelley, C. Spencer Larsen (Eds.), *Advances in dental anthropology* (pp. 13-31).

Uhle, M. (1903). *Pachacamac: Report of the William Pepper, M.D., LL.D. Peruvian Expedition of 1896*. Philadelphia, PA: Department of Archaeology of the University of Pennsylvania.

Ullinger, J. M. (2018). Early Christian pilgrimage to a Byzantine monastery in Jerusalem—A dental perspective. *Dental Anthropology Journal*, *16*(1), 22–25. https://doi.org/10.26575/daj.v16i1.166

Van Pool, T. L., & Van Pool, C. S. (2018). Visiting the horned serpent's home: A relational analysis of Paquimé as a pilgrimage site in the North American Southwest. *Journal of Social Archaeology*, *18*(3), 306–324. https://doi.org/10.1177/1469605318762819

Velasco, M. C. (2016). *Mortuary tradition and social transformation during the Late Intermediate Period (A.D. 1100-1450): A bioarchaeological analysis of above-ground burials in the Colca Valley, Peru* [Doctoral dissertation]. Vanderbilt University.

Velasco, M. C. (2018). Open sepulchers and closed boundaries? Biodistance analysis of cemetery structure and postmarital residence in the late prehispanic Andes. *American Journal of Physical Anthropology*, *166*(4), 906–920. https://doi.org/10.1002/ajpa.23594

Verano, J. W. (1987). *Cranial microvariation at Pacatnamu: A study of cemetery population variability* [Doctoral dissertation]. University of California Los Angeles.

Verano. J.W. (2001) The Physical Evidence of human sacrifice in ancient Peru. In E. P. Benson and A. G. Cook (Eds.), *Ritual sacrifice in ancient Peru* (pp. 165-184). University of Texas Press.

Villacorta, L. F. (2004). Los palacios en la Costa Central durante los Periodos Tardíos: De Pachacamac al Inca. *Bulletin de l'Institut Français d'Études Andines, 33*(3), 539–70.

Waddington, C. H. (2012). The epigenotype. *International Journal of Epidemiology*, *41*(1), 10–13. (Original work published 1942). https://doi.org/10.1093/ije/dyr184

Wade, A. D., & Nelson, A. (2013). Radiological evaluation of the evisceration tradition in ancient Egyptian mummies. *Homo, 64*(1), 1-28. https://doi.org/10.1016/j.jchb.2012.11.005

Wade, A. D., Holdsworth, D. W., & Garvin, G. J. (2011). CT and micro-CT analysis of a case of Paget's disease (osteitis deformans) in the Grant skeletal collection. *International Journal of Osteoarchaeology*, *21*(2), 127–135. https://doi.org/10.1002/oa.1111

Washburn, S. L. (1951). The new physical anthropology. *Transactions of the New York Academy of Sciences*, *13*, 298-304. https://doi.org/10.1111/j.2164-0947.1951.tb01033.x

Watson Jiménez, L. C. (2016). *Vida y muerte en la costa central del Perú do los periodos tardíos (800 d.C.-1532 d.C.): Análisis de los fardos funerarios de Ancón desde la perspectiva bioarqueológica* [Doctoral dissertation]. Universidad Nacional Autónoma de México.

Watson Jiménez, L. C. (2019). *Los fardos de Ancón – Perú (800d.C.-1532d.C.): Una perspectiva bioarqueológica de los cambios sociales en la Costa Central del Perú*. BAR International Series.

Wauters, V. (2016). Imperial Needs, Imperial Methods: Chimú Ceramic Manufacturing Process Through CT Scan Analysis of Stirrup-Spout Bottles. *Latin American Antiquity*, *27*(2), 238–256. https://doi.org/10.7183/1045-6635.27.2.238

Weinhold, B. (2006). Epigenetics: The science of change. *Environmental Health Perspectives*, *114*(3), 160-167. https://doi.org/10.1289/ehp.114-a160

Wernick, M., Yang, Y., Brankov, J., Yourganov, G., & Strother, S. (2010). Machine learning in medical imaging. *IEEE Signal Processing Magazine*, *27*(4), 25–38. https://doi.org/10.1109/MSP.2010.936730

White, C. D. (1996). Sutural effects of fronto-occipital cranial modification. *American Journal of Physical Anthropology*, *100*(3), 397–410.

White, C. D., Nelson, A. J., Longstaffe, F. J., Grupe, G., & Jung, A. (2009). Landscape bioarchaeology at Pacatnamu, Peru: Inferring mobility from $\delta^{13}C$ and $\delta^{15}N$ values of hair. *Journal of Archaeological Science, 36*(7), 1527–1537. https://doi.org/10.1016/j.jas.2009.03.008.

Wilson, A. S., Brown, E. L., Villa, C., Lynnerup, N., Healey, A., Ceruti, M. C., Reinhard, J., Previgliano, C. H., Araoz, F. A., Diez, J. G., & Taylor, T. (2013). Archaeological, radiological, and biological evidence offer insight into Inca child sacrifice. *Proceedings of the National Academy of Sciences of the United States of America*, *110*(33), 13322–13327. https://doi.org/10.1073/pnas.1305117110

Wind, J. (1984). Computerized X-ray tomography of fossil hominid skulls. *American Journal of Physical Anthropology*, *63*(3), 265–282. https://doi.org/10.1002/ajpa.1330630303

Zesch, S., Panzer, S., Rosendahl, W., Nance, J. W., Schönberg, S. O., & Henzler, T. (2016). From first to latest imaging technology: Revisiting the first mummy investigated with X-ray in 1896 by using dual-source computed tomography. *European Journal of Radiology Open*, *3*, 172–181. https://doi.org/10.1016/j.ejro.2016.07.002

Appendix

Appendix A: Semi-automated segmentation of fardos using Segmentation Wizard (Seg Wiz) in Dragonfly.

(Step 1) Import the dataset into Dragonfly. Adjust the window levelling to ensure the volume is visible and select the appropriate "Views" option to observe the volume in 3D as well as multiple 2D views.

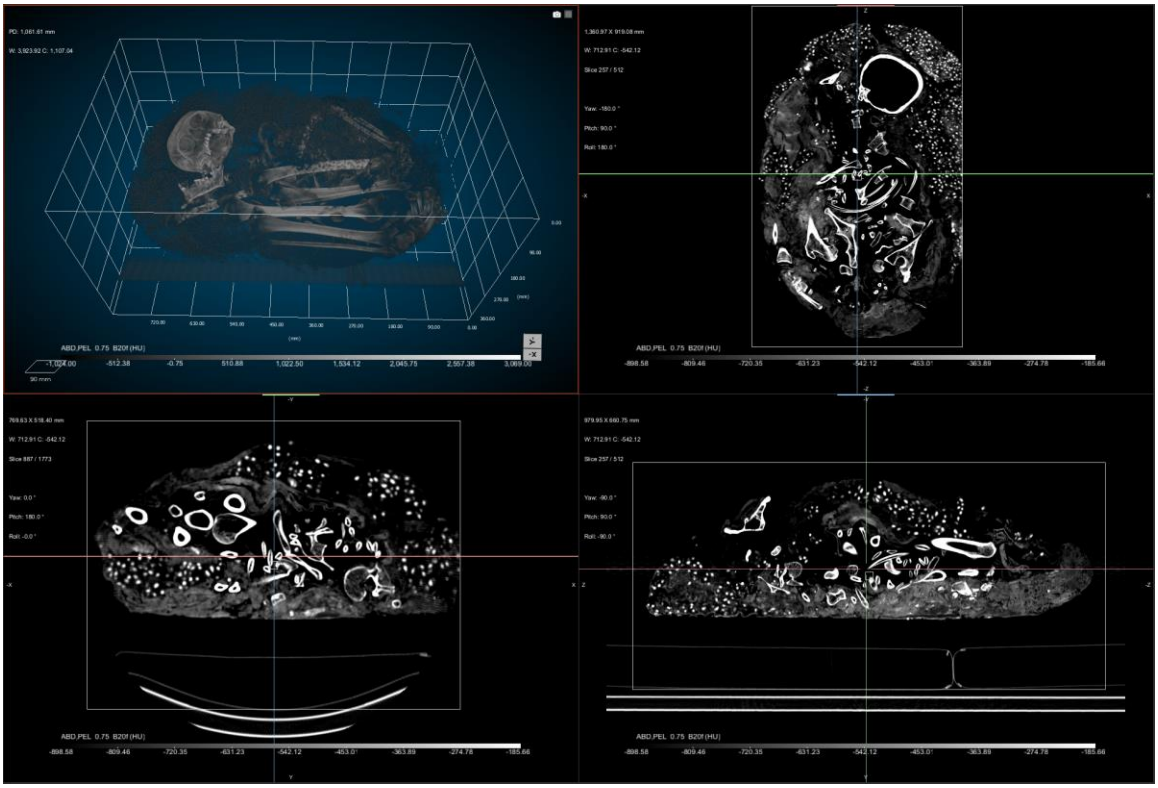

Figure A.1 Fardo E82S before cropping to skull. Image by Cameron Beason.

(Step 2) Select the "Clip" tool in the "Properties" tab. A box marking the clipping boundaries will appear. Use this tool to define the cropping area and isolate the cranium and mandible, consulting the 3D and 2D views to ensure the most accurate cropping of the dataset. Once the box is placed around the cranium and mandible, right click the dataset in the image channel located in the "Properties" tab and select "Modify and transform" and "Crop…".

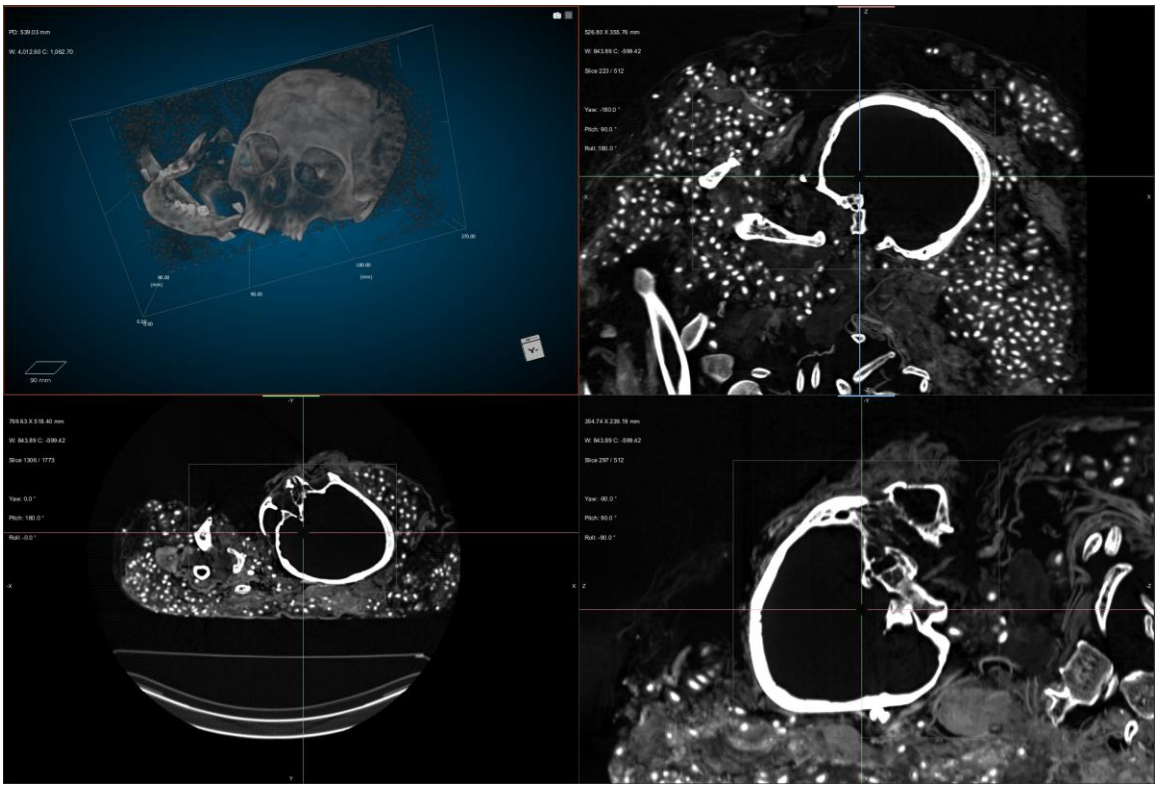

Figure A.2 Fardo E82S cropped to the skull. Image by Cameron Beason.

(Step 3) Once the skull is cropped, right click the cropped dataset in the image channel and select “Segmentation Wizard”. This will open a new instance of Dragonfly with the selected dataset show in the image plane. Cycle to slice 1 in the dataset and select “Add” under the “Frames” menu. This will add a frame to the available training data. Scroll through the dataset, adding training frames as necessary. The training frames were added at a fixed interval (every 50 slices) in this study to ensure uniformity during the early experimentation with these tools to determine the most effective method.

(Step 4) Once the frames have been created, create labels for the classes in the region of interest (ROI). This study employs a binary segmentation, separating the skull (with a ROI labelled “Skull”) from the remaining “clutter” present in the fardo (with an ROI labelled “ETC.”). The “ETC.” ROI includes any other objects that are not the cranium or mandible of the individual, such as the postcranial remains, wrappings, desiccated soft tissue, artifacts, cotton seeds, and the air or empty space in between

objects. To create the training data for the models, manually segment the frames as accurately as possible using the ROI painting tools in Segmentation Wizard.

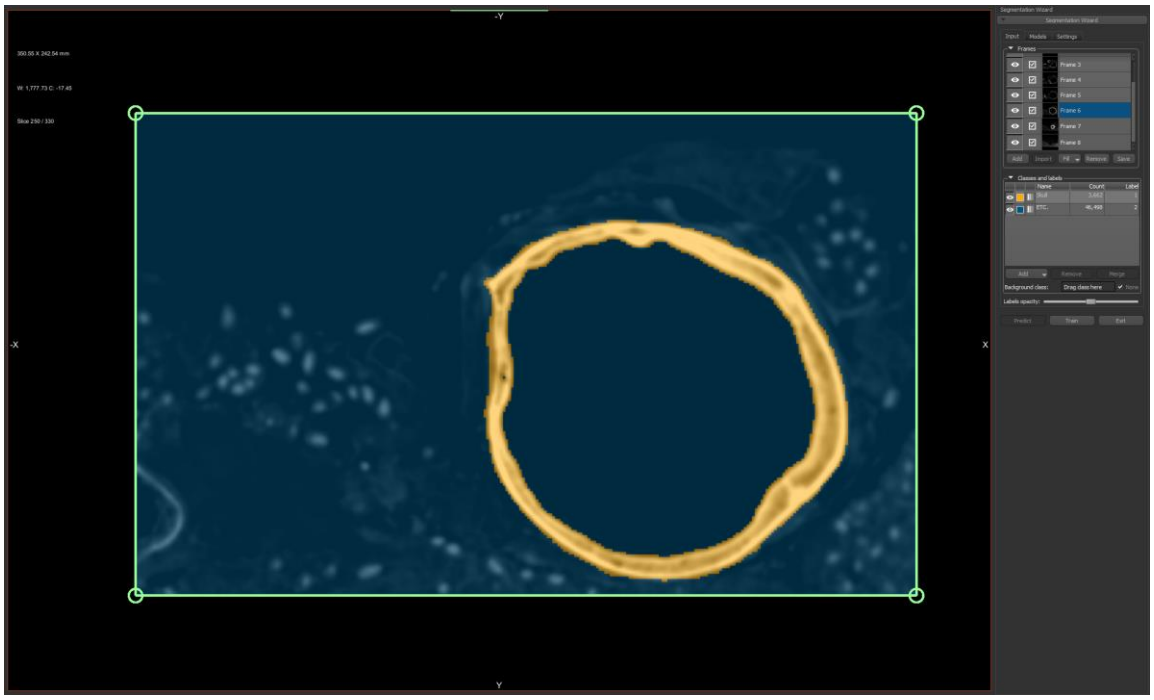

Figure A.3 Example of a training frame painted in Segmentation Wizard on fardo E82S. Image by Cameron Beason.

(Step 5) Once the training frames are labelled, select the “Models” tab. Pre-existing models can be imported or new models can be generated from this menu. Both machine learning and deep learning architectures are available. Select “Train” to begin training. The training is set to stop early if the value of the loss function does not improve after ten epochs. Once the training is complete, the three most successful models will be displayed below the training frames.

(Step 6) The arrow key at the top right of each training output can be used to promote the model’s output into the training data. Once the preferred output is promoted, the frame can be corrected to ensure greater accuracy in the next round of training with the ROI painting tools. Once the desired results have been achieved, the models can be saved in Dragonfly when exiting Segmentation Wizard. The Segmentation Wizard session will now appear in the image channel and can be reopened for further training.

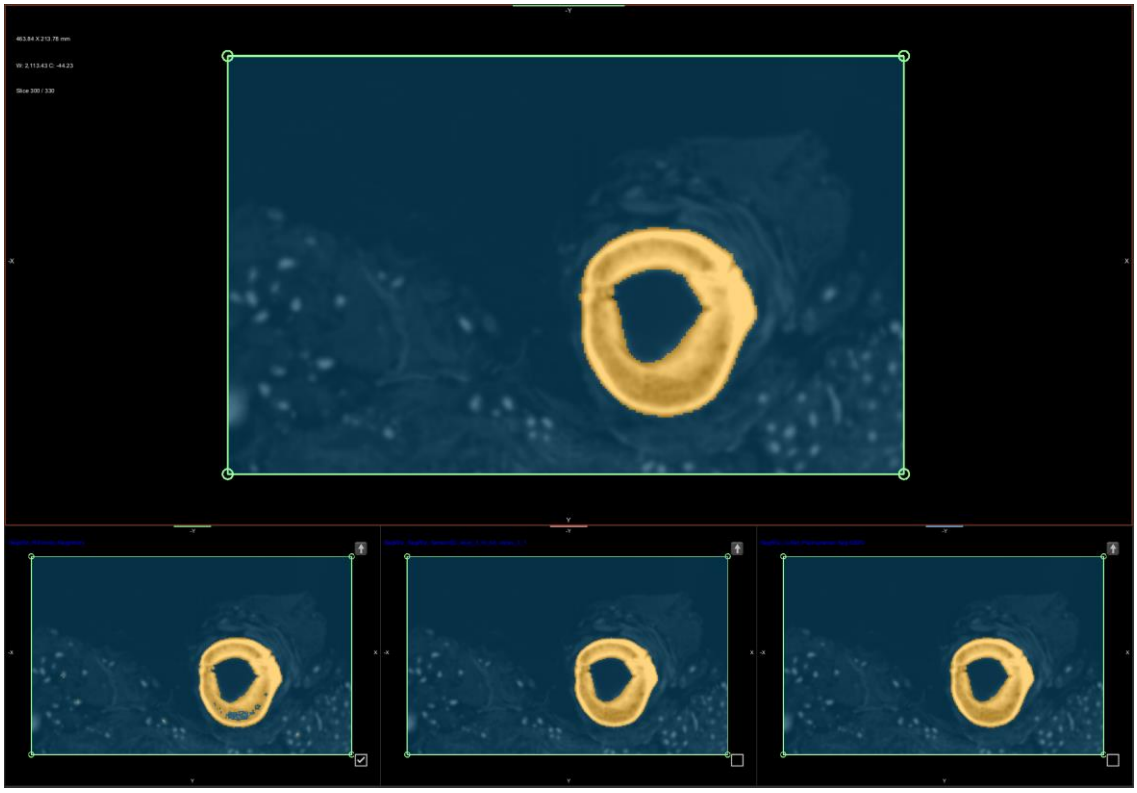

Figure A.4 Results of model training in Segmentation Wizard on fardo E82S. Image by Cameron Beason.

(Step 7) Finally, to apply a model to the full volume, exit Segmentation Wizard, select the desired volume to be segmented in the image channel, and select the "Segment" tab or right click the image channel and select "Segment with AI". From this menu, the image to be segmented and the model used can be selected. This will produce a new ROI with the output segmentation.

(Step 8) Manually correct the segmentation output. With the output segmentation ROI selected, and using the ROI painter tool, correct any false positives and false negatives. Use left CTRL + left click to add voxels to the selected class and SHIFT + left click to remove.

In my experience, the best results have come from correcting only the "Skull" ROI, erasing any labels on pixels that do not correspond with the skull and adding labels to pixels that do correspond with the skull but were incorrectly labelled "ETC." by the model (see Figure 4.2). The 2D ROI painting tool will add voxels to the ROI only on the

current 2D slice. The 3D painting tool can be used for long series of similar slices when there is a lot of overlap in the structures moving from one slice to the next; however, be cautious of overpainting/erasing as slices above and below the current view will be affected.

Appendix B: Semi-automated segmentation of fardos using the Deep Learning Tool in Dragonfly.

The Deep Learning Tool is useful for creating models and training pre-existing models. First, follow the same steps to crop the volume down to the skull. Then, create a new ROI assigned to the geometry of the cropped skull, select the "Create as a Multi-Class ROI" option, and specify the number of classes required. Manually label the entire image stack as accurately as possible. The model will not be able to train unless all of the pixels in the ROI are assigned to a class. This makes this approach the most time-consuming of the three methods tested in this thesis. It is not recommended as the procedure with Segmentation Wizard is much quicker and enables a comparison between model architectures.

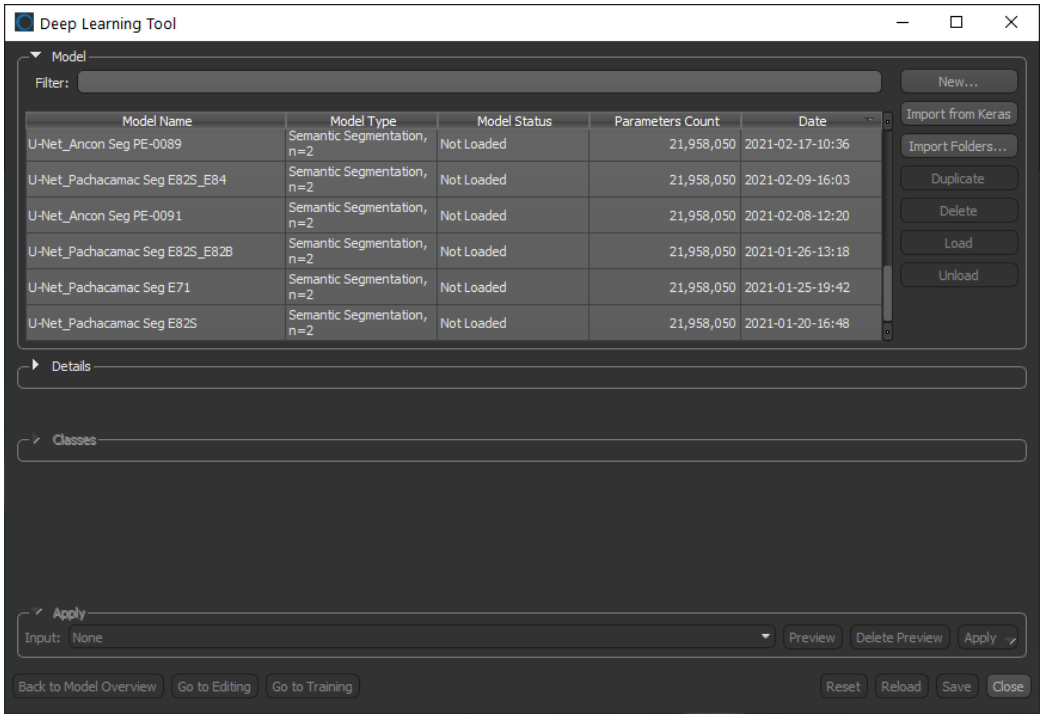

Figure B.1 The Deep Learning Tool interface in Dragonfly. Image by Cameron Beason

Select "Deep Learning Tool" from the "Artificial Intelligence" menu. Select a pre-existing model and select "Load" or create a new model by selecting "New…". Select "Go to Training", choose an input (the volume on which the training data was prepared), an output (the ROI used as the ground truth or training data). In this menu, the user can adjust the various training parameters (outlined in section 3.4.2). Selelect

"Train" and the system will begin to run through the training epochs. Once complete, save the model and follow Steps 7-8 (outlined in Appendix A) to apply the model to a new image and manually correct the output for the final segmentation.

Appendix C: Instructions given by Dr. Natalie Reznikov on the "manual abridged stack method"

In August 2020, Dr. Natalie Reznikov offered advice on obtaining suitable results with the deep learning segmentation in Dragonfly. I refer to this method as the "manual abridged stack method" in which a handful of slices (taken at 50-slice intervals) were selected, compiled, and used as the training input. This enables the use of image processing tools in Dragonfly to, for example, increase the edge detection and contrast between objects in the image for a more accurate ground truth or input.

With the image loaded in the 2D slice view, right click the image and select "Image Plane". Then, right click the image and select "Show Marked Slices Indicator"; a check box will appear in the bottom right of the screen. Scroll through the slices and check one slice at a fixed interval. On the image channel, right click the dataset and select "New Image from Marked Slices". This will create a new stack of images containing only the slices marked during the previous step.

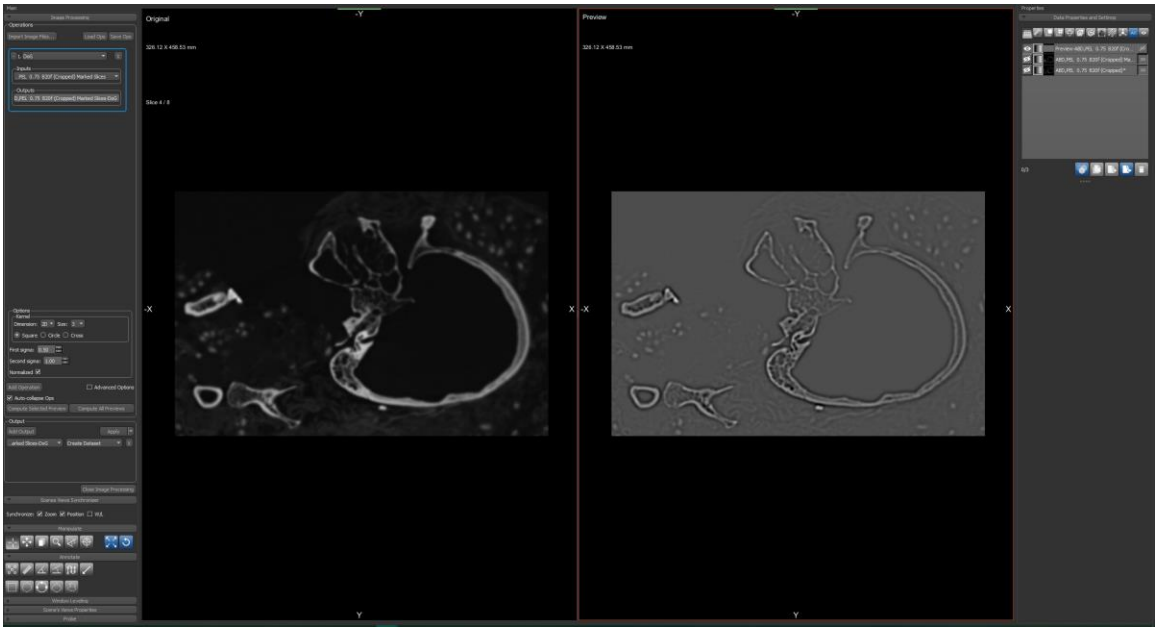

Figure C.1 Advanced image processing panel interface in Dragonfly. Image by Cameron Beason.

To apply image processing, select the “Image Processing Panel under the “Main” tab and select “Advanced…”. This will open a new instance of Dragonfly and allows the selection of various image processing tools with a view of the original image and the new processed image for comparison.

Once complete, select “Close Image Processing” and the new stack of processed images will appear in the image channel. Create a ROI with this new image and follow the steps outlined in Appendix B to train a model with the Deep Learning Tool, using the abridged stack of processed slices as the input and use the ROI as the output. The image processing allows the user to label the features in the image more accurately and saves time over the procedure in Appendix B. Finally, follow steps 7-8 outlined in Appendix A for the manual correction of the output.

Appendix D: Full battery of traits analyzed in this study. (For traits used in biodistance analysis, see Table 3.3).

Table E.1 List of nonmetric traits analyzed in this study with coding, coding used by Ossenberg (2013), criteria for scoring as present, and references with image page numbers from Hauser & DeStefano (1989).

Trait name	Coding	Ossenberg Coding	Bilateral?	Present	Source	
Metopic Suture*	MSR	METO	N	Complete	Hauser & De Stefano, 1989, p. 41	p. 45, Plate VI
Fronto-temporal Articulation	FTA L/R		Y	Present	Hauser & De Stefano, 1989, p. 216	p. 211, Plate XXXI
Supraorbital Foramen*	SOF L/R	SOF L/R*	Y	Present	Hauser & De Stefano, 1989, p. 50	p. 52, Plate VII
Supraorbital Notch*	SON L/R	SOF L/R*	Y	Present	Hauser & De Stefano, 1989, p. 50	p. 52, Plate VII
Parietal Foramen	PFP L/R		Y	Present	Hauser & De Stefano, 1989, p. 78	p. 79, Plate XII
Tympanic Dehiscence/Foramen of Huschke*	FOH L/R	TYM L/R	Y	Present	Hauser & De Stefano, 1989, p. 143	p. 145, Plate XXII
Condylar Canal*	CCP L/R	ICC L/R	Y	Open	Hauser & De Stefano, 1989, p. 114	p. 105, Plate XVII
Divided Hypoglossal Canal*	DHC L/R	HYP L/R	Y	Complete Division	Hauser & De Stefano, 1989, p. 120	p. 123, Plate XXI
Foramen Ovale Incomplete*	FOI L/R	FSP L/R***	Y	Open	Hauser & De Stefano, 1989, p. 149	p. 150, Plate XXIII
Foramen Spinosum Incomplete*	FSO L/R	FSP L/R***	Y	Open	Hauser & De Stefano, 1989, p. 149	p. 150, Plate XXIII
Accessory Lesser Palatine Foramen	APF L/R		Y	>1 Present	Hauser & De Stefano, 1989, p. 163	p. 168, Plate XXV
Zygomatico-facial Foramen	ZFA L/R		Y	Present	Hauser & De Stefano, 1989, p. 229	p. 229, Plate XXXI
Multiple Infraorbital Foramina	MIF L/R		Y	>1 Present	Hauser & De Stefano, 1989, p. 70	p. 71, Plate X
Coronal Ossicle	COP L/R		Y	Present	Buikstra & Ubelaker, 1994, p. 88	p. 88, Figure 59
Sagittal Ossicle	SOB		N	Present	Buikstra & Ubelaker, 1994, p. 88	p. 88, Figure 59
Lambdoid Sutural Bone	LOP L/R		Y	Present	Buikstra & Ubelaker, 1994, p. 88	p. 88, Figure 59
Occipito-mastoid Bone*	OMB L/R	OMB L/R	Y	Present	Buikstra & Ubelaker, 1994, p. 88	p. 88, Figure 59
Bregmatic Bone	OAB		N	Present	Buikstra & Ubelaker, 1994, p. 88	p. 88, Figure 59
Apical Bone*	ABP	APIC	N	Present	Buikstra & Ubelaker, 1994, p. 88	p. 88, Figure 59
Pterion/Epipteric Bone	EBP L/R		Y	Present	Buikstra & Ubelaker, 1994, p. 88	p. 88, Figure 59
Asterionic Bone*	OAA L/R	AST L/R	Y	Present	Buikstra & Ubelaker, 1994, p. 88	p. 88, Figure 59
Parietal Notch Bone*	PNB L/R	PNB L/R	Y	Present	Hauser & De Stefano, 1989, p. 207	p. 200, Plate XXIX
Os Japonicum*	OJP L/R	JAP L/R	Y	Present	Hauser & De Stefano, 1989, p. 222	p. 211, Plate XXXI
Inca Bone*	IBP	INCA	N	Present	Hauser & De Stefano, 1989, p. 99	p. 100, Plate XVI
Torus Maxillaris	MTP L/R		Y	Present	Hauser & De Stefano, 1989, p. 180	p. 181, Plate XXVII

Torus Palatinus	PTP		N	Present	Hauser & De Stefano, 1989, p. 174	p. 175, Plate XXVI
Auditory Exostosis	ATP L/R		Y	Present	Hauser & De Stefano, 1989, p. 186	p. 181, Plate XXVII
Double Condylar Facet	CFD L/R		Y	Double	Hauser & De Stefano, 1989, p. 116	p. 113, Plate XIX
Precondylar Tubercle*	PCT	PCTB	N	Present	Hauser & De Stefano, 1989, p. 134	p. 119, Plate XX
Infraorbital Suture*	IOS L/R	CON L/R	Y	Present	Hauser & De Stefano, 1989, p. 67	p. 71, Plate X
Mylo-hyoid Bridge*	MHB L/R	MHB L/R	Y	Present	Hauser & De Stefano, 1989, p. 234	p. 231, Plate XXXIII
Torus Mandibularis*	TMP L/R	TMP	Y	Present	Hauser & De Stefano, 1989, p. 182	p. 181, Plate XXVII
Multiple Mental Foramen*	MMF L/R	MEN L/R	Y	>1 Present	Hauser & De Stefano, 1989, p. 230	p. 231, Plate XXXIII

*Indicates traits on which both the Peruvian and Chilean material were scored.

**Ossenberg scored the supraorbital foramen and notch as one trait but distinguished between the two forms when scoring. An individual was scored ‘1’ if two or more foramina were present and a ‘2’ if a notch was present. The scores were separated for comparability with the scoring in this thesis.

***Ossenberg scored all variants of the foramen spinosum and ovale as one trait with no further distinction. Therefore, the separate frequencies of open foramen spinosum and ovale were pooled into one trait for the Pachacamac, Maranga, Ancón, and San Jose de Moro samples for comparability with the Ossenberg dataset.

Appendix E: Nonmetric trait scores for all individuals observed in this thesis (see Table 3.5 for trait abbreviations).

Site	ID	Sex	MSR	SOFL	SOFR	SONL	SONR	FOHL	FOHR	CCPL	CCPR	DHCL	DHCR	FOIL	FOIR	OMBL	OMBR	ABP	OAAL	OAAR	PNBL	PNBR	OJPL	OJPR	IBP	PCT	IOSL	IOSR	MHBL	MHBR	MMFL	MMFR
Pachacamac	E76E	F	0	1	0	0	1	1	0	1	0	0	0	0	1	9	9	0	1	1	9	9	0	0	0	0	0	0	0	0	0	0
Pachacamac	E82C	M	0	1	1	0	0	1	1	0	1	0	0	0	0	9	9	1	1	1	9	0	0	0	1	0	0	0	0	0	0	0
Pachacamac	E82F	M	0	0	0	1	1	0	0	0	0	0	0	0	0	0	0	0	1	1	9	9	0	0	0	0	0	0	0	9	9	9	9
Pachacamac	E82S	M	0	1	1	0	0	0	0	0	0	0	0	0	0	0	0	0	0	0	9	9	0	0	0	0	0	0	1	1	0	0
Pachacamac	E84	M	9	9	9	9	9	1	1	0	9	0	0	0	0	0	0	0	1	1	0	1	0	0	0	0	0	9	0	0	0	0
Ancon	PE-0087	M	0	1	1	0	0	0	0	0	0	0	0	1	0	1	1	1	1	1	0	1	0	0	0	0	0	0	9	9	9	9
Ancon	PE-0088	M	0	0	0	1	1	0	9	0	0	0	0	0	0	9	0	9	9	1	9	0	0	0	9	0	0	0	0	0	0	0
Ancon	PE-0089	F	0	1	1	0	0	0	0	0	9	0	0	0	0	9	9	0	1	1	9	9	0	0	0	0	0	0	0	0	0	0
Ancon	PE-0091	M	0	0	0	0	1	0	0	0	0	0	0	0	1	1	1	0	1	1	9	9	0	0	1	0	0	0	1	1	0	0
Ancon	PE-0093	M	0	0	1	1	0	1	1	0	0	0	0	0	0	1	1	0	1	1	0	0	0	0	0	0	1	9	0	0	0	0
Ancon	PE-0100	F	0	1	0	0	1	0	0	9	1	0	0	0	0	1	1	1	1	1	0	0	0	0	0	0	0	0	1	1	0	0
Ancon	PE-0101	F	0	0	0	1	1	1	1	0	0	1	1	0	0	0	1	1	0	1	0	0	0	0	0	0	0	0	0	0	1	0
Ancon	PE-0102	F	0	1	0	0	1	1	9	0	0	1	0	1	1	9	9	0	0	1	0	0	0	0	0	0	0	0	0	0	0	0
Ancon	PE-0103	F	0	0	0	1	1	9	0	9	0	1	0	0	0	0	0	0	0	0	9	9	0	0	0	0	0	0	0	0	0	0
Ancon	PE-0104	M	0	0	0	1	1	0	0	0	0	1	0	0	1	0	1	0	1	1	0	1	0	0	1	0	0	0	0	0	0	0
Maranga	JC-AE-228	F	0	0	1	1	0	0	0	9	9	0	0	0	1	0	0	0	0	0	0	0	0	0	0	0	9	0	0	0	0	0
Maranga	JC-AE-230	M	0	1	0	0	1	0	0	0	0	0	0	0	0	0	0	0	1	1	0	1	0	0	0	0	0	0	0	0	0	0
San Jose de Moro	SJM-301	F	9	1	1	0	0	1	1	9	9	9	9	9	9	0	0	0	0	0	0	0	9	9	0	9	9	9	0	0	0	0
San Jose de Moro	SJM-311	M	9	9	9	9	9	0	0	9	9	9	9	9	9	9	9	9	9	9	9	9	9	9	9	9	9	9	0	0	9	9
San Jose de Moro	SJM-313	F	0	9	9	9	9	0	9	9	9	9	9	9	9	9	9	9	9	9	9	9	9	9	0	9	9	9	0	0	0	0
San Jose de Moro	SJM-316	F	0	9	0	9	1	9	9	9	9	9	9	9	9	9	9	9	9	9	9	9	9	9	9	9	9	9	9	9	1	0
San Jose de Moro	SJM-319	M	0	9	9	9	9	1	1	9	9	9	9	9	9	0	0	0	1	1	0	0	0	0	0	9	9	9	0	0	0	0
San Jose de Moro	SJM-320	M	0	9	9	9	9	9	9	9	9	9	9	9	9	0	0	0	0	0	0	0	9	9	9	9	9	9	0	0	9	9
San Jose de Moro	SJM-321	F	9	9	9	9	9	9	0	9	9	9	9	9	9	9	9	9	9	9	9	9	9	9	9	9	9	9	9	9	9	9
San Jose de Moro	SJM-405	F	0	0	1	0	0	0	1	9	9	9	9	9	9	0	0	0	0	0	9	9	9	9	0	9	9	9	1	1	9	9
San Jose de Moro	SJM-412	F	1	0	0	1	1	1	0	9	9	0	1	1	0	0	0	0	0	0	1	1	9	0	0	9	1	1	0	0	0	1
San Jose de Moro	SJM-413	M	0	1	1	0	0	9	9	9	9	9	9	9	9	9	9	9	9	9	9	9	9	9	9	9	9	9	0	0	0	0
San Jose de Moro	SJM-414	M	9	9	9	9	9	1	9	9	9	9	9	9	9	9	9	9	9	0	0	9	9	9	9	9	9	9	9	9	0	0
San Jose de Moro	SJM-415 1	M	1	0	0	1	0	1	1	1	1	0	1	0	0	0	0	0	0	0	0	0	0	0	0	0	9	9	0	0	0	1
San Jose de Moro	SJM-415 2	M	1	0	0	1	1	0	0	1	0	1	1	0	9	0	1	1	0	0	0	0	0	0	0	0	9	9	9	9	9	9
San Jose de Moro	SJM-415 3	M	0	9	0	9	1	0	0	0	0	0	0	0	0	0	0	0	0	0	0	0	0	0	0	0	9	9	9	9	9	9
San Jose de Moro	SJM-415 4	M	0	0	1	1	0	9	1	9	9	0	0	9	9	0	0	0	0	0	0	0	0	0	0	0	9	9	9	9	9	9
San Jose de Moro	SJM-415 5	M	0	0	0	1	1	0	0	0	0	0	0	1	1	9	1	0	1	1	0	0	1	0	0	0	9	9	9	9	9	9
San Jose de Moro	SJM-415 6	M	1	0	1	1	0	0	0	9	9	9	9	9	9	0	9	1	0	9	0	9	9	0	0	9	9	9	9	9	9	9
San Jose de Moro	SJM-418	M	0	9	9	9	9	9	9	9	9	9	9	9	9	9	9	0	9	9	9	9	9	0	9	9	9	9	9	9	9	9
San Jose de Moro	SJM-501	F	0	1	1	0	0	1	0	0	9	9	9	9	9	0	0	1	0	0	0	0	0	0	0	0	9	9	1	1	0	0
San Jose de Moro	SJM-502	F	0	9	1	9	0	1	9	9	9	0	9	0	9	0	0	0	9	0	0	0	1	9	0	0	1	9	9	9	0	0
San Jose de Moro	SJM-503	M	0	0	0	1	1	9	1	0	0	1	1	0	1	0	0	0	1	1	9	1	0	1	0	9	9	9	0	0	0	0
San Jose de Moro	SJM-509 A	F	0	1	0	0	1	9	9	9	9	9	9	9	9	9	9	9	9	9	9	9	0	0	1	9	9	9	1	1	0	0
San Jose de Moro	SJM-512	M	0	0	1	1	0	9	9	9	9	9	9	9	9	0	1	0	0	0	9	9	9	9	0	9	9	9	9	9	9	9
Araucanian	VL 3239	M	0	1	0	0	0	1	1	0	1	0	0	1	1	0	0	0	1	1	0	0	9	0	0	0	0	0	9	9	9	9
Araucanian	VL 3342	M	0	1	1	0	0	0	0	1	0	1	0	1	1	1	0	0	1	0	0	0	0	0	0	0	0	0	9	9	9	9
Araucanian	VL 3343	M	0	1	0	0	1	1	1	0	0	0	1	0	1	1	1	0	0	0	0	0	0	0	1	0	1	0	0	9	9	9
Araucanian	VL 3344	M	0	0	0	0	0	0	0	0	0	0	0	1	0	1	0	0	0	0	0	0	0	0	0	0	0	0	0	0	9	9
Arica	391/717	M	1	0	1	0	0	1	1	1	1	0	1	0	1	0	0	0	1	0	0	1	1	0	0	0	1	1	9	9	9	9
Arica	391/718	M	0	1	0	0	1	0	0	0	1	1	0	0	1	0	0	1	0	0	0	1	0	0	1	0	0	0	0	0	0	0
Arica	VL 258	M	0	1	0	0	1	0	1	0	0	0	0	1	0	0	0	1	0	0	1	1	0	0	0	0	0	0	9	9	9	9
Coquimbo	39/3942	M	0	1	0	0	0	0	0	0	0	0	0	0	0	0	9	1	1	9	0	0	0	0	0	0	9	9	0	0	0	0
Coquimbo	39/3943	M	0	0	0	0	1	0	0	0	0	0	0	0	0	0	1	1	0	0	0	0	0	0	9	0	0	0	0	0	0	0
Coquimbo	39/3944	M	0	1	1	0	0	1	1	1	0	1	0	0	0	0	1	0	0	1	0	0	0	0	9	0	0	0	0	0	0	0
Coquimbo	39/3945	F	0	0	0	0	0	0	1	0	0	1	0	0	0	0	1	1	1	0	1	1	0	0	9	0	0	0	0	0	0	0
Coquimbo	39/3946	M	0	1	0	0	1	1	0	9	9	0	0	0	9	9	0	0	9	0	0	0	0	0	9	0	0	0	9	9	9	9
Coquimbo	39/3947	M	0	0	0	0	0	9	9	9	9	0	0	9	0	9	9	0	9	9	9	9	9	1	0	9	9	0	0	0	0	0
Coquimbo	39/3948	M	0	0	1	0	0	1	1	0	1	0	0	0	0	1	0	0	1	1	0	0	0	0	9	0	0	0	0	9	9	9
Coquimbo	39/3949	M	0	0	1	1	0	9	9	9	9	9	9	9	9	1	1	1	9	1	0	0	0	0	0	0	0	0	0	1	1	0
Iquique	391/756	M	0	0	1	0	0	0	0	0	0	0	0	9	0	9	9	0	1	9	9	0	1	0	0	0	0	0	9	9	9	9
Iquique	VL 190	IND	0	1	1	0	0	1	0	0	1	0	0	1	0	1	1	0	1	0	1	1	0	0	0	0	0	0	0	0	0	0
Iquique	VL 199	M	0	0	0	0	0	0	0	0	1	0	0	1	0	0	0	0	0	0	0	1	1	9	0	0	0	0	9	9	9	9
Iquique	VL 277	F	0	1	0	0	0	1	1	1	1	0	0	0	0	0	0	0	0	0	0	1	0	0	1	0	0	0	9	9	9	9
Junin grave 10	391/753	F	1	1	0	0	0	1	1	9	9	9	9	0	0	0	1	0	0	0	1	9	0	1	0	9	0	0	0	0	0	1
Junin grave 15	391/754	M	0	0	0	0	0	0	0	1	1	1	1	0	0	0	0	0	0	0	0	0	0	0	0	0	0	0	1	0	0	0
Punta Pichalo	391/720	M	0	1	1	0	0	1	1	1	1	0	1	0	0	0	0	0	0	0	0	0	9	0	0	0	0	0	9	9	9	9
Punta Pichalo	391/729	F	0	0	0	0	0	0	1	1	0	0	1	1	1	1	0	0	0	0	1	1	0	1	0	0	0	0	9	9	9	9
Punta Pichalo	391/731	F	0	0	0	0	0	0	0	1	1	0	0	0	0	0	0	0	0	0	0	0	0	0	0	0	0	1	1	0	0	0
Punta Pichalo	391/732	M	0	0	0	0	0	1	1	0	0	0	1	0	0	9	9	9	9	9	9	9	0	0	9	0	0	9	0	9	0	9
Punta Pichalo	391/735	M	0	0	0	0	0	1	0	1	0	0	0	0	0	0	0	0	0	0	1	1	0	0	0	0	0	0	0	0	0	0
Punta Pichalo	391/736	F	0	0	0	0	0	0	0	1	0	0	0	0	0	1	1	0	0	0	0	0	0	0	0	0	0	0	9	9	9	9
Punta Pichalo	391/739	F	0	0	0	0	0	1	1	1	0	0	0	0	0	0	0	0	1	1	0	0	0	0	0	0	0	0	0	0	0	0
Punta Pichalo	391/740	M	0	1	0	0	0	1	1	0	0	0	1	1	0	0	0	0	0	0	1	0	0	0	0	0	0	0	1	0	0	0
Punta Pichalo	391/741	M	0	0	0	0	0	0	0	0	1	1	1	0	0	0	0	0	0	0	0	0	0	0	0	0	0	0	0	0	0	0
Punta Pichalo	391/742	F	0	1	0	0	0	0	0	0	1	9	0	0	1	1	9	0	0	0	1	1	9	9	0	0	9	0	1	1	1	0
Punta Pichalo	391/745	M	0	0	0	0	0	0	0	1	1	1	0	0	0	0	0	0	0	0	0	0	0	0	0	0	0	0	0	1	0	1
Punta Pichalo	391/749	M	0	0	0	0	0	0	0	1	9	0	0	0	0	0	0	0	0	1	1	1	0	0	0	0	0	0	1	1	0	0

Appendix F: Nonmetric trait scores for all Peruvian Individuals (see Table 3.5 for trait abbreviations).

Site	ID	Sex	MSR	FTAL	FTAR	SOFL	SOFR	SONL	SONR	PFPL	PFPR	FOHL	FOHR	CCPL	CCPR	DHCL	DHCR	FOIL	FOIR	FSOL	FSOR	APFL	APFR	ZFAL	ZFAR	MIFL	MIFR	COPL	COPR	SOB	LOPL	LOPR
Pachacamac	E76E	F	0	0	0	1	0	0	1	1	0	1	0	1	0	0	0	0	0	0	1	0	0	1	0	1	0	0	0	0	1	1
Pachacamac	E82C	M	0	9	9	1	1	0	0	0	0	1	1	0	1	0	0	0	0	0	0	0	1	0	0	0	0	1	0	0	1	1
Pachacamac	E82F	M	0	0	0	0	0	1	1	1	0	0	0	0	0	0	0	0	0	0	0	0	0	1	1	0	0	0	0	1	0	0
Pachacamac	E82S	M	0	0	0	1	1	0	0	1	1	0	0	0	0	0	0	0	0	0	0	0	0	1	1	0	0	9	1	0	1	0
Pachacamac	E84	M	9	0	0	9	9	9	9	1	1	1	1	0	9	0	0	0	0	9	9	1	0	0	0	0	9	0	9	0	1	1
Ancon	PE-0087	M	0	0	0	1	1	0	0	0	1	0	0	0	0	0	0	0	0	1	0	1	0	1	1	1	0	0	0	0	1	1
Ancon	PE-0088	M	0	0	0	0	0	1	1	1	0	0	9	0	0	0	0	0	0	9	0	9	9	1	1	0	0	1	0	0	9	9
Ancon	PE-0089	F	0	9	9	1	1	0	0	0	0	0	0	0	9	0	0	0	0	0	0	9	9	0	0	0	0	9	9	9	1	1
Ancon	PE-0091	M	0	9	0	0	0	0	1	1	0	0	0	0	0	0	0	0	1	0	1	0	0	0	0	0	0	0	0	0	1	1
Ancon	PE-0093	M	0	0	0	0	1	1	0	0	1	1	1	0	0	0	0	0	0	0	0	0	0	1	1	1	9	0	0	0	1	1
Ancon	PE-0100	F	0	0	0	1	0	0	1	0	0	0	0	9	1	0	0	0	0	9	9	9	0	1	1	0	0	9	9	9	0	0
Ancon	PE-0101	F	0	0	0	0	0	1	1	0	0	1	1	0	0	1	1	0	0	0	0	0	0	1	1	1	0	0	0	0	1	1
Ancon	PE-0102	F	0	0	0	1	0	0	1	0	0	1	9	0	0	1	0	0	1	1	1	1	1	1	0	0	0	0	0	0	0	0
Ancon	PE-0103	F	0	9	9	0	0	1	1	0	0	9	0	9	0	1	0	0	0	0	0	9	9	0	0	9	9	0	0	0	1	1
Ancon	PE-0104	M	0	9	0	0	0	1	1	0	0	0	0	0	0	1	0	0	0	0	1	1	1	0	0	1	0	0	0	9	1	1
Maranga	JC-AE-2288	F	0	1	1	0	1	1	0	0	1	0	0	9	9	0	0	0	1	0	1	0	0	0	0	0	0	0	0	0	0	0
Maranga	JC-AE-2305	M	0	0	0	1	0	0	1	1	1	0	0	0	0	0	0	0	0	0	0	0	0	1	1	0	0	0	0	0	1	1
San Jose de Moro	SJM-301	F	9	9	9	1	1	0	0	0	0	1	1	9	9	9	9	9	9	9	9	9	9	9	9	9	9	0	0	0	1	0
San Jose de Moro	SJM-311	M	9	9	9	9	9	9	9	9	9	0	0	9	9	9	9	9	9	9	9	9	9	9	9	9	9	9	9	9	9	9
San Jose de Moro	SJM-313	F	0	9	9	9	9	9	9	9	9	0	9	9	9	9	9	9	9	9	9	9	9	9	9	9	9	9	9	9	9	9
San Jose de Moro	SJM-316	F	0	9	9	9	0	9	1	0	1	9	9	9	9	9	9	9	9	9	9	9	9	9	9	9	9	9	9	9	9	9
San Jose de Moro	SJM-319	M	0	9	9	9	9	9	9	9	9	1	1	9	9	9	9	9	9	9	9	9	9	9	9	9	9	0	0	0	0	0
San Jose de Moro	SJM-320	M	0	9	9	9	9	9	9	9	9	9	9	9	9	9	9	9	9	9	9	9	9	9	9	9	9	0	0	0	0	0
San Jose de Moro	SJM-321	F	9	9	9	9	9	9	9	9	9	9	0	9	9	9	9	9	9	9	9	9	9	9	9	9	9	9	9	9	9	9
San Jose de Moro	SJM-405	F	0	9	9	0	1	0	0	0	0	0	1	9	9	9	9	9	9	9	9	9	9	9	9	9	9	0	0	0	0	0
San Jose de Moro	SJM-412	F	1	0	0	0	0	1	1	0	0	1	0	9	9	0	1	0	0	1	0	0	0	1	9	1	1	1	1	0	1	0
San Jose de Moro	SJM-413	M	0	9	9	1	1	0	0	9	9	9	9	9	9	9	9	9	9	9	9	9	9	9	9	9	9	9	9	9	9	9
San Jose de Moro	SJM-414	M	9	9	9	9	9	9	9	9	1	9	9	9	9	9	9	9	9	9	9	9	9	9	9	9	9	9	9	9	9	9
San Jose de Moro	SJM-415 1	M	1	0	0	0	0	1	0	0	0	1	1	1	1	0	1	0	0	0	0	9	9	0	0	9	1	0	0	0	0	0
San Jose de Moro	SJM-415 2	M	1	0	0	0	0	1	1	0	1	0	0	1	0	1	1	0	9	0	9	9	9	0	1	0	0	0	0	0	1	1
San Jose de Moro	SJM-415 3	M	0	0	0	9	0	9	1	1	0	0	0	0	0	0	0	0	0	0	0	9	9	9	9	9	9	0	0	0	0	0
San Jose de Moro	SJM-415 4	M	0	9	9	0	1	1	0	0	1	9	1	9	9	0	0	9	9	9	9	9	9	9	9	9	9	0	0	0	0	0
San Jose de Moro	SJM-415 5	M	0	0	0	0	0	1	1	1	0	0	0	0	0	0	0	1	1	1	1	9	9	1	1	0	0	0	0	0	1	1
San Jose de Moro	SJM-415 6	M	1	9	9	0	1	1	0	0	1	0	0	9	9	9	9	9	9	9	9	9	9	9	1	9	1	0	0	0	0	1
San Jose de Moro	SJM-418	M	0	9	9	9	9	9	9	0	1	9	9	9	9	9	9	9	9	9	9	9	9	9	9	9	9	9	0	9	1	1
San Jose de Moro	SJM-501	F	0	0	0	1	1	0	0	0	0	1	0	0	9	9	9	9	9	9	9	9	9	1	1	0	0	0	0	0	0	1
San Jose de Moro	SJM-502	F	0	9	9	9	1	9	0	0	1	1	9	9	9	0	9	0	9	0	9	9	9	9	9	9	9	0	0	1	0	0
San Jose de Moro	SJM-503	M	0	0	0	0	0	1	1	0	1	9	1	0	0	1	1	0	1	0	0	9	9	1	1	9	1	0	0	0	1	1
San Jose de Moro	SJM-509 A	F	0	9	9	1	0	0	1	9	9	9	9	9	9	9	9	9	9	9	9	9	9	9	0	0	1	1	9	0	1	9	1
San Jose de Moro	SJM-512	M	0	9	9	0	1	1	0	0	0	9	9	9	9	9	9	9	9	9	9	9	9	0	9	0	9	0	0	0	1	1

Appendix F: Nonmetric trait scores for all Peruvian Individuals (cont.) (see Table 3.5 for trait abbreviations).

Site	ID	Sex	OMBL	OMBR	OAB	ABP	EBPL	EBPR	OAAL	OAAR	PNBL	PNBR	OJPL	OJPR	IBP	MTPL	MTPR	PTP	ATPL	ATPR	CFDL	CFDR	PCT	IOSL	IOSR	MHBL	MHBR	TMPL	TMPR	GEPL	GEPR	MMFL	MMFR
Pachacamac	E76E	F	9	9	0	0	9	9	1	1	9	9	0	0	0	0	0	0	0	0	0	0	0	0	0	0	0	0	0	0	0	0	0
Pachacamac	E82C	M	9	9	0	1	9	0	1	1	9	0	0	0	1	0	0	0	0	0	9	9	0	0	0	0	0	0	0	1	1	0	0
Pachacamac	E82F	M	0	0	0	0	0	9	1	1	9	9	0	0	0	0	0	0	0	0	9	9	0	0	0	9	9	9	9	9	9	9	9
Pachacamac	E82S	M	0	0	0	0	9	9	0	0	9	9	0	0	0	0	0	0	0	0	9	9	0	0	0	1	0	0	0	0	0	0	0
Pachacamac	E84	M	0	0	9	0	9	9	1	1	0	1	0	0	0	0	0	0	0	0	0	0	0	0	9	0	0	0	0	0	0	0	0
Ancon	PE-0087	M	1	1	0	1	0	0	1	1	0	1	0	0	0	0	0	0	0	0	0	0	0	0	0	9	9	9	9	9	9	9	9
Ancon	PE-0088	M	9	0	0	9	0	9	9	1	9	0	0	0	9	0	0	0	9	0	0	0	0	0	0	0	0	0	0	0	0	0	0
Ancon	PE-0089	F	9	9	9	0	9	9	1	1	9	9	0	0	0	0	0	0	0	0	0	0	0	0	0	0	0	0	0	1	0	0	0
Ancon	PE-0091	M	1	1	0	0	9	9	1	1	9	9	0	0	1	0	0	0	1	1	0	0	0	0	0	1	0	0	0	1	1	0	0
Ancon	PE-0093	M	1	1	0	0	0	0	1	1	0	0	0	0	0	0	0	0	0	0	1	1	0	1	9	0	0	0	1	0	0	0	0
Ancon	PE-0100	F	1	1	9	1	9	9	1	1	0	0	0	0	0	0	0	0	0	0	0	0	0	0	0	1	1	0	0	0	0	0	0
Ancon	PE-0101	F	0	1	0	1	0	0	0	1	0	0	0	0	0	0	0	0	0	0	0	0	0	0	0	0	0	0	0	1	1	1	0
Ancon	PE-0102	F	9	9	0	0	0	0	0	1	0	0	0	0	0	0	0	0	0	0	0	0	0	0	0	0	1	0	0	0	0	0	0
Ancon	PE-0103	F	0	0	0	0	9	9	0	0	9	9	0	0	0	0	0	0	1	1	0	0	0	0	0	0	1	0	0	0	0	0	0
Ancon	PE-0104	M	0	1	0	0	0	0	1	1	0	1	0	0	1	0	0	1	1	1	0	0	0	0	0	0	0	0	0	1	0	0	0
Maranga	JC-AE-2288	F	0	0	0	0	0	0	0	0	0	0	0	0	0	0	0	0	0	0	9	9	9	0	0	0	0	0	0	1	1	0	0
Maranga	JC-AE-2305	M	0	0	0	0	1	0	1	1	0	1	0	0	0	0	0	0	0	0	0	0	0	0	0	0	0	0	0	1	1	0	0
San Jose de Moro	SJM-301	F	0	0	0	0	9	9	0	0	0	0	9	9	0	9	9	0	0	0	9	9	9	9	9	0	0	9	9	1	1	0	0
San Jose de Moro	SJM-311	M	9	9	9	9	9	9	9	9	9	9	9	9	0	9	9	0	0	0	9	9	9	9	9	0	9	0	0	1	1	9	9
San Jose de Moro	SJM-313	F	9	9	1	9	9	9	9	9	9	9	9	9	0	0	0	0	0	0	9	9	9	9	9	0	0	0	0	1	1	0	0
San Jose de Moro	SJM-316	F	9	9	9	9	9	9	9	9	9	9	9	9	9	0	0	0	9	9	9	9	9	9	9	9	0	0	0	9	1	1	0
San Jose de Moro	SJM-319	M	0	0	0	0	0	0	1	1	0	0	0	0	0	9	9	0	9	9	9	9	9	9	9	0	0	0	0	0	0	0	0
San Jose de Moro	SJM-320	M	0	0	0	0	0	0	0	0	0	0	9	9	9	1	1	0	0	9	9	9	9	9	9	0	9	9	9	1	1	9	9
San Jose de Moro	SJM-321	F	9	9	9	9	9	9	9	9	9	9	9	9	9	0	0	9	9	0	9	9	9	9	9	9	9	9	9	9	9	9	9
San Jose de Moro	SJM-405	F	0	0	0	0	9	9	0	0	9	9	9	9	0	0	0	0	0	0	9	9	9	9	9	1	0	0	0	0	0	9	9
San Jose de Moro	SJM-412	F	0	0	0	0	0	0	0	0	1	1	9	0	0	0	0	1	0	0	0	0	9	1	1	0	0	0	0	0	0	0	1
San Jose de Moro	SJM-413	M	9	9	9	9	9	9	9	9	9	9	9	9	9	9	9	9	9	9	9	9	9	9	9	0	0	9	9	0	0	0	0
San Jose de Moro	SJM-414	M	9	9	9	9	9	9	0	0	9	9	9	9	9	9	9	9	0	0	9	9	9	9	9	9	9	0	0	0	9	0	0
San Jose de Moro	SJM-415 1	M	0	0	0	0	0	0	0	0	0	0	0	0	0	0	0	0	0	0	0	0	0	9	9	0	0	0	0	1	1	0	1
San Jose de Moro	SJM-415 2	M	0	1	0	1	9	9	0	0	0	0	0	0	0	0	0	0	0	0	0	9	0	9	9	9	9	9	9	9	9	9	9
San Jose de Moro	SJM-415 3	M	0	0	0	0	9	9	0	0	0	0	0	0	0	9	9	0	0	0	0	0	0	9	9	9	9	9	9	9	9	9	9
San Jose de Moro	SJM-415 4	M	0	0	0	0	9	9	0	0	0	0	0	0	0	9	9	9	9	0	0	0	0	9	9	9	9	9	9	9	9	9	9
San Jose de Moro	SJM-415 5	M	9	1	0	0	9	9	1	1	0	0	1	0	0	0	0	0	0	0	0	0	0	9	9	9	9	9	9	9	9	9	9
San Jose de Moro	SJM-415 6	M	0	9	0	1	9	9	0	9	0	9	9	0	0	0	0	0	0	0	9	9	9	9	9	9	9	9	9	9	9	9	9
San Jose de Moro	SJM-418	M	9	9	9	0	9	9	9	9	9	9	9	9	0	9	9	9	9	0	9	9	9	9	9	9	9	9	9	9	9	9	9
San Jose de Moro	SJM-501	F	0	0	0	1	9	9	0	0	0	0	0	0	0	0	0	0	0	0	0	0	0	9	9	1	9	0	0	1	1	0	0
San Jose de Moro	SJM-502	F	0	0	0	9	9	9	0	0	0	1	9	0	0	0	0	0	0	0	0	0	1	9	9	9	0	0	0	0	0	0	0
San Jose de Moro	SJM-503	M	0	0	0	0	9	9	1	1	9	1	0	1	0	0	0	1	0	0	0	0	0	9	9	0	9	0	0	1	1	0	0
San Jose de Moro	SJM-509 A	F	9	9	9	9	9	9	9	9	9	9	0	0	1	0	0	0	9	9	9	9	9	9	9	1	1	0	0	0	0	0	0
San Jose de Moro	SJM-512	M	0	1	0	0	9	9	0	0	9	9	9	9	0	9	9	9	9	9	9	9	9	9	9	9	9	9	9	9	9	9	9

Curriculum Vitae

Name: Cameron Beason

Post-secondary Education and Degrees:

The University of Western Ontario
Master of Arts
London, Ontario, Canada
2019-2021

The Ohio State University
Bachelor of Science
Columbus, Ohio, United States of America
2013-2017

Honours and Awards:

Western Graduate Research Scholarship
2019-2020, 2020-2021

Related Work Experience:

Graduate Teaching Assistant
The University of Western Ontario
2019-2021

Affiliations:

Western Anthropology Graduate Society (WAGS)
2019-2020 Member
2020-2021 VP Finance

Publications:

Atkinson, L. A. H.; Beason, C. J.; Boettinger, C. E. K.; Eastaugh, E.; Muggridge, T.; Philips, N. K.; Poeta, L. S.; Roberge, É.; Seston, D.; Vesely, I. V. (2020). "Finding those once lost: The analysis of the Potter's Field at Woodland Cemetery, London, ON". Archaeology eBook Collection. 1. https://ir.lib.uwo.ca/archaeology_ebooks/1